A Robot for Gait Rehabilitation

by

Michael H. Roberts

B.S. Mechanical Engineering
Massachusetts Institute of Technology, 2002

Submitted to the Department of Mechanical Engineering
in Partial Fulfillment of the Requirements for the Degree of
Master of Science in Mechanical Engineering

at the

MASSACHUSETTS INSTITUE OF TECHNOLOGY

June 2004

Signature of Author...
Department of Mechanical Engineering
May 7, 2004

Certified by...
Hermano Igo Krebs
Principal Research Scientist
Thesis Supervisor

Accepted by...
Ain Sonin
Chairman, Department Committee on Graduate Students

A Robot for Gait Rehabilitation

by

Michael H. Roberts

Submitted to the Department of Mechanical Engineering
on May 7, 2004 in partial fulfillment of the
requirements for the degree of
Master of Science in Mechanical Engineering

Abstract

After a stroke, persons suffer from neurological impairments that affect gait, and so require rehabilitation to regain ambulatory function. While 82% of patients recover the ability to walk, current methods including physiotherapy and partial body-weight supported treadmill training (PBWSTT) are monotonous and require intense therapist effort. The Mechanized Gait Trainer and the LOKOMAT are two robotic devices that have been developed to improve gait rehabilitation, but neither provides the facilitation of pelvis movements afforded by traditional methods. In addition, neither device is truly backdrivable. As shown by Hogan and Krebs, backdrivable, impedance-controlled robots are ideal for rehabilitation because of their stable interaction properties. Robots for the arm/shoulder, wrist, ankle, and hand have already been developed.

This thesis describes the design of a robot for gait rehabilitation through the facilitation of pelvis movements. Four degrees of freedom (DOF) are actuated: vertical, lateral, and frontal translations as well as the rotation about the vertical axis. Vertical forces support part of the patient's weight. Lateral forces assist the weight shift from stance leg to swing leg and are a part of physiotherapy and treadmill training. Frontal forces help pace the subject as on a treadmill. Pelvic rotations can impart energy into the swing leg without direct actuation of the hip and knee muscles. A four DOF mechanism was designed to control these movements, consisting of a three-DOF planar linkage with a vertical prismatic translation. A mockup of the configuration was designed and tested to show that the non-actuated pelvis DOFs are not adversely affected by the device. Design calculations include finding the optimal linkage configuration, selecting ballspline shafts for the vertical DOF, selecting actuators, and designing the robot arm cross-sections and joints. A final design for the four-DOF module is presented.

Thesis Supervisor: Hermano Igo Krebs
Title: Principal Research Scientist

Acknowledgements

The research contained in this thesis would not have been possible without the help of many people. Igo Krebs has been a terrific mentor throughout my two years as a grad student. His advice related to both engineering and non-engineering topics has been helpful and appreciated. Professor Neville Hogan has also helped me through this project with his technical expertise and eerily penetrating insights.

Many others contribute to the atmosphere at the Newman Lab and make it a great place to work. Jason Wheeler was a partner in gait research and design. Steve Buerger was the resident controls guru and answered my many foolish questions. Jerry Palazzolo has expertise in a variety of subjects, including how to provoke Steve into entertaining rants. Susan Fasoli had valuable input as the research group's resident therapist. Sarah Mendelowitz bought the best group meeting food and also helped me proofread this thesis. Chan Rhyou always greeted me with a smile. Laura DiPietro and Doug Eastman also made my time here more enjoyable, along with now-ex-Newman lab members James Celestino, Miranda Newbery, Tom Bowers, and Belle Kuo.

When I began this work I knew nothing about gait or rehabilitation. Several people conspired to cure me of this affliction. Richard Hughes at the Spaulding Rehabilitation Hospital was always happy to loan me reading material and to sit and discuss ideas for this robot. Dr. David Krebs and Dov Goldvasser from the Biomotion Lab at the Massachusetts General Hospital were kind enough to lend their gait analysis equipment and their knowledge for use in my research. Kevin McQuade, Rich Macko, Larry Forrester, and Chris Bever all dedicated much time to travel from Baltimore to learn about the gait robot and to offer input into this project.

Numerous people have lent technical help as well. Gerry Wentworth at the Laboratory for Manufacturing Productivity helped through all the machining for the mockup. Randy Jezowski dedicated much time to sitting with me and suggesting improvements to the final design. Mike Sandman, Antonio Makiyama, and Dustin Williams at Interactive Motion Technologies all gave considerable contributions to this project: Mike designed the housing for the frameless motors, Antonio spent much time on finite element analysis, and Dustin coordinated the orders for the components.

I would also like to thank my parents and my family for their support throughout my life. And finally I must thank Kelli Griffin, who makes my life infinitely better even from the other side of the country.

Table of Contents

List of Figures

List of Tables

Chapter 1: Introduction

1.1 Scope of thesis

This thesis describes the design of a robot for gait rehabilitation through the facilitation of pelvis motions. It begins by describing the requirements and specifications for this robot, which is itself one module of a complete gait rehabilitation system as shown in Figure 1.1-1. The pelvis module contains five sub-modules that cover the following functions: pelvis actuation, body-weight support, fall prevention, forward propulsion, and patient connection.

This thesis focuses on the pelvis actuation sub-module. A concept using a three-degree-of-freedom horizontal linkage with a prismatic vertical joint was selected for this module, and a mockup of this concept was built and tested to ensure that it did not adversely affect gait. Further refinements of this concept involve the selection of methods for actuation, for providing vertical motion, for bearing loads on the robot arms, for connecting the robot arms to move together vertically, for providing body-weight support forces, and for chassis construction. Detailed calculations are then carried out on the robot arms, actuators, and vertical motion elements.

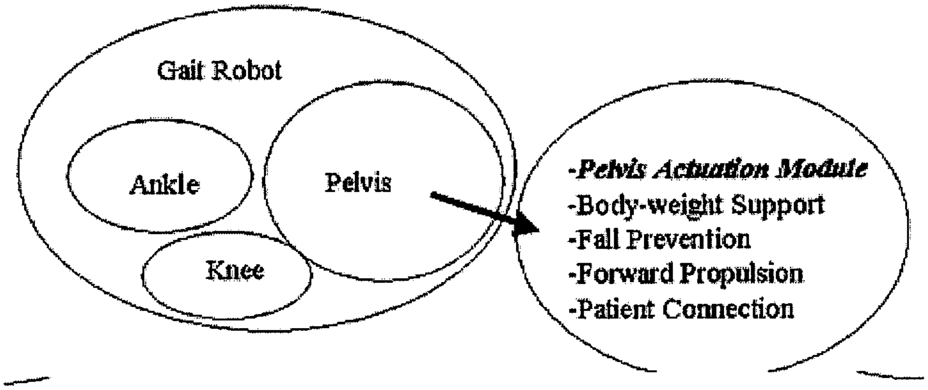

Figure 1.1-1: Modularization of the gait robot

Much future work remains. It includes the design of the remaining pelvis module components shown in Figure 1.1-1; of these, the forward propulsion sub-module will be the most mechanically complex. In addition, the pelvis actuation module described here must still be manufactured, assembled, characterized, and controlled. Then the sub-modules of the pelvis robot can be integrated into a cohesive unit. When the mechanical implementation is complete, clinical trials could begin so that the effectiveness of the device can be tested.

1.2 Motivation

As of 1999, stroke was the third most common cause of death in the United States, claiming 160,000 lives annually [69]. An estimated 730,000 strokes occur every year, and about 4 million people suffer from the after-effects of stroke [69]. While 82% of stroke survivors recover the ability to walk, the process of gait rehabilitation is difficult and labor-intensive. As such, it is a perfect application for an impedance-controlled rehabilitation robot.

Rehabilitation robotics is the use of electromechanical devices to assist the recovery of function following a stroke or other disabling event. The Newman Laboratory for Biomechanics has developed robots for the rehabilitation of the arm and shoulder, wrist, and ankle [34, 6, 4, 78, 76]. These robots are backdrivable and impedance-controlled: they do not impose a force or a position on the patient. Instead, they define a combination of force and motion (i.e. impedance) that can interact stably with the patient and can provide adjustable assistance based on the patient's ability.

The purpose of this thesis is to extend the application of impedance control to gait rehabilitation, particularly through actuating the pelvis. Pelvic facilitation is already a method used by physiotherapists [15], and newer treadmill-based therapies also include pelvis movement in their programs [72]. While current robotic gait trainers focus on the legs and feet [10, 9], evidence from two sources indicate that a pelvis-based robot could have a large impact on gait. First, computer simulations have shown that moving the pelvis can impart swing energy to the leg even when hip and knee muscles are weak [73]. Second, a pilot study found that patients who were being rehabilitated through pelvis actuation showed more brain activity than those who were rehabilitated by moving the legs through gait [38].

These results suggest that the pelvis robot could be effective as a stand-alone device. However, future clinical applications could include the integration of this device with other robots, in particular a recently designed, impedance-controlled ankle robot [76]. In addition, a robot to actuate the knee could be added if clinical trials with the pelvis robot show that such a device is necessary.

While this device is intended for use with stroke patients, it should be just as useful for use with patients suffering from spinal cord injuries, multiple sclerosis, or Parkinson's disease. Furthermore, it could be used in orthopedics, for example, to aid in recovery after hip replacement surgery.

1.3 Chapter overview

This thesis is divided into eight chapters. After this introduction, a *Background* chapter provides context on stroke, gait, gait therapy, and rehabilitation robotics. Chapter three covers the *Functional Requirements and Target Specifications*; these are the tasks the device must execute and quantitative measures of performance it must meet. The next stage in the design is the *Concept Selection* in chapter four, which involves considering the options for fulfilling each requirement and selecting the best one. At this point a mockup of the selected concepts are incorporated in to a mockup; the *Mockup Design and Testing* are described in chapter five. Chapter six included detailed *Design Analysis* for the alpha prototype pelvis robot. This chapter is the longest of this thesis and some of its sections are on linkage design, actuator selection, robot arm design, and robot joint analysis. Chapter seven shows an overview of the *Final Design Details*, including assembly drawings and exploded views of the pelvis actuation module. Finally, the *Conclusions* of this thesis are presented in chapter eight.

Chapter 2: Background

This chapter gives background information about stroke, gait, rehabilitation, and impedance control. Concepts from all four subjects are used in the design of this gait therapy robot.

2.1 Stroke and rehabilitation

Strokes, also called cerebrovascular accidents (CVAs), occur when blood ceases to reach part of the brain because of a blocked or ruptured artery. Symptoms of stroke can vary based on the size and location of the lesion: some CVAs leave no residual signs of the event while others are fatal in as little as five minutes [69]. After a stroke occurs, the patient receives acute care for two to four days and is then either allowed to go home or sent to another facility for further treatment [69].

Neurological damage originating from a stroke commonly leads to paralysis of one side of the body called hemiparesis. Hemiparetic patients suffer from reduced muscle strength, abnormal muscle tone, reduced sensation, and difficulty in controlling movements [69]. While modern medicine cannot regenerate neurons, the effects of the stroke can be reduced over time through rehabilitation: studies show that "58% of patients regain independence in activities of daily living (ADL) and 82% learn how to walk" [69]. Some studies also show that, in addition to being beneficial in the first 3-6 months after CVA, rehabilitation can also improve function many years post-stroke [69].

Rehabilitation is helpful to those who have suffered a stroke. But what is rehabilitation? According to Charness, "Rehabilitation can ... be defined as restoring the patient to the highest functional level possible within the limits of his CNS (*central nervous system*) damage, at all times keeping alive and maximizing the potential of the affected parts of the body" [7]. Specifically, modern rehabilitation aims to improve functional outcomes and so focuses on tasks instead of on exercises [69].

It is thought that rehabilitation is possible because neurons can assume new functions in two ways: first, by recruiting nearby neurons to aid with a skilled task; and second, by activating dormant connections within the brain. An example of the former process is the tendency of healthy string players to have a disproportionally large group of neurons controlling their left hand [27]. The latter phenomenon is observed in stroke patients as neural activation on the opposite side of the brain as the damaged area in response to a stimulus at the affected limb [41].

Although rehabilitation can improve function, some studies have shown that starting training too soon after stroke may increase neural damage [27]. Therefore, it is "... recommended that stroke patients be admitted to specialized stroke units with specially trained medical and nursing staff, coordinated multidisciplinary rehabilitation, and education programs for patients and their families" [27].

2.2 Gait

Gait is a very complex process in terms of the motions that comprise it, the forces it produces, and the neural control it requires. This section provides an introduction to the kinematics of gait, the impairments associated with stroke, the differences between overground and treadmill walking, and the central gait pattern generator.

2.2.1 Kinematics of gait

The phases of gait shown in Figure 2.2-1 and the six elements of gait described by Inman et al [26] combine for a simple yet useful description of gait kinematics. A gait cycle is defined as the time between subsequent right heel contacts. Each gait cycle includes two periods of single support and two periods of double support. A leg in contact with the ground is called a stance leg and one that is not in contact with the ground is called a swing leg. For example, at about the 25% point on the gait cycle the person is the right single support phase, the right leg is the stance leg and the left leg is the swing leg [26].

The basic gait pattern in Figure 2.2-1 defines terminology for the process of putting one leg in front of the other. More detail is added to this framework via accompanying motions called the elements of gait [26]: these elements are motions that are progressively added to the 'compass model' of gait in Figure 2.2-2 to better approximate human walking. A compass model has a pelvis in a fixed-orientation and two straight legs so that the pelvis travels through a trajectory of intersecting arcs with radius equal to the leg length [26]. Each element of gait added to this model reduces the vertical excursion of the pelvis, and so together they minimize the energy expenditure against gravity.

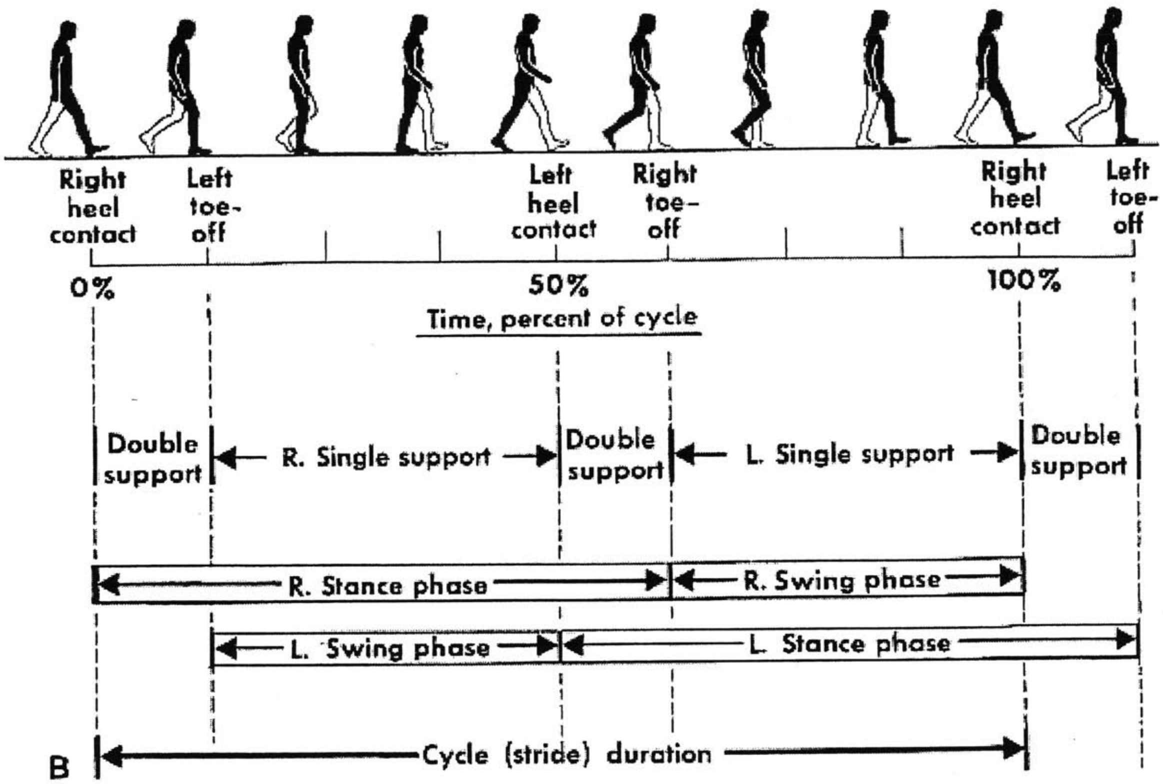

Figure 2.2-1: Time dimensions of walking cycle [26]

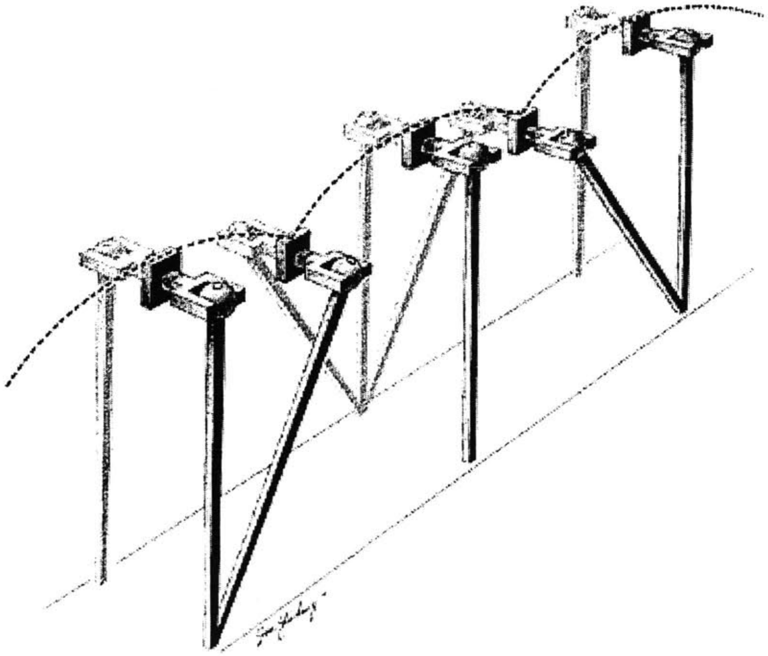

Figure 2.2-2: Compass model of gait [26]

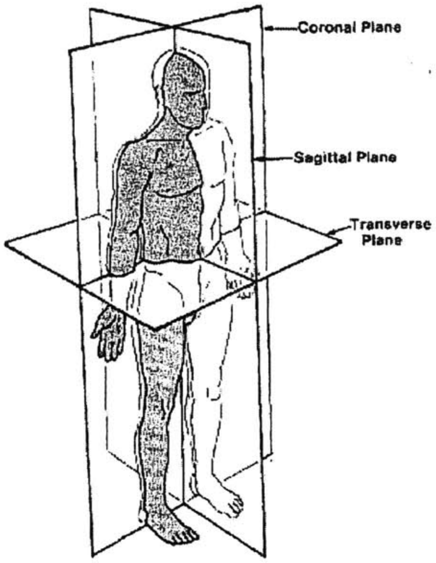

Figure 2.2-3: Clinical terms for the planes of the human body [26]

Before describing the elements of gait it is necessary to define the terminology in Figure 2.2-3. The three planes of the body are labeled according to their clinical designation: the transverse plane cuts the body horizontally, the coronal plane cuts the body vertically from left to right and the sagittal plane cuts the body vertically from front to rear [26]. These planes will be used throughout this thesis to refer to an orientation relative to the human body.

The first element of gait is a transverse rotation of the pelvis that increases the step length. Next, the pelvis rotates in the coronal plane so that the swing side hip is lower than the stance side hip; this is the second element of gait. The third element is stance-side knee flexion, which further reduces the maximum height of the center of gravity. The first three elements combine to make the center of mass, located on the pelvis, pass through a trajectory of intersecting arcs with radii equal to 2.2 times the length of the legs [26].

The fourth and fifth elements of gait are foot and ankle functions that smooth the trajectory of the pelvis from a "series of interconnected arcs into a sinusoidal path" [26] as shown in Figure 2.2-4. The mere presence of a foot reduces the vertical excursion of the knee; adding ankle muscle activation slows the downward acceleration of the body's center of gravity after heel strike and smoothes the transition to upward acceleration [26].

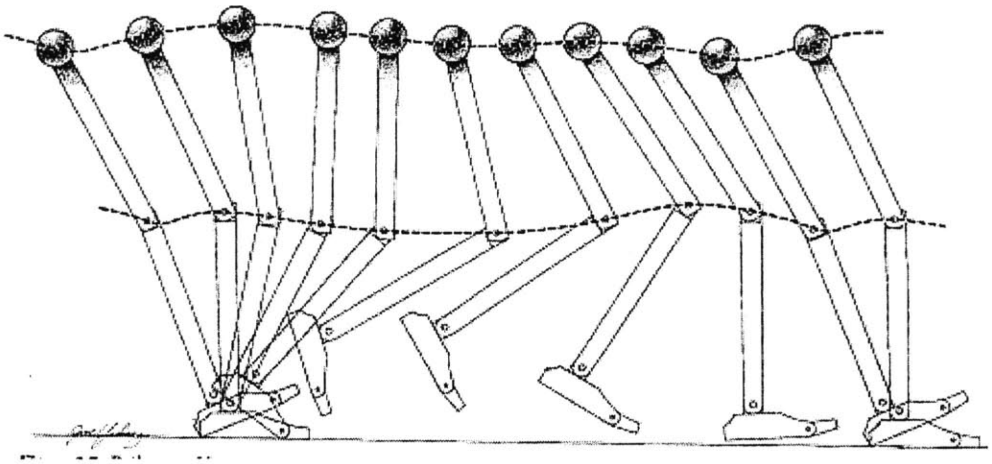

Figure 2.2-4: Pathway of knee and hip during gait [26]

The sixth and final element of gait is the lateral displacement of the body; this motion is reduced with the introduction of a coronal angle between the shin and the thigh. In other words, when the shins are placed vertically the knees are closer to the body's centerline than are the hips [26].

2.2.2 Gait impairments due to stroke

Stroke causes physiological as well as neurological changes in the body. Umphred writes, "the primary impairments of stroke that relate to functional recovery of movement include changes in strength, changes in muscle tone, muscle activation or control changes (sequencing, firing, initiation), and changes in sensation" [69]. One study estimated a decrease in strength of 50% at the ankle plantar flexors and 20% at the hip flexors [40]. These physical changes result in abnormal gait patterns. Some patients have decreased muscle activation on the affected side and need compensatory strategies to maintain balance. Others have increased and/or inappropriate muscle activation that disrupts the sequence of gait movements [69].

Two common strategies to compensate reduced activation in the knee flexors and ankle plantar flexors are hip hiking and circumduction. A hip hike occurs when the patient raises the swing hip, causing an increase in thigh coronal angle relative to normal gait [29]. In circumduction the patient swings the leg in an arc away from his or her body to create an increase in thigh coronal angle with respect to the vertical axis [29]. Inappropriate activation of the ankle plantar flexors early in the gait cycle is another abnormal gait pattern. Instead of creating push-off forces the plantar flexors rotate the shin backwards and lock the knee in hyperextension [69].

2.2.3 Differences between overground and treadmill gait

Analysis of treadmill and overground walking shows that the two cases are equivalent for a constant belt speed [70]. However, kinematic [63] and kinetic [77] differences have been reported between the two conditions. One study comparing overground gait to treadmill gait found that at the same gait speed, subjects increased their step frequency and decreased their stride length while walking on a treadmill relative to walking on the ground [63]. The same study also observed changes in balance-related stance parameters while treadmill walking, including wider stance and increased outward rotation of the feet [63]. Another study found that while the ground reaction forces in treadmill and overground walking shared similar time histories, treadmill gait generated larger mid-stance forces and smaller push-off forces than overground gait [77]. The latter study also reported treadmill belt speed variations of about +/- 4% [77].

While the second study measured belt speed it did not compare those results with the ground reaction forces [77]. The author suggests that push-off forces impart energy to the belt and increase its speed, thereby altering the force generated by the subject at that stage of gait [77]. Another interesting observation is that "the shortest subjects (height <1.65 m) tended to have the greatest change in force magnitudes in late-stance for the fastest walking speed." [77]. No hypothesis or conjecture is offered to explain this effect. Perhaps a short subject can take long steps relative to leg length; increases in leg angle at heel strike and toe-off could increase the amount of force the subject applies to the treadmill in the frontal direction.

The difference between treadmill and overground walking can also be due to differences in sensory inputs. To isolate the effect of visual input on treadmill walking, a dome-shaped device was placed in front of subjects as they walked on a self-pacing treadmill. This device projected an "optic flow pattern ... chosen to elicit the illusion of viewing a tunnel or a corridor" [48]; the effect of visual input was measured as the change in the subjects' self-selected walking pace. The study concluded that visual inputs have a significant effect on self-selected walking speed.

Therefore, to provide the same walking condition on a treadmill as on the ground it is necessary to both maintain a constant belt speed and to provide visual simulation of forward progress. For a hemiparetic patient, the small differences in gait described above might not be significant in the presence of gait impairments. In fact, treadmill walking produces a more symmetric, less variable gait pattern in stroke patients relative to walking overground [20, 22]. However, these changes could be a result of the treadmill belt forcing the patient to maintain a constant walking speed; no evidence exists to prove or disprove the possibility.

2.2.4 Central pattern generator

Studies point to the existence of a central pattern generator responsible for the gross muscle activation pattern of gait. A patient with a complete spinal cord lesion was placed on a treadmill while a harness supported 75% of his body weight. While no voluntary motion of the lower limbs was possible, the patient still showed muscle activation while a therapist guided the legs through a gait pattern [16]. A patient who suffered from an incomplete spinal cord injury began the study unable to walk but was able to take 20-30 unsupported steps after four months of therapy. However, the patient was not able to increase the voluntary force output of the lower limbs [16].

Activation patterns of the hip abductor and adductor muscles in hemiparetic patients also suggest the existence of a central pattern generator [31]. These muscles control the coronal thigh angle relative to the pelvis. They stabilize posture in the presence of lateral forces and they maintain a level pelvis during the single support phase of gait. While hemiparetic subjects were not able to properly activate the hip abductor and adductor muscles in the presence of a lateral postural disturbance, the same muscles showed a relatively normal activation pattern when taking a step [31].

The existence of a central pattern generator has strong implications for gait rehabilitation following stroke. Instead of rebuilding neural pathways from the brain to each muscle used in gait, therapists can instead try to reconnect the brain to the pattern generator.

2.3 Gait therapy

Therapy following stroke is highly recommended as a means to recover lost function [27]. The ability to relearn gait seems to be helped by the existence of the central pattern generator [31], given that 82% of stroke patients relearn how to walk while only 40-70% of patients regain arm function [69]. Until recently, physiotherapy was the only available gait therapy. However, studies in body-weight supported treadmill training have arguably shown it to be superior to standard physiotherapy, and robotic gait trainers have been developed to capitalize on the benefits of treadmill training while reducing the therapist's time and effort required for the treatment.

2.3.1 Physiotherapy

The theory behind physiotherapy states that before a patient practices to walk, he or she must demonstrate the functional ability for stance and swing. A patient is ready for the stance phase of walking when he or she is able to stand on the affected leg without either a cane or a walker and without hyper-extending the knee. The patient is ready for the swing phase of walking if he or she can take a step forward with the affected leg without making abnormal trunk movements [15]. If the therapist begins to walk with a patient before these abilities are achieved then there is a risk of developing compensatory gait patterns that will be difficult for the patient to correct. Within these constraints, however, the patients should be made to walk as soon as possible [15].

Unlike treadmill therapy, physiotherapy does not consist of a single gait pattern. Rather, it is a collection of interventions designed to address specific gait impairments including hyperextension of the knee during stance, unstable thoracic spine, and inadequate arm motions [15]. As an example of these techniques, the method for walking with a patient to prevent the affected knee from hyperextending is described here.

The therapist stands beside the patient, places the affected side hand on the patient's side, and uses the thumb to push on the head of the femur. The other hand is placed at the patient's unaffected side. During the swing phase of the affected limb, the therapist pushes down to prevent hip hiking and rotates the pelvis forwards. Immediately after heel strike on the affected foot the therapist guides the affected side hip over that foot and prevents the hip from moving backwards, thus preventing the knee from locking. During the rest of the affected side stance phase the therapist aids in lateral weight shift and in hip extension [15].

2.3.2 Treadmill training

Treadmill training is gait therapy using a treadmill. The techniques used for treadmill training vary both in the number of therapists employed and the type of device, if any, used to provide partial body-weight support to the patient as he or she walks. The most common form of treadmill training uses two therapists and a body-weight support device, as shown in Figure 2.3-1. One therapist sits on the paretic side of the treadmill and guides the knee and ankle through gait motions. The other therapist stands behind the patient and facilitates the lateral weight shift required for stepping [72]. In some cases a third therapist guides the unaffected knee and ankle.

There are also a variety of methods in use to supply body-weight support forces. While it is generally accepted that BWS forces should not surpass 40% and that they should be decreased as soon as possible [79], some research groups use rigid cables to provide support while others use soft springs. A testing device to determine the effects of vertical compliance on gait has been constructed [8] but results are not yet available.

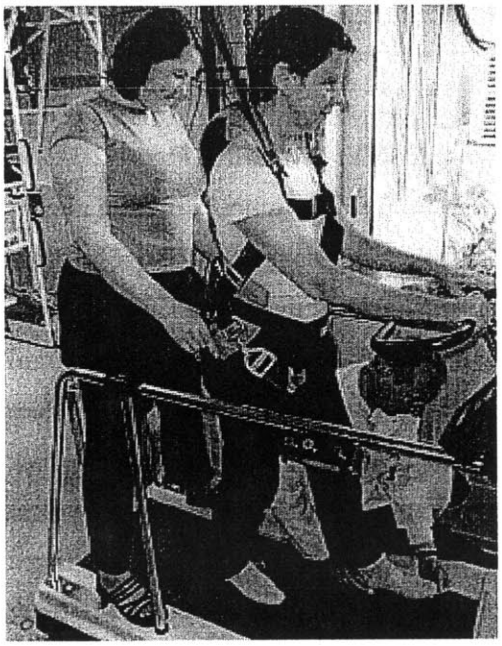

Figure 2.3-1: Treadmill training with two therapists [75]

Novel treadmill-training protocols have been tested to target recovery in specific functions. Using principles of sport physiology, one research group almost tripled the maximum overground speed reached by a group of mildly affected stroke patients [47]. The training regimen included bursts at maximum speed followed by periods of recovery at a slower pace. Another variation on treadmill therapy targeted the cardiovascular fitness of stroke patients [35]. In this protocol patients walked three times a week in low-intensity aerobic workouts while receiving no body-weight support. As a result of the intervention the patients reduced their energy expended in walking at a linear rate for the six-month duration of the intervention.

Treadmill therapy is effective, especially in the training of very impaired subjects who would otherwise be unable to practice walking [32]. Still, therapists cannot sustain the effort required to facilitate leg motion for more than fifteen minutes at a time [9]. In addition, fitting the patient with a body-weight support harness can be challenging and can take a significant amount of time.

2.3.3 Robotic gait trainers and rehabilitation devices

Treadmill training is repetitive yet intense. Thus, that type of rehabilitation is a perfect application for robotic devices: by using machines to provide the high forces and repetitive motions necessary for gait training, these robotic trainers allow therapists to concentrate on providing better overall care rather than focusing on gait alone. Two gait trainers are currently in use: the Mechanized Gait Trainer and the LOKOMAT.

The Mechanized Gait Trainer (MGT) is shown in Figure 2.3-2. This single-degree-of-freedom device consists of two footplates that follow an elliptical path and a body-weight support harness that moves vertically and laterally to shift the center of gravity [23]. Motion of the pelvis in the vertical direction follows a 2 cm amplitude sinusoid and that in the lateral direction follows a 4 cm sinusoid [23]. The trainer can attain step rates of up to 140 steps per minute, which translates to 1.12 m/s when coupled with the 0.95 m stride length [23]. The principal advantage of this device is its relative simplicity: gait motions are generated using only a single actuator. However, the drawback to this approach is that some patients preferred standard treadmill training because they did not think the footplate movement was realistic [75]. Still, the MGT allows the training of even severely impaired patients with only one therapist to oversee the process. In addition, many patients preferred the MGT to the treadmill training because it was less demanding and required less manipulation from the therapists [75].

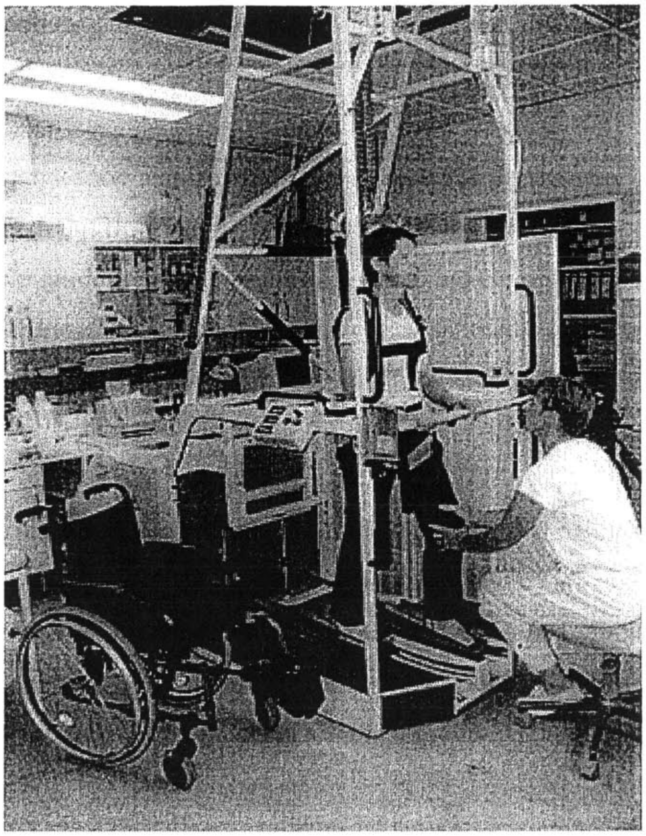

Figure 2.3-2: Mechanized Gait Trainer in use [75]

The makers of the Mechanized Gait Trainer are designing a more advanced version dubbed the Robotized Gait Trainer (RGT) [50]. A preliminary model of the RGT is shown in Figure 2.3-3. The new model will continue to simulate gait by moving the feet while they are attached to footplates. Unlike the previous design, however, the robotized version has footplates that can each move in three degrees of freedom: the vertical and frontal translations as well as a rotation about the horizontal axis [51]. The RGT is meant to be highly dynamic and backdrivable; specifications for the foot plates include a maximum linear acceleration of 3.22 g and a maximum angular acceleration of 7450 degrees/sec^2 to achieve a maximum gait speed of 1.4 m/s [50] and to simulate stumbling and walking over rough ground. The footplates must support a patient weighing up to 100 kg.

Colombo et al. designed the LOKOMAT driven-gait orthosis shown in Figure 2.3-4 [9]. This design has ball-screw-driven hip and knee flexors, passive ankle lifters, and an air spring-supported vertical degree of freedom [10]. No motion out of the sagittal plane is allowed by the mechanism. The ball-screw actuators produce 50 N-m and 30 N-m of continuous torques about the hip and knee joints, respectively, and about five times that amount of torque is available under peak conditions [9]. These output torques allow the LOKOMAT to train gait at up to 0.83 m/s with cadence up to 90 steps per minute [9].

Prior to use, the device must be adjusted in eight dimensions; once a patient has completed the set-up it can be recorded and duplicated quickly in future sessions [9]. If the machine's joints are not properly aligned with the subject's joints the device can cause painful rubbing on the skin. This problem can arise both due to improper adjustment at set-up and due to the orthosis shifting relative to the patient as the patient walks. An improved harness was proposed to maintain the position of the device relative to the subject and prevent this problem [9].

The gait pattern must also be programmed into the machine. At first the program was based on published data, but the foot clearance was inadequate so the machine was reprogrammed by removing the drive systems and measuring the gait of healthy subjects as they walked in the device [9]. To further increase foot clearance, the healthy subjects walked over 3 cm obstacles. This additional foot clearance was needed because many degrees of freedom were not actuated or allowed to move by the trainer [9].

As with the Mechanized Gait Trainer, the LOKOMAT allows the training of gait with only one therapist to set up the machine and to oversee the therapy. While the design of the two gait trainers is different the result is the same: repeatable gait therapy that can last up to 60 minutes without requiring intense effort from one or more therapists.

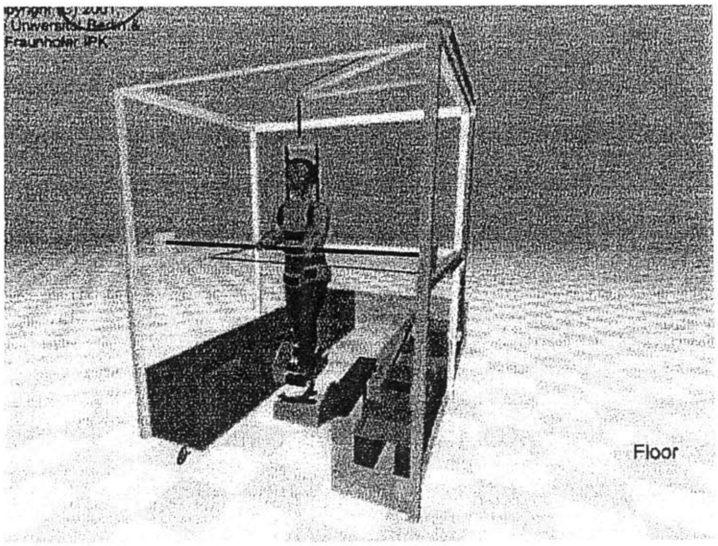

Figure 2.3-3: Robotized Gait Trainer [51]

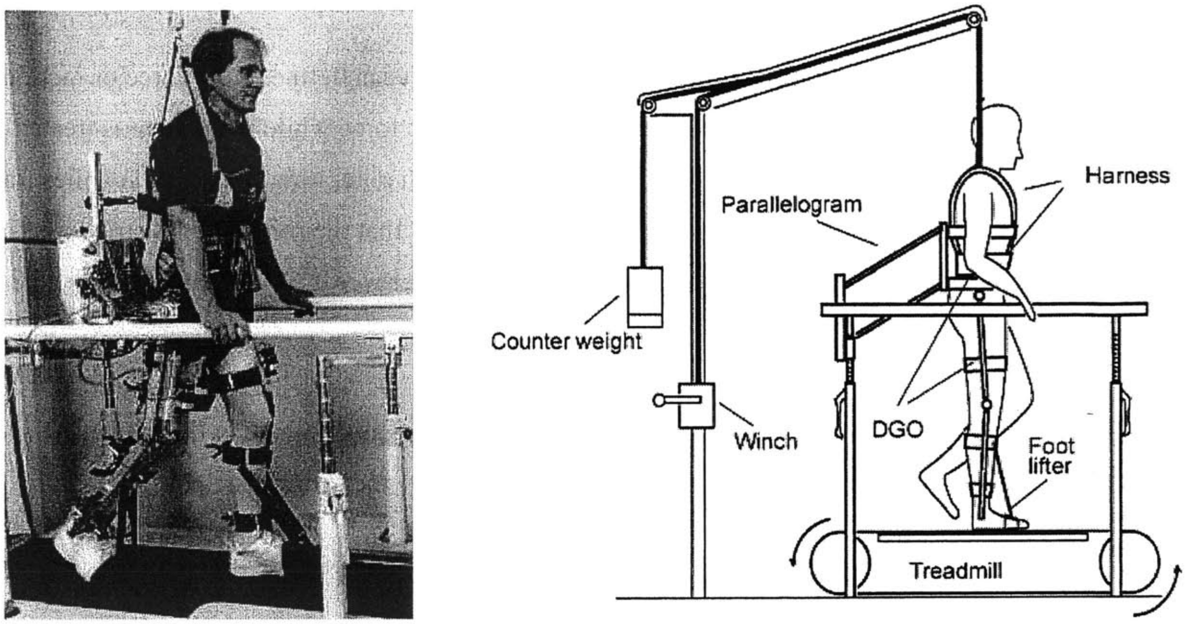

Figure 2.3-4: LOKOMAT driven gait orthosis [9]

2.4 Impedance control

Most industrial robots, i.e. welding robots, are position-controlled devices: the user is interested in the endpoint position and the mechanical design and control is intended to reduce the error resulting from position disturbances. Other robots have relied on force control, in which a force is specified but position is ignored. Neither approach is suitable for stroke rehabilitation because of the nature of the interaction: the robot must apply forces to the patient depending on the motion that the patient generates. In other words, the robot must be impedance-controlled [24].

Impedance is the relationship between motion and force. Linear impedance is called stiffness when it represents a force-position relationship, damping when it represents a force-velocity relationship, and inertia when it represents a force-acceleration relationship. General impedance can be one of the above linear forms with positive or negative force constant, or it can be in a general non-linear form. In rehabilitation, a common way to apply impedance control is to specify a 'target trajectory' and then have the robot provide a spring-damper system about that trajectory. Using this control strategy, the patient receives no help from the robot if he or she can move along the trajectory, but if the patient cannot properly aim or lags behind the robot the robot assists motion with the necessary force. Larger deviations from the target generate larger robot forces due to the stiffness term.

Causality limitations stipulate that each port in an interaction can define either force or motion. For rehabilitation, the robot is defined as an impedance that provides force while the patient is treated as an admittance that moves in response to the force. This point is worth reiterating: the robot supplies force, the patient moves in response. Mechanically, this relationship means that the robot cannot strictly define the position of its endpoint so the robot must be backdrivable. In other words, the patient must be able to move the robot endpoint [24].

Backdrivability has been the defining principle behind the robots designed at the Newman Laboratory for Biomechanics. This robot for gait rehabilitation shares the same principle.

Chapter 3: Functional Requirements and Target Specifications

This chapter divides the need for a new gait therapy robot into components called functional requirements and then derives corresponding target specifications that the new machine must attain.

3.1 Functional requirements

This thesis describes the design of a robot for impedance-controlled gait rehabilitation through the facilitation of the pelvis. The robot was conceived to help a person walk, to improve standing balance, and to practice stepping onto a platform. These top-level goals are separated into functional requirements that the robot must fulfill, including backdrivability, facilitation of the pelvis, partial body-weight support, forward propulsion, patient connection, and fall prevention. The robot must also satisfy implicit functional requirements. The functional requirements are summarized in Table 3.1-1 and are discussed in detail below.

Backdrivability is the key to the purpose of this robot. Like the MANUS family of upper-body rehabilitation tools developed at the Newman Laboratory [34, 4, 5], the gait trainer must be able to interact stably with the environment at all times. Instead of practicing voluntary point-to-point movements [34], however, the new robot is allowing the patient to train gait.

The backdrivability requirement applies to every degree of freedom in the body. Therefore, the combination of actuation, mechanism, and attachment to the patient must have low endpoint impedance in the actuated direction(s) without constraining motion in non-actuated direction(s). Endpoint impedance includes damping and inertia as well as non-linear qualities like backlash, cogging, and static friction. The impedance of the robot affects stability and feel; in general, smooth and consistent impedances (e.g. linear damping) feel good and promote stability while unpredictable or variable impedances like backlash feel poor and limit stability.

Table 3.1-1: Functional requirements

▪ Backdrivability
▪ Facilitate pelvis motions
1. Vertical
2. Lateral
3. Frontal
4. Transverse rotation
5. Coronal rotation
6. Sagittal rotation
▪ Partial body-weight support
▪ Forward propulsion
▪ Patient connection
▪ Fall prevention
▪ Implicit functional requirements
o Ease of manufacturing, assembly, and maintenance
o Aesthetically pleasing
o Safe at all times

The second functional requirement is that the robot must facilitate motion of the pelvis. Facilitation is the act of applying forces to the body during walking to improve gait. The pelvis is chosen for this module because, while both physiotherapy and treadmill therapies facilitate pelvic motions, the currently available robotic gait trainers do not. In addition, the module that actuates the pelvis will be the starting point for a new family of modular robots akin to the upper extremity MANUS designs. Additional robots for the knee and ankle would combine with the pelvis robot to provide total gait therapy.

Which pelvis degrees of freedom (DOFs) should the robot actuate? The six pelvis DOFs are listed below in order from highest to lowest actuating priority. The final number of actuated degrees of freedom will be determined by the choice of concept used to actuate the pelvis.

The highest priority pelvic degree of freedom is vertical translation. In treadmill training, vertical forces are called body-weight support (BWS) forces. Studies show that treadmill training of stroke patients using BWS is more effective than treadmill training with no BWS [72]. By supporting part of the patient's weight this machine would reduce the amount of muscle function required to walk, making it possible for a patient to begin walking sooner. Vertical robot forces could also help the patient transfer energy between gravitational potential and kinetic forms [26, 17] to make his or her gait more energy-efficient.

The second-highest priority pelvic degree of freedom is lateral translation. This motion represents the weight shift towards the stance leg that allows the swing leg to be lifted. Asymmetric deficiencies due to stroke cause patients to have difficulty balancing on their paretic limb. Facilitation of lateral weight shift is included in both treadmill-based therapy and conventional physiotherapy for stroke patients [15, 72]. Actuation of this degree of freedom would also allow standing balance exercises [36, 30].

The third-ranked pelvis degree of freedom is frontal translation relative to average forward displacement. Average forward displacement is discussed below as a separate functional requirement. Frontal forces could improve gait symmetry [17, 22] and gait speed [47] as in treadmill training, or they could alter treadmill gait to reduce belt speed fluctuations and to make treadmill walking more like overground walking [70]. Combined frontal and vertical forces could be used to modulate the energy transfer between kinetic and gravitational potential forms during gait. Frontal and lateral forces would allow omni-directional postural disturbances to train balance reactions while standing or walking [36, 30].

The fourth-ranked pelvis degree of freedom is transverse rotation. This motion occurs when the hips move frontally relative to each other. A computer simulation of walking shows that actuating this movement allows some control of the swing leg without using the hip- or knee-joint muscles [73]. Combined frontal force and transverse torque could also prevent knee hyperextension associated with improperly timed calf muscle activation in stroke patients [15]. Conversely, transverse rotation can never be actuated without also actuating the frontal translation because if rearward forces are created at the stance hip they could cause knee hyperextension.

The fifth-ranked pelvis degree of freedom is coronal rotation. This motion occurs when one hip rises relative to the other. Some stroke patients produce abnormal coronal rotations while walking to increase ground clearance for paretic leg swing [29]. This 'hip hike' is thought to originate from lack of muscle activation at the ankle and knee and not from problems at the hip. Physiotherapists combat the problem by pushing down on the affected side hip during swing [15], but a robot that mimics this action risks tripping the patient if the patient fails to compensate for the reduced ground clearance during the paretic side swing phase.

The sixth-ranked pelvis degree of freedom is sagittal rotation, or rotation of the pelvis about the axis that connects the hips. This motion is not among the elements of gait defined in [26] and no reason to actuate it has been found in the literature.

To summarize, the pelvis has six degrees of freedom but not all of them must be actuated. In deciding which DOFs are actuated priority is given first to the vertical translation followed by lateral translation, frontal translation, transverse rotation, coronal rotation, and sagittal rotation. The pelvis must maintain its natural range of motion in all six directions to comply with the backdrivability requirement.

The next functional requirement is to provide partial body-weight support to the patient. The effects of variations in BWS during the gait cycle have not been studied [79]. However, the body-weight support system should be selected such that variations in force due to inertia, stiffness, and friction are minimized. That way, an actuator can be used to add and adjust any desired force modulations.

The fourth functional requirement is to move forward; this is the task the patient performs during therapy. Forward propulsion is considered the average forward velocity of the person as he or she walks.

The fifth functional requirement is to connect the patient to the machine in a safe, stiff, and comfortable way. The attachment should fit the majority of patients and should be quick to don and doff. Wilson suggests that a harness support the buttocks, thighs, and ribcage while allowing free movement of arms and legs [79].

The final explicit functional requirement is that the gait trainer must prevent falls. This gait robot produces large forces that can destabilize a person. Should the patient fall he or she could strike the machine and suffer serious injury. Even a study using low intensity treadmill exercise with stroke outpatients used a safety harness to prevent falls [35]. A fall support system also increases confidence and imparts a sense of safety in both the patient and the therapist.

Besides satisfying the above explicit functional requirements, the gait robot must also be easy to use; easy to manufacture, assemble, and maintain; aesthetically pleasing; and safe at all times. These traits are called implicit functional requirements because they apply to the whole machine instead of to a module or component.

3.2 Target specifications

The specifications are the quantitative targets a device must reach to satisfy the functional requirements. The gait therapy robot must meet specifications related to anthropometrical data, overground use, endpoint impedance, output force, and other areas.

3.2.1 Anthropometrical data and related specifications

Using anthropometrical data to design a machine ensures that the machine will be compatible with a large percentage of the population. For this gait trainer, the important anthropometrical data include relevant dimensions of humans, the range of motion of the pelvis during gait, the machine workspace derived from these ranges of motion, and the required clearance behind the patient leg.

Human dimensions used in this design are shown in Table 3.2-1. These measurements include the height and weight, waist height and width, crotch height, hip width, and foot length. Figure 3.2-1 shows the locations of some measurements on the human body. The minimum value for each measurement in Table 3.2-1 corresponds to the smallest 1% of women and the maximum value corresponds to largest 1% of men [67]. Maximum weight, however, is based on the 160 kg load rating of the *Litegait* body-weight support system [37].

The amplitude of pelvis motion during gait in each of its six degrees of freedom is shown in Table 3.2-2. From the point of view of the person, fore/aft is movement forwards and backwards, lateral translation is left-to-right, and vertical translation is up and down. The rotations of the pelvis are named by the planes in which they occur (see Figure 2.2-3). Transverse rotation occurs about the vertical axis, sagittal rotation occurs about a lateral axis, and coronal rotation occurs about a fore/aft axis.

The amplitudes of pelvic motions during gait are used to size the minimum workspace of the machine as shown in Table 3.2-3. The fore/aft workspace is sized for the step-up task. When the patient steps onto the platform, he moves forward one length of his shoe; the largest expected shoe is 331 mm [67]. The pelvis moves an additional 60 mm fore/aft from Table 3.2-2. Fore/aft workspace is the sum of these motions, which is rounded to 400 mm. The vertical workspace is also sized for the step-up task. A standard step is 180 mm [57] tall, and the maximum expected vertical deviation of the pelvis is 90 mm [26]. An extra 30 mm of clearance is added, resulting in a 300 mm vertical workspace.

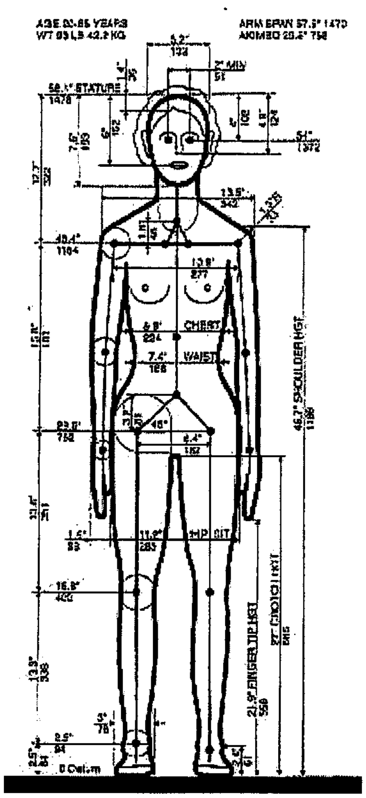

Figure 3.2-1: Measurements of humans [67]

Table 3.2-1: Relevant dimensions of humans

Parameter	Min	Max	Units	Source
Weight	42.2	160	*kg*	67, 39
Overall height	1476	1920	*mm*	67
Hip height	753	1018	*mm*	67
Hip width	158	198	*mm*	67
Waist width	285	464	*mm*	67
Crotch height	686	914	*mm*	67
Shoulder width	342	523	*mm*	67
Stride width	30	60	*mm*	67, 58
Stride length	1229	1664	*mm*	67, 79
Foot length	210	298	*mm*	67

Table 3.2-2: Amplitude of pelvic motions

Degree of Freedom	Max	Units	Source
Fore/Aft deviation from average	30	*mm*	26
Lateral Translation	80	*mm*	58, 26
Vertical Translation	45	*mm*	26
Transverse Rotation	25	*degrees*	26
Sagittal Rotation	4	*degrees*	26
Coronal Rotation	5	*degrees*	26

Table 3.2-3: Workspace size

Degree of Freedom	W.S. Size	Units	Source
Fore/aft workspace	400	*mm*	67, 26
Lateral workspace	200	*mm*	58
Vertical workspace	300	*mm*	26, 57
Transverse rotation workspace	± 25	*degrees*	26
Sagittal rotation workspace	± 4	*degrees*	26
Coronal rotation workspace	± 5	*degrees*	26
Hip height adjustment	753-1018	*mm*	67

The lateral workspace consists of the 160 mm of expected motion from Table 3.2-2 plus 40 mm for clearance and to allow variation during walking and deviation from a straight path. Thus, the total lateral workspace is 200 mm. For the three rotational degrees of freedom, the machine workspace in Table 3.2-3 is equal to the maximum expected pelvic motions from Table 3.2-2.

A hip height adjustment dimension is also shown in Table 3.2-3. It represents the robot's ability to adjust so that the center of the vertical workspace is at the proper height relative to the patient. The presence of this adjustment reduces the size of vertical workspace required.

The robot should allow the patient to extend the hip by up to 20 degrees [28]. In addition, the robot should not interfere with knee flexion and so should not have components below the knee height. Table 3.2-4 shows anthropometric data related to thigh length and hip height. As shown in Figure 3.2-2, the minimum clearance behind the patient is

3.2-1 $$351mm \cdot \tan(20°) = 128mm$$

The shortest thigh length is used for the calculation because the robot will not extend down below the shortest thigh; a longer thigh would extend below the robot under full extension.

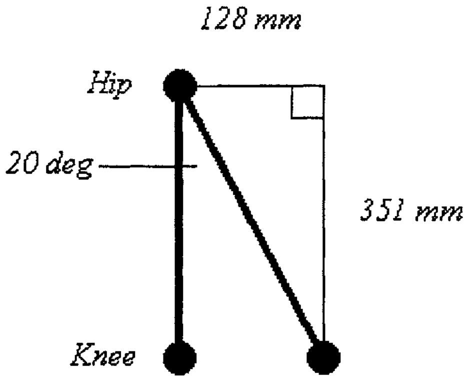

Figure 3.2-2: Clearance required behind patient

Table 3.2-4: Dimensions relevant to leg clearance

Dimension	Value	Units	Source
Maximum hip extension	20	*degrees*	28
Hip height	753-1018	*mm*	67
Knee height	402 - 551	*mm*	67
Hip-to-knee distance	351 - 467	*mm*	67
Minimum horizontal clearance	128	*mm*	

3.2.2 Overground use specifications

The functional requirements of the gait trainer dictate that the machine must be able to move overground. Such a machine must conform to specifications that dictate its overall size, the speed and acceleration that it can achieve overground, and its ability to navigate obstacles it may encounter.

The overground-mobile machine must be sized such that it can operate in a building that meets the accessibility section of the building code. Two levels of accessibility are specified for this machine.

Universal accessibility specifications would allow the robot to reach any wheelchair-accessible areas. Hospital accessibility specifications limit the gait trainer to use within a hospital. Maximum overall machine dimensions are shown in Table 3.2-5. These dimensions are the overall length, width, and height of the machine as well as its turning diameter and weight. The robot described in this thesis is designed to meet hospital accessibility specifications.

The robot must be able to move fast enough to accommodate the fastest expected stroke therapy. The fastest population of stroke patients in the literature is in a study by Pohl, which specifically aimed to increase patient speed by training at short bursts of maximal speed [47]. Pohl's treatment group reached average maximum walking speeds of 1.63 +/- 0.8 m/s, or 3.65 +/- 1.8 mph. Corresponding values for step rate are 128.8 +/- 30.1 steps per minute, or 2.15 +/- 0.50 steps per second. Therefore, the gait trainer must be able to achieve this speed, as shown in Table 3.2-6. A minimum speed of 0.083 m/s is also necessary, as is the ability to change speeds at 0.042 m/s increments [79].

Table 3.2-5: Limits on machine overall dimensions

Parameter	**Hospital**	**Universal**	***Units***	**Source**
Max. Height	80	80	*in*	57
Max. Width	44	32	*in*	57, 61
Max. Length	60	48	*in*	57
Min. Turning Diameter	72	60	*in*	57
Max. Weight	1000	500	*lbs.*	57

Table 3.2-6: Speed and acceleration

Parameter	**Max**	**Units**	**Source**
Overground speed	1.63	*m/s*	47
Treadmill speed	1.63	*m/s*	47
Step rate	2.15	*steps/sec*	47
Speed increment	0.042	*m/s*	79
Minimum speed	0.083	*m/s*	79
Overground acceleration	0.09	*g*	33

The required acceleration shown in Table 3.2-6 is calculated by assuming that the patient accelerates from rest to walking at half the maximum speed in one step. Thus, he or she will reach 0.82 m/s in the time required to take one step, or 0.93 seconds. These values are calculated using the maximum speed and step rate from Table 3.2-6. The resulting average acceleration a is

3.2-2 $$a = \frac{v}{t} = \frac{0.82 m/s}{0.93 s} = 0.88 m/s^2 = 0.09 g$$

where v is the velocity achieved, t is the time elapsed, and g is the acceleration of gravity, 9.81 m/s^2. The distance d covered in this time is

3.2-3 $$d = \tfrac{1}{2} a t^2 = 0.5 \cdot 0.88 m/s^2 \cdot 0.86 s^2 = 0.38 m$$

So, the gait trainer should be able to accelerate from a standing start at 0.09g or be able to reach 0.82 m/s in 0.38 m. For comparison, the average maximum acceleration of 10 elite athletes ages 19-25 is 0.35 g [33].

The building code permits certain minor obstacles to be included in wheel chair-accessible buildings. The gait trainer must be able to navigate these obstacles, which include [57]

- Vertical Step: The machine must be able to cross the maximum allowable steps of 1/4" vertical and 1/2" of 50% slope.
- Floor Slope: The machine must be able to navigate the maximum allowable floor slope of 1 in 48, and should be able to navigate the slope of ramps at 5%.
- Gratings: The machine must be able to navigate over allowable gratings of maximum .5" spacing along the direction of travel.
- Protrusions: The machine should not endanger the patient when encountering allowable protrusions of 4" when the leading edge is more than 27" above the floor, and 12" when the leading edge is less than 27" above the floor.

In addition to allowing the inclusion of the above obstacles in a building, the building code also stipulates that floor surfaces must have a coefficient of friction > 0.5 and must be "stable and firm" [57].

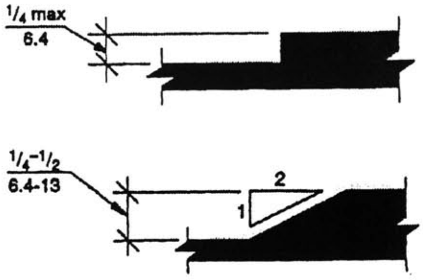

Figure 3.2-3: Vertical step allowable per the building code [57]

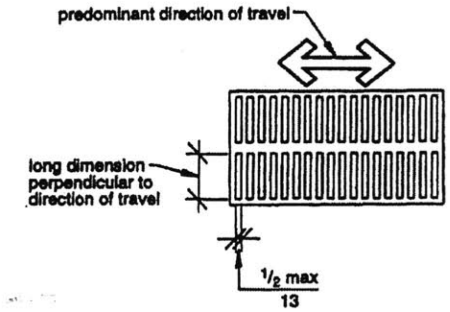

Figure 3.2-4: Gratings allowable per the building code [57]

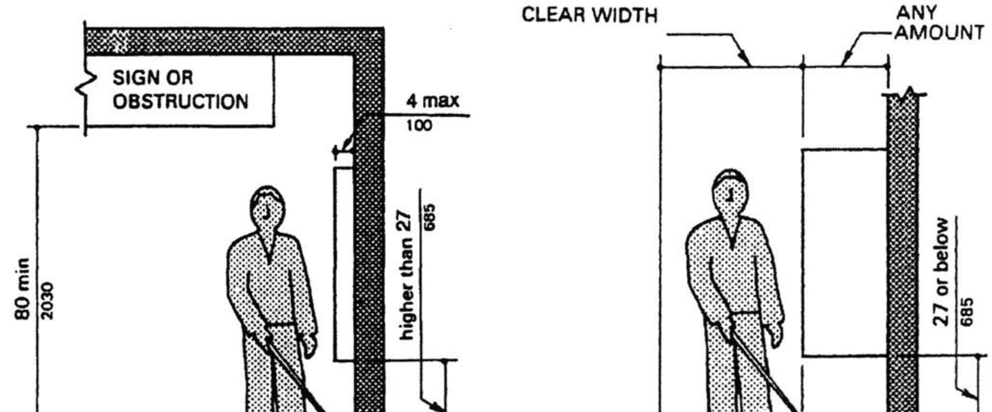

Figure 3.2-5: Protrusions allowable per the building code [57]

3.2.3 Endpoint impedance specifications

The endpoint impedance of the robot is the relation between the motion at the endpoint and the force produced in the machine. The functional requirements stipulate that the gait trainer must be backdrivable. Therefore, the forces produced at the endpoint as a result of endpoint motions must be low enough that they do not affect the gait of the patient. Endpoint impedance is divided into four parts: inertia, static friction, viscous friction, and stiffness.

Previous work in rehabilitation robotics suggests that the inertia of the robot should be less than the inertia of the body for each actuated degree of freedom [6, 78]. The inertia limit for the pelvis robot is thus the inertia of the human along the pelvis degrees of freedom.

A NASA publication presents regression equations to find the mass of a portion of the body based on the total body weight [59]. Other regression equations tailored for older adults were published in a paper by Pavol et al, but those equations require specific body dimensions that are not available so the equations are not applicable [46]. The pertinent equations in the former source are

3.2-4 $$W_{head,neck,torso} = 0.5940 \cdot TBW - 2.20$$

3.2-5 $$W_{torso} = 0.50 \cdot TBW$$

3.2-6 $$W_{thorax} = 0.438 \cdot W_{torso}$$

3.2-7 $$W_{lumbar} = 0.294 \cdot W_{torso}$$

3.2-8 $$W_{pelvis} = 0.268 \cdot W_{torso}$$

where W_x is the weight of body segment x and TBW is the total body weight in kilograms. The thorax is the portion of the torso about the ribcage, and the lumbar is the lower back between the ribcage and pelvis.

The sum of the inertias for the head, neck and torso is a reasonable estimate for vertical body inertia because all three segments move in unison as the person moves vertically. Lateral and frontal inertia can be estimated by summing only the pelvis and lumber inertias because a person may thrust the pelvis in these directions while keeping the ribcage and head stationary. Substituting 42.2 kg for *TBW* of a 1% female from Table 3.2-1 into equations 3.2-4 through 3.2-8 gives the following approximate human body inertias for pelvis translations:

3.2-9 $$I_{vertical} = 0.5940 \cdot 42.2 - 2.20 = 22.9kg$$

3.2-10 $$I_{planar} = 0.50 \cdot 42.2 \cdot (0.294 + 0.268) = 11.9kg$$

The moment of inertia of the body in pelvic rotation about the vertical axis is computed using the same formulas presented above. For a 5% male weighing 65.2 kg, the moment of inertia of the torso about the vertical axis is 0.34175 kg-m^2 [59]. Two further operations are required: first, the inertia must represent the inertia of the pelvis and lumbar and not the whole torso, and second, the inertia must apply to the 1% female instead of the 5% male. These changes are represented in the formula

3.2-11 $$I_{pel,lum,1\%} = I_{torso,5\%} \cdot \frac{W_{lumbar} + W_{pelvis}}{W_{torso}} \cdot \frac{TBW_{1\%}}{TBW_{5\%}}$$

3.2-12 $$I_{rotation} = 0.34175 \cdot (0.294 + 0.268) \cdot \frac{42.2}{65.2} = 0.1243kg \cdot m^2$$

where the values in equations 3.2-11 and 3.2-12 are as defined above. Table 3.2-7 summarizes the target specifications for endpoint inertia.

Table 3.2-7: Machine inertia specifications

Body Segment	Direction		Target Inertia	Source
Head, neck, and torso	Vertical	z	22.9 kg	59, 67
Pelvis and lumbar	Horizontal translation	x, y	11.9 kg	59, 67
Pelvis and lumbar	Transverse rotation	Φ	0.1243 kg-m^2	59, 67

The second component of endpoint inertia is static friction. The patient feels static friction at the robot endpoint as a force applied to his or her pelvis. A study that tested the postural stability of stroke patients in response to lateral force disturbances found that some stroke patients could not resist disturbances equal to 2% of their body weight [30]. From Table 3.2-1 the minimum expected body weight is 42.2 kg, so the maximum static friction forces felt by the patient should be no greater than 8.3 N.

Another component of endpoint impedance is viscous friction, or damping. Damping does not adversely affect the qualitative feel of a device as much as static friction. In addition, damping is linear and so it is easier to reduce through control algorithms. Therefore, no value is specified for the minimum viscous friction.

The final aspect of endpoint impedance is the achievable endpoint stiffness. Experiments show that blindfolded subjects cannot distinguish between 4150 N/m stiffness and a solid wall. Thus, this machine should have suitable resolution of both position and force to achieve that stiffness smoothly.

Table 3.2-8 summarizes the endpoint static friction, damping, and stiffness specifications.

Table 3.2-8: Endpoint friction and stiffness specifications

Parameter	Max	Units	Source
Static friction	8.3	*N*	30
Viscous friction	--	*N-s/m*	
Achievable stiffness	4150	*N/m*	64

3.2.4 Output force specifications

This gait robot is designed to interact with a stroke patient. This section describes specifications for the minimum output force that guarantees that the machine can guide the patient through therapy.

In facilitating the motion of the pelvis, the gait robot produces forces in the transverse plane. The magnitude of these forces could be estimated by measuring forces exerted by therapists during training, but the result would be limited by the strength of the therapist. Therefore, the force output of the machine is estimated from the force required to stabilize an inverted pendulum at a displacement equal to the maximum amplitude of lateral pelvic motion, as shown in Figure 3.2-6.

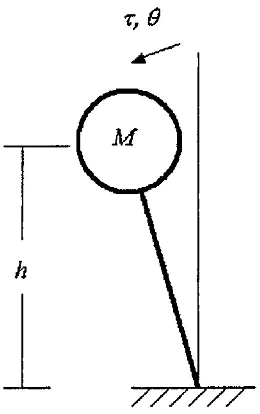

Figure 3.2-6: Inverted pendulum model used to estimate the planar force required

The inverted pendulum in question has a mass M equal to the mass of the heaviest patient and a height h equal to the shortest patient's hip height. Using the values from Table 3.2-1 yields a 753 mm long, 160 kg pendulum. The force required to stabilize such a pendulum depends on the displacement from the vertical axis A as

3.2-13
$$F = \frac{MgA}{h}$$

where g is the acceleration of gravity, $g = 9.81\ m/s^2$. From Table 3.2-2, $A = 80\ m\ m$ so the maximum planar force required of the machine is $F_{max} = 167\ N$. Stabilizing the inverted pendulum allows the robot to apply destabilizing forces safely because if the patient fails to resist these disturbances the robot can re-stabilize stance before a fall occurs.

In addition to forces in the transverse plane, the robot must also apply body-weight support (BWS) forces to the patient. Three studies examined treadmill walking with BWS up to 60% of patient weight [21, 42, 54], but one found that BWS over 40% resulted in increased oxygen cost [54] and one found that BWS above 30% reduced EMG activity in weight-bearing muscles [21]. Another study limited BWS to 40% because higher forces prevented some patients from making proper heel contact [71]. A fifth study limited BWS to 30% with no reason cited [13]. In light of these findings, the gait trainer should be capable of applying BWS forces up to 40% of the heaviest stroke patient encountered, or 160*0.40 = 64 kgf = 628 N.

The body-weight support forces should be generated with as compliant a spring as possible. Experience with the gait robot mockup (see *Chapter 5: Mockup Design and Testing)* showed that a spring with less than 700 N/m stiffness is desired. Also, the robot must be able to support the patient in case of a fall; the fall support load is the full weight of the patient multiplied by a safety factor of four, or 6280 N. The target specifications for the forces produced by the gait trainer are summarized in Table 3.2-9.

Table 3.2-9: Gait trainer force specifications

	Max	Units	Source
Planar force produced	167	*N*	67, 37, 26
Body weight support loads	628	*N*	13, 21, 42, 54, 71
BWS stiffness	700	*N/m*	Mockup
Fall support loads	6280	*N*	79, 44

3.2.5 Additional specifications

The gait trainer should ensure the safety of the patient and the operator at all times. A safety factor of four should be used for design loads because the robot will likely experience moderate shock loads throughout its life [44].

Safety systems should be included with the overground propulsion module to prevent accidents. These systems can be either mechanical or electronic but they must prevent the device from driving off a curb, hitting a wall or other obstacle, or injuring the patient in any foreseeable way. Also, the moving parts of the gait robot should have large enough spaces between them to prevent pinch points. Robot arms, gears, and linear motion elements should be covered to prevent injury to the operator and to the patient.

Therapy sessions should be at least 30 minutes long [42, 47]. All other aspects of training including the travel to and from the robot location, robot set-up, patient briefing, and ingress/egress time should take less than 30 minutes so the entire procedure can be scheduled in standard one-hour time slots. Ingress/egress time for the patient should be under 5 minutes, although a faster-release attachment is desirable in case of emergencies. The attachment to the patient should not create discomfort or reduced circulation. In addition, a fall must not cause undue pain from poorly distributed restraints.

Table 3.2-10: Other specifications

	Max	Units	Source
Safety factor	4		79, 44
Minimum pinch point	6	*mm*	Estimate
Length of therapy session	30	*minutes*	42, 47
Ingress/egress time	5	*minutes*	Estimate
Service interval	6	*months*	Estimate

Components with finite life used on the gait robot should last six months of 40 therapy-hours per week, or 1040 hours of operation, before replacement. The service interval can be adjusted depending on the difficulty and cost of replacing individual components.

A summary of the additional specifications of the gait robot is found in Table 3.2-10.

Chapter 4: Concept Selection

This chapter first generates potential concepts to fulfill the functional requirements and then evaluates the concepts in terms of their abilities to meet the specifications. Because a concept is only a general selection of approach to solving a problem, detailed calculations are not carried out in this chapter; at most, rough calculations are carried out to show if an approach would be feasible. An overall approach made up of top-level concepts is first selected for the entire machine. Then, the top-level concept for actuating the pelvis is divided into sub-modules and concepts are selected for those sub-modules.

4.1 Overall approach

The overall approach is the group of concepts that fulfill the top-level functional requirements outlined section 3.1. Concepts must be selected to provide forward motion, actuate the pelvis, generate body-weight support forces, connect the patient to the machine, and prevent falls. Other functional requirements impose conditions on the concepts; for example, the requirement that the machine be backdrivable and safe affects the choice of mechanism to actuate the pelvis.

4.1.1 Provide forward motion

The first functional requirement is that the gait trainer has to allow forward motion. One way to achieve this function is to move the machine and another is to move the ground. The latter case is more common in current practice and is implemented by using a stationary machine base combined with a treadmill as in the LOKOMAT shown in Figure 2.3-4. The former option involved making a mobile machine base to follow the patient overground as shown in Figure 4.1-1.

The principal advantage to designing a machine that works with a stationary base is the ability to use an off-the-shelf treadmill to provide forward motion, thus saving time and money that would have to be spent on a custom solution. Using a treadmill also allows gait training to take place in a small room dedicated to the robot. Furthermore, because the patient is stationary, the therapist has easy access to the patient's body to facilitate degrees of freedom not actuated by this robot. A machine with a stationary base also allows for multiple structures to attach to the patient simultaneously, for example, one structure could support the pelvis actuation module while another independent structure supports the patient in case of falls. The separate fall-support structure could be an off-the-shelf component. Finally, a stationary machine can have as larger footprint because it can be assembled in place.

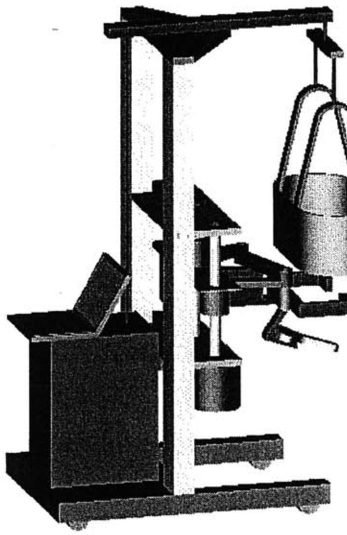

Figure 4.1-1: Gait trainer concept with moving base

The main disadvantages to a stationary machine is the fact that walking on a treadmill is not equivalent to walking on the ground, as discussed in section 2.2.3. Also, using a treadmill limits the patient to walking in a straight line at a constant speed and so does not allow the patient to practice starting and stopping.

A moving-base robot would allow the person to walk in a straight line as well as to turn, and to receive all the sensory feedback associated with walking. Such a robot could be used to answer clinical questions about the relative merit of conducting gait therapy on the ground versus conducting the same therapy on a treadmill.

The added capabilities of a mobile robot come with added cost and complexity. As will be discussed in section 6.3, the pelvis actuation module requires large and heavy actuators. Thus, the actuators to drive the robot on the ground will have to be large and powerful. The robot also must have a compact base of support to allow indoor maneuverability. Also, the additional compliances between the robot endpoint and the ground (e.g. shafts, bearings, wheels) will lower the natural frequency of structural vibrations. Finally, the robot must have a tether that provides power. In all, a mobile robot considerably increases the complexity of the design.

Despite the drawbacks inherent in the mobile-robot concept, this approach is favored due to the clinical advantages it possesses. The ability to maneuver, turn, and vary speeds while allowing the patient to experience all the sensory inputs associated with walking are too important to overlook, despite the added effort required to bring the mobile concept to fruition. Rather than settle for a simple off-the-shelf solution that severely limits the capabilities of the robot it is better to attempt the next step in gait rehabilitation robotics.

4.1.2 Body-weight support

Body-weight support is actuating the pelvis in the vertical direction. It could be included in the pelvis actuation concept selection, but because the magnitude of the force is much larger than for the other degrees of freedom it is considered separately. There is also a difference in the time-history of the two types of forces: planar forces can occur in any direction at any time according to the gait cycle while vertical forces are generally constant and directed upwards only. These differences suggest that a fundamentally different way of providing the vertical force will be required. The two principal alternatives are shown in Figure 4.1-2: the first is to use a cable or other device to pull up on the robot endpoint directly and the second is to use the mechanism that actuates the pelvis to transmit the vertical forces to the patient.

Using a cable to pull up on the robot endpoint directly is advantageous because it allows the horizontal and the vertical load components to be borne by separate robot modules. Also, cables can support very large vertical loads relative to their size and weight because they are only loaded in tension; in fact, the loads supported by a cable would be large enough to support the full weight of the patient in case the patient trips or falls. However, this approach is hard to package; it must be as close to vertical as possible to reduce horizontal forces and it should be as close to the patient as possible to reduce the moment arm. Therefore the cable must be supported from a point above the patient's head; as stated in the specifications, the tallest person expected is 75.6 inches tall and the machine must be less than 80 inches tall to fit through doors, leaving only 4.4 inches to hold a structure for supporting the vertical loads.

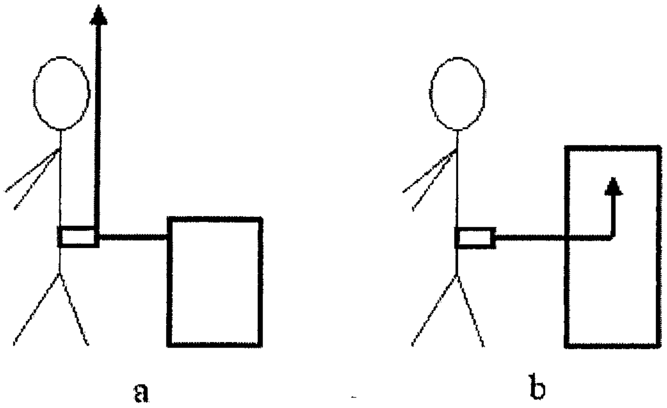

Figure 4.1-2: Two options for providing body-weight support forces: a) cable directly to the robot endpoint, b) transmit vertical forces through the mechanism that actuates the pelvis degrees of freedom

In addition, as the patient moves in the horizontal plane the cable becomes angled and part of the vertical force is projected into the horizontal plane. The patient should not be allowed to feel these forces because they will alter his or her balance. Figure 4.1-3 shows the effect of planar motions on the BWS force direction in an endpoint-cable arrangement. The maximum height of the machine is given in Table 3.2-5 as 80 inches or about 2 meters, while the maximum hip height is given in Table 3.2-1 as just over 1 m. The workspace of the machine must be 0.4 meters in the frontal direction per Table 3.2-3. Therefore, the planar force F_{plane} resulting from maximum body-weight support F_{BWS} being applied at the furthest point in the frontal workspace is

4.1-1
$$F_{plane} = F_{BWS} \tan\theta = 624 \cdot \frac{0.2}{1.0} = 125N$$

which is almost as large as the maximum specified actuation force of 166 N. For this reason, using a cable at the robot endpoint is not a feasible alternative for transmitting body-weight support force.

The second alternative for transmitting the vertical forces to the patient is to route them through the pelvis actuation module. This approach is deemed desirable because it creates a more streamlined and integrated design; all forces are transmitted to the patient through the same module. Furthermore, if the pelvis actuation system has a prismatic vertical degree of freedom no coupling occurs between horizontal and vertical forces.

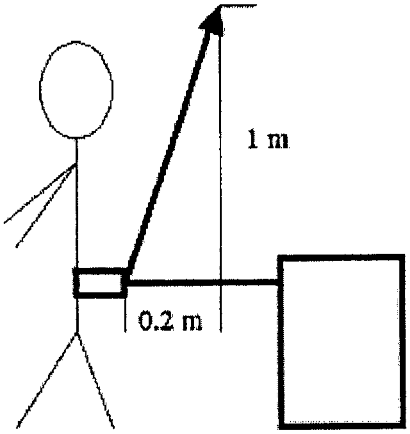

Figure 4.1-3: Cable for BWS at the endpoint

The disadvantage of transmitting the vertical forces through the pelvis actuation module is that grouping these two functions into one module is akin to replacing two independent design problems with one design problem that has conflicting requirements. The output impedance of the pelvis actuation module should be minimized, so the inertia and therefore the weight should be reduced. But the mechanism will also have to carry significant vertical loads so it will have to be strong and stiff, so the weight must be increased.

The second option is more difficult to implement, but using a separate cable to provide vertical forces is not feasible in light of the large workspace and limited available height. Therefore, the pelvis actuation mechanism must provide vertical support to the patient as well as forces the other degrees of freedom it will actuate.

4.1.3 Pelvis actuation

The third top-level functional requirement is that the robot must actuate the pelvis, i.e. it must be able to impart forces to the pelvis in a controlled manner. These forces can occur along any number of degrees of freedom depending on the mechanism used to generate them. In accordance with the functional requirements outlined in section 3.1, the actuated degrees of freedom must at least include vertical and lateral components. More degrees of freedom can be added according to the relative importance assigned. Furthermore, because the machine must be backdrivable, all un-actuated pelvic degrees of freedom must be free to move through their natural range while a person walks. Finally, as just discussed in section

4.1.2, the same mechanism that actuates the pelvis must also transmit the vertical body-weight support forces to the patient. This section will evaluate possible concepts for actuating the pelvic, beginning with a simple two-degree-of-freedom concept and ending with a six-DOF mechanism.

The simplest concept allowed by the functional requirements is a two-degree of freedom mechanism like the ones shown in Figure 4.1-4. These mechanisms actuate the vertical and the lateral degree of freedom. One option consists of a parallelogram that translates in the vertical direction and can rotate to actuate the lateral direction. Another alternative is to use prismatic joints in an orthogonal arrangement; this set-up maintains the independence of the degrees of freedom. The third option is a combination of the two previous ones and it uses prismatic vertical motion and rotary lateral motion.

The principal drawback of the two-degree-of-freedom designs involves backdrivability: of the concepts shown in Figure 4.1-4 only the second and third options provide freedom of fore/aft movement. In addition, the third option with the prismatic-plus-rotary arrangement has a variable moment arm for lateral motions. As the person moves forward and backwards the torque required to produce a constant force will vary, and because a passive force source for body-weight support is desired (as will be discussed in section 4.2.5) this approach is not advisable. Of these two-degree-of-freedom concepts only the Cartesian mechanism is feasible.

As discussed in section 3.1, the third translational degree of freedom should be actuated to mimic the benefits of treadmill use. In addition, a robot that does not actuate the frontal translation will not be able to correct knee hyperextension associated with premature calf activation [15].

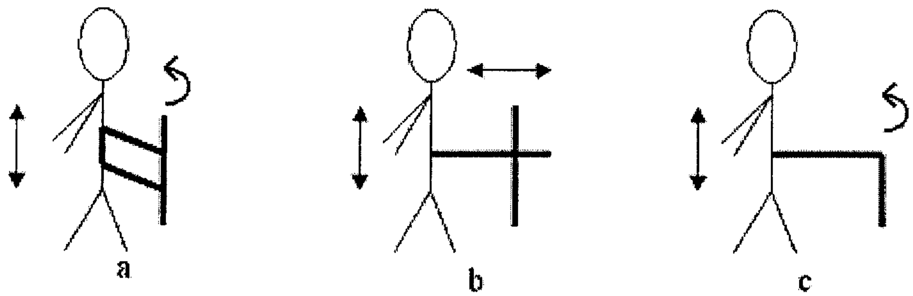

Figure 4.1-4: Two-degree-of-freedom concepts for actuating the pelvis: a) parallelogram b) Cartesian and c) prismatic vertical plus rotary lateral

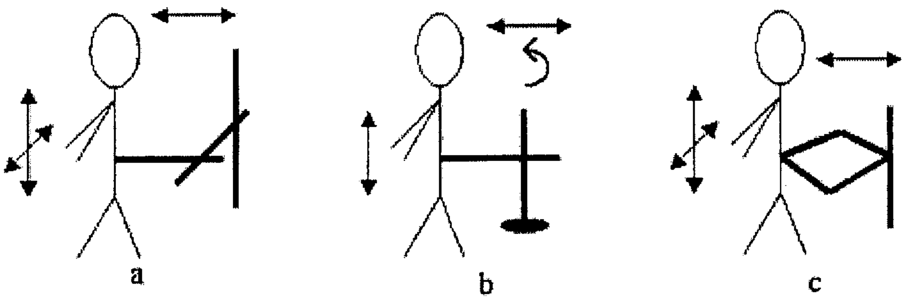

Figure 4.1-5: Three-degree-of-freedom concepts for actuating the pelvis: a) Cartesian, b) cylindrical, c) SCARA plus prismatic vertical

Examples of mechanisms with three DOFs are shown in Figure 4.1-5. The mechanisms shown actuate the pelvis in the vertical, lateral, and frontal directions. The first concept is a Cartesian arrangement with three orthogonal prismatic joints. The cylindrical option uses prismatic joints for vertical and frontal motion and rotary joint for lateral motion. Finally, a SCARA plus prismatic robot uses two rotary joints for lateral and frontal motion and a prismatic joint for vertical motion. A possibility not shown in the figure is the spherical configuration that uses two rotary joints for vertical and lateral motion and a prismatic joint for frontal motion.

The acronym SCARA stands for selective compliance assembly robot arm. This configuration consists of links whose joints are aligned parallel to the vertical axis. As outlined in the design for the arm rehabilitation robot, a SCARA configuration allows the use of rotary joints and generally has lower inertia and friction than a comparable prismatic joint design [6]. A SCARA design does not inherently have a vertical degree of freedom, however, so an additional prismatic joint must be provided.

SCARA configurations can have three planar degrees of freedom actuated in parallel, as shown in Figure 4.1-6. Both two- and three-degree-of-freedom SCARA configurations require an additional vertical joint. The additional degree of freedom of the latter case allows the ability to produce a torque about the vertical axis. This torque equates to pushing forward on one hip joint while pulling back on the other, and as discussed in *Chapter 2: Background*, applying that torque can yield improvements in the swing phase of gait without having to actuate the hip joint or the knee joint [73]. Furthermore, being able to push forward on the stance-side hip joint can help prevent knee hyperextension [15].

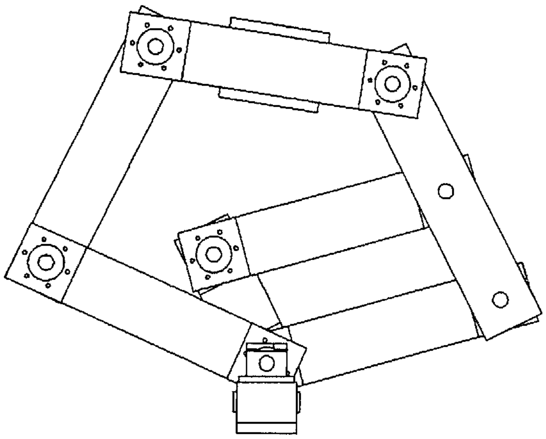

Figure 4.1-6: Sample three-degree-of-freedom SCARA mechanism

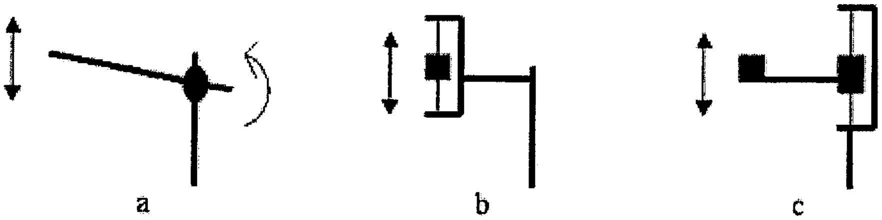

Figure 4.1-7: Sources of vertical motion: a) rotational elevation, b) prismatic joint at endpoint, c) prismatic joint at base

The vertical motion can come from one of three mechanisms: a rotational elevation joint, a prismatic joint at the endpoint, and a prismatic joint at the actuator base. These possibilities are sketched in Figure 4.1-7. Each of these options is discussed in detail below.

A robot with a rotary elevation joint allows the use of large actuators in a serial configuration so that they rotate with the robot arms as the patient moves vertically; because the vertical inertia that the patient feels depends on the rotary inertia of the mechanism instead of on its mass, inertia is still low. A rotary joint at the base can be enclosed in a small volume and still produce large motions at the endpoint, whereas a prismatic joint must be as large as the motion it is producing.

The rotary elevation joint is not feasible for this design because, as discussed in section 4.1.2, body-weight support forces are to travel through the pelvic actuation mechanism to reach the patient. The lever arm between elevation and vertical force depends on the linkage orientation, so a mechanical spring would not be able to provide a near-constant vertical force. Furthermore, in this design, elevation torque projects to a combination of vertical and horizontal forces. To estimate the magnitude of the horizontal forces, recall that the arm must elevate 0.15 m or half the workspace. Maximum angle occurs at the shortest arm length; the minimum clearance is 0.13 m so assume a minimum arm length of 0.3 m. This configuration is shown in Figure 4.1-8. The planar force F_{plane} resulting from this angle is

4.1-2 $$F_{plane} = F_{BWS} \tan\theta = 624 \cdot \frac{0.15}{0.3} = 312N$$

This force is larger than the maximum planar actuation force required.

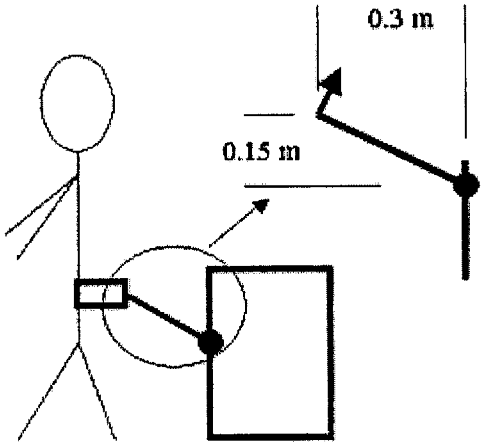

Figure 4.1-8: Tilt BWS system at maximum angle

The second possibility for adding vertical motion to the three-degree-of-freedom SCARA mechanism is to place a prismatic joint at the endpoint. This approach was used on the vertical extension of the MIT-MANUS arm therapy robot [4]. The prismatic vertical joint provides true vertical motion independent of the horizontal degrees of freedom so a mechanical spring can be used to aid in generating vertical forces. The actuators for the horizontal degrees of freedom can be sized strictly according to force needs in that plane. This configuration also has very low inertia in the vertical direction because the only components that move vertically are those at the endpoint.

Locating the prismatic joint at the endpoint means that the entire mass of the vertical actuator is felt as horizontal inertia by the patient. The design would have very low vertical inertia and high planar inertia, but the specifications stipulate that the planar inertia must be low in magnitude. The additional mass at the endpoint also lowers the natural frequency of the robot arms in the vertical direction so they must be made larger and stiffer to compensate. Finally, the actuator at the endpoint could also create problems with interference with the patient, since it must be at least as long as the desired travel.

The final configuration proposed in Figure 4.1-7 is a three-degree-of-freedom SCARA arm with a prismatic joint at the base of support. Kinematically, this mechanism would be identical to the one having a prismatic joint at the endpoint. Moving the prismatic joint to the base of support negates some of the disadvantages of the latter arrangement: the robot endpoint can now be more compact so that it doesn't interfere with the patient and the robot inertia in the plane is lower because it does not include the mass of the vertical actuator.

The most serious problem with locating the prismatic joint at the base is the larger inertia in the vertical direction. While moving the prismatic joint to the base removed the mass of the vertical actuator from the horizontal inertia, doing so means that the vertical inertia now includes the mass of the SCARA arms and the actuators that drive it! As will be seen in section 4.2.1, the planar actuators will be large, so a configuration in which they must be moved by the patient is not feasible. A solution to this problem is to insert a transmission element between the rotary actuators and the SCARA arms that allow the arms to move vertically relative to the motors while the two components are still constrained to rotate together. Such a design is shown in Figure 4.1-9. These added transmission elements increase compliance and complexity in the system, but they are a necessity in this configuration.

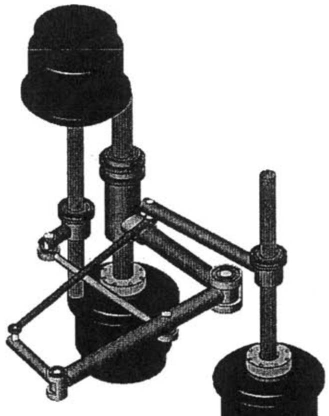

Figure 4.1-9: Four-degree-of-freedom parallel mechanism consisting of a 3-DOF SCARA linkage floating on prismatic, torque-transmitting joints

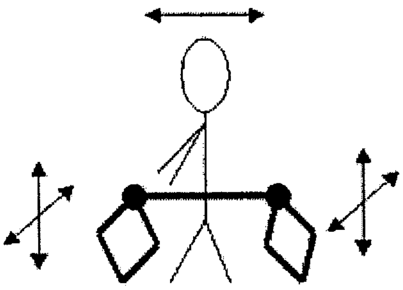

Figure 4.1-10: Twin-SCARA, five-degree-of-freedom mechanism

The next concept considered is a twin-SCARA, five-degree-of-freedom device shown in Figure 4.1-10. This design is based on a two-degree-of-freedom SCARA mechanism discussed above. However, in the five-degree-of-freedom arrangement, two such mechanisms are placed in a parallelogram to actuate two translations and two rotations. Lateral translation is achieved by moving the parallelogram like a four-bar linkage with an additional rotary actuator. The fact that the SCARA linkages must rotate means that this design is not truly parallel.

This five-degree-of-freedom design is modular: the two sides could be identical modules, and the robot would be symmetric with the possible exception of the lateral actuator. Two more arms could be mounted below the pelvis-actuating arms to actuate the knees. Also, knowledge gained from prior designs [6] could be applied to this design. A problem with this design is that it would place part of the burden of generating vertical forces on the same actuators that generate the horizontal forces. This problem is compounded by the fact that the links start out closer to vertical than to horizontal, so that the high stiffness of the SCARA arms perpendicular to their plane of motion cannot be used to support the largest forces.

Another complication is that the SCARA arms must be placed far enough to the side to allow room for the widest patients, so that the overall width of the machine would be much larger than the maximum specified in section 3.2. Also, the inertia of the design is inherently high in the rotation about the vertical axis because of the long lever arm, while the inertia of the human body is relatively small about that axis.

This five-degree-of-freedom design actuates rotation in the coronal plane, a degree of freedom that is not ranked as very important in section 3.1. This fact coupled with the added complexity of the extra degree of freedom and the other problems inherent in the design make the twin-SCARA configuration less appealing than the three- and four-degree-of-freedom mechanisms described above.

The final actuation mechanism considered here is the six-degree-of-freedom Stewart platform shown in Figure 4.1-11. This is a fully parallel design that uses six prismatic joints to locate an endpoint. This configuration was deemed unfeasible for the pelvis robot because of the large platform size required to generate the necessary workspace, in particular for the large frontal motions.

The two most promising concepts to actuate the pelvis are the two-degree-of-freedom SCARA plus prismatic joint at the base and the three-degree-of-freedom SCARA plus prismatic joint at the base. The second design adds the transverse rotation degree of freedom; unlike coronal rotation, transverse rotation has large amplitude and has more evidence of being important in gait and rehabilitation [15, 38, 73]. The added degree of freedom is part of the planar SCARA linkage, so actuating the transverse rotation does not add as much complexity as the switch to a whole new configuration (such as a Stewart platform) would. Therefore, the concept selected for actuating the pelvis is the four-degree-of-freedom design that consists of a 3-DOF planar linkage and a prismatic vertical DOF at the linkage base.

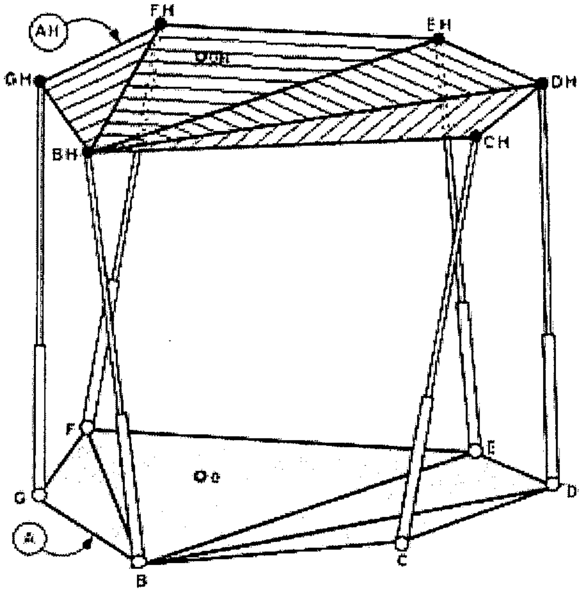

Figure 4.1-11: Six-degree-of-freedom Stewart platform [45]

4.1.4 Patient attachment

The patient attachment transmits forces from the pelvis actuation module to the patient. According to the functional requirements, the attachment should be comfortable, highly adjustable, fast to don and doff, and relatively stiff in the actuated degrees of freedom. There are four overall approaches to this problem: a parachute-style harness, a rigid frame that surrounds the patient, an inflatable harness, and a bicycle seat.

The first style of patient attachment is a parachute harness like the one shown in Figure 2.3-1 on page 31. This type of harness has a lower section that tightens around the pelvis and an upper section that fits over the torso. It is currently used for body-weight supported treadmill training, so it is a proven solution. Another benefit of this approach is that there are many sized harnesses so any size patient can use them.

Harnesses are not the best solution for a few reasons. First, the easiest way to secure the patient in the parachute harness is while the patient is lying down. This process can take up to fifteen minutes, or a substantial portion of a one-hour therapy session. Also, some patients find the straps that surround the pelvis uncomfortable. Finally, for this application it is important to transmit horizontal forces to the patient, and the parachute harness is not designed with this ability in mind. The harness would transmit horizontal forces by pulling on straps that are wrapped around the body, so the pulling forces are orthogonal to the strap. While this last point is not a serious issue, an attachment that applies forces by pushing on the relative body part would be better.

A patient attachment that applies all forces by pushing is the rigid frame like the one shown in Figure 4.1-12. Between the two sides of the frame, force and torque in all three planar degrees of freedom can be applied to the patient through pushing action alone. This trait makes the rigid frame the closest approximation to therapy by a human.

While the rigid frame is the best attachment in the horizontal plane, it is the most complicated of the concepts presented. It is also the heaviest and the most difficult to adjust. Still, its ability to push in all planar degrees of freedom gives this mechanism the best functionality if an implementation is deemed feasible.

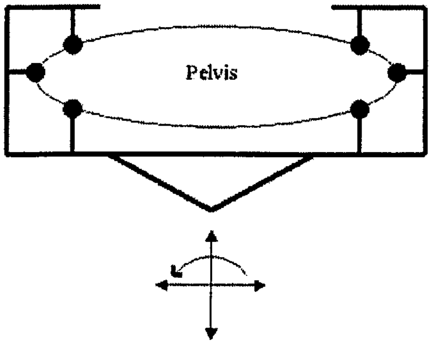

Figure 4.1-12: A rigid frame method of connecting to the patient

The opposite of the rigid frame is the inflatable harness. In this concept, a harness is fitted around the patient and inflatable pockets exert pressure over a large surface area. Whereas the rigid frame relied on pushing to transmit forces, the inflatable pockets distribute pressure evenly. This design could transmit forces through shear at the surface of the body. Also, as in the parachute harness, the inflatable harness would be easy to adjust to all patient sizes. While relying on shear and friction at the body's surface to transmit force limits the stiffness of the connection to the patient, this concept is still a feasible option.

Finally, an approach that uses the lone good place on which to push upwards on the human body is the bicycle seat. Although similar systems are not currently in use for therapy, the bicycle-seat body-weight support device shown in Figure 4.1-13 was used to test gait in simulated reduced gravity [17]. Also, the mockup of this machine described in *Chapter 5: Mockup Design and Testing* uses the same principle to support the subject. The bicycle seat works very well for transmitting loads in the vertical direction comfortably even while the patient is standing, and it can be mounted such that its position is adjustable to suit the preferences of the patient. Nevertheless, because it only contacts the patient below the groin this concept is unsuitable for transmitting horizontal loads.

The previous discussion suggests that a combination of all four concepts would be the best approach to the patient attachment. A bicycle seat provides vertical forces, an inflatable harness holds the patient comfortably but securely in all directions and transmits some forces through surface traction, and a rigid frame pushes directly around the hip joints to move the pelvis. Some deficiencies would remain, such as the fact that the rigid frame would be challenging to design well and the fact that using three different attachments means locating and adjusting three different items. In the end, the only way to evaluate an attachment method is to build it and gauge the response of the therapists and the patients, but the combination of a bicycle seat, inflatable harness, and rigid frame is a good start.

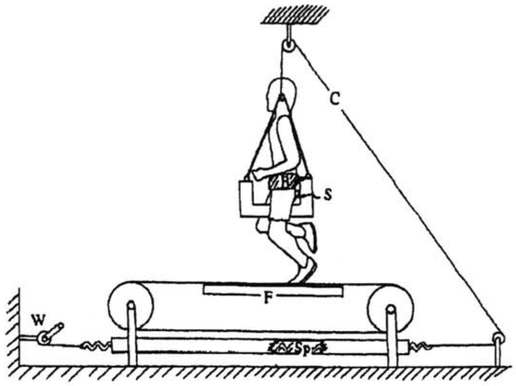

Figure 4.1-13: Device for body-weight support using bicycle seat [17]

4.1.5 Fall support

It is imperative that there be no danger of injury while a patient undergoes gait therapy. Therefore, as outlined in the functional requirements, some support must be provided in case of a fall. Moreover, the robot must be designed with falls in mind as part of the normal routine so that a fall does not cause damage to the robot. In a similar way to the body weight support force source, there are two ways to fulfill this requirement: with an independent mechanism or with a pelvis actuation module that can withstand fall loads.

The latter of these two options is similar to the concept selected earlier to provide body-weight support forces. However, because the magnitude of fall loads is nearly ten times as much as the already-large body-weight support forces it is not practical to design the pelvis actuation module in this manner.

The independent fall-support is thus the better option. Unlike the case of body-weight support forces, fall loads do not have to act at all times and do not have to coexist with planar forces. This fact makes it feasible to carry fall loads on a cable that does not need to remain vertical, as shown in the sample mechanism in Figure 4.1-14. The same limitations of machine size exist with this mechanism as with the body-weight support mechanism, so the robot cannot be large enough to have an overhead gantry to support these vertical loads. However, a device can be mounted lower and next to the patient without interfering with normal walking.

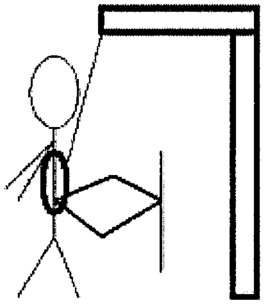

Figure 4.1-14: Independent fall support system

4.2 Detail concepts of the pelvis actuation module

This section focuses on one module selected above: the pelvis actuation module. It features a three-degree-of-freedom linkage to actuate in the horizontal plane and a prismatic joint at the base for the degree of freedom in the vertical direction. In addition the pelvis actuation module is responsible for transmitting body-weight support forces form the base to the patient. The first sub-module discussed is the transmission for the linkage actuation. Next, the mechanism that guides vertical motion is selected. After that the linkage is discussed in terms of how the vertical loads will be divided between the links, followed by the method of connecting all the arms so that they move vertically in unison. A source for body-weight support forces is then selected. Subsequently a method is chosen for constructing the chassis that ties all components of the pelvis actuation module into a self-sustained package. The end result of this section is a more detailed conceptual picture of the pelvis actuation module.

4.2.1 Planar actuators and transmission

The three-degree-of-freedom linkage requires an actuator with high-torque and low output impedance. The actuator can be directly connected to the links or it can be coupled with a gear, capstan, or fluidic transmission. This application involves slow movements with high torques; continuous stall torque is the driving factor behind motor size (as opposed to peak power). Therefore, using a transmission would allow a smaller motor to be used to achieve the desired output torques.

Transmissions have disadvantages. For example, a transmission element introduces compliance between the output shaft and the actuator. Some transmissions, such as gear trains, also introduce backlash. Transmissions also change the output impedance of the motor in such a way as to make them unsuitable for this robot. If an ideal, zero loss transmission is used to increase the output torque N times, the output inertia increases by N^2 times and the static friction torque increases by N times. A direct-drive system was chosen because of the desirable friction properties and because the construction of a direct-drive system is simpler. In the future, a capstan transmission design could be attempted, such as the one on the PHANTOM robot [52]. Capstan drives have high stiffness, low friction, and zero backlash [56, 74].

4.2.2 Source of vertical motion

At the base of the three-degree-of-freedom SCARA linkage is a prismatic joint. This joint must allow vertical motion of the linkage while transmitting torque from the actuators to the links. In addition, because body-weight support forces travel through the linkage, this joint must be strong enough to handle the significant moment loads that arise from applying a force to the patient at a distance governed by the linkage position. Only two ways of achieving this objective are discussed here: using linear bushings on two or more shafts and using ball splines.

The former option, using linear bushings on two or more shafts, is built up from simple parts. Linear bushings allow rotation and translation along a cylinder, which is why two shafts are needed for each link. The fact that the assembly must withstand significant moment loads means that large cylinders are needed. Also, because the shafts are offset from the motor axis they add a large amount of inertia to the rotation of the motors. Finally, the two-shaft assembly poses alignment and overconstraint problems.

A ball spline is shown in Figure 4.2-1. It is an off-the-shelf component that consists of a shaft with grooves cut along its length so that a nut, guided by balls that sit in said grooves, can slide in the axial direction but cannot rotate relative to the shaft. As is the case for the previous concept, the large moment loads at the base require a large shaft cross section for strength. Also, the fact that the shaft and the spline nut are connected only through six trains of balls limits the radial and angular stiffness of the spline nut compared to that of a plain bearing. However, the ball trains can be preloaded to increase stiffness in all directions; this property of the spline nut makes them stiff enough for this design but increases friction [65]. The properties of the ball spline make it the preferred method for providing vertical motion in this design.

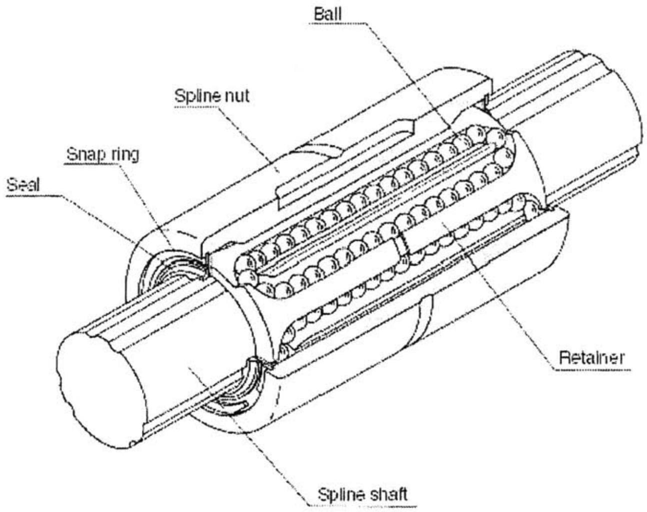

Figure 4.2-1: THK ball-spline [65]

4.2.3 Number of load-bearing arms

The pelvis actuation module uses direct-drive rotary motors and ball splines to drive the arms while allowing the linkage to translate vertically. The next step is to transmit to the endpoint the vertical force generated at the base.

The three-degree-of-freedom SCARA linkage is composed of 8 links and 9 joints. In a design where every link can support a vertical load, each joint allows one rotation and restricts the other five degrees of freedom. Each joint then represents an axis with one degree of freedom; in order for the linkage to work well every axis must be aligned parallel and located vertically or else there will be overconstraint forces. The only solutions are to either increase the clearance in the system or to decrease the stiffness; that way, the size of the forces required to bring the components into geometric compatibility is reduced.

In contrast, a design with only one load-bearing arm, like the one in Figure 4.2-2, has three joints that transmit moments and six joints that constrain translations but allow all rotations. The extra degrees of freedom allow for geometric compatibility even with misalignments. Furthermore, the fact that one arm carries the vertical loads means that the load-bearing arm can be designed for the worst-case vertical load with confidence that small misalignments will not affect its load rating.

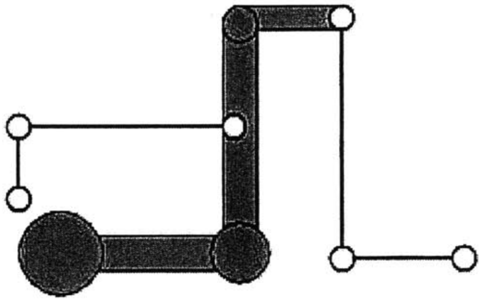

Figure 4.2-2: Linkage arrangement with all vertical loads supported by one arm

4.2.4 Connection between vertically-translating elements

Because the linkage will have one load-bearing arm and six spherical joints, a connection is needed between the three spline-nuts and the linear actuator. The connection must not overconstrain the components. The spline-nuts must rotate with respect to each other, so rotary bearings are mounted on the outer diameter of the spline nut housings. These bearings must be connected by a structure, which is rigidly mounted to the load-bearing spline nut. The other two spline-nuts and the linear actuator must each be allowed two angular and two translational misalignments in relation to the connecting structure. These motions can be allowed in two ways: through plain bearings or through flexural bearings.

Because each plain bearing allows two degrees of freedom, a four-degree-of-freedom mechanism can be built with two plain bearings as shown in Figure 4.2-3. Each plain bearing is positioned so that its axis intersects the center of the spline shaft, making the rotational misalignments have negligible moment arms. A plain bearing design is simple, straightforward, and has the potential for large displacements. However, plain bearings can suffer from play or low stiffness, depending on the details of the design.

The four-degree-of-freedom flexure mechanism in Figure 4.2-4 is similar to the plain bearing system. As with the plain bearings, each flexure nominally allows a translation and a rotation: the former in the form of a bending deflection and the latter in the form of a twisting rotation. The flexures shown in the figure are of the clamped variety, so the flexure blades are separate pieces that are bolted into an assembly. Flexures are advantageous because they have no static friction, they have no play, and they have very high stiffness in the desired direction. However, flexural bearings have a much more limited range of motion than plain bearings. Also, flexures must be designed to withstand fatigue, and unforeseen deflections or vibrations can hasten wear on the flexures and cause them to fail unexpectedly.

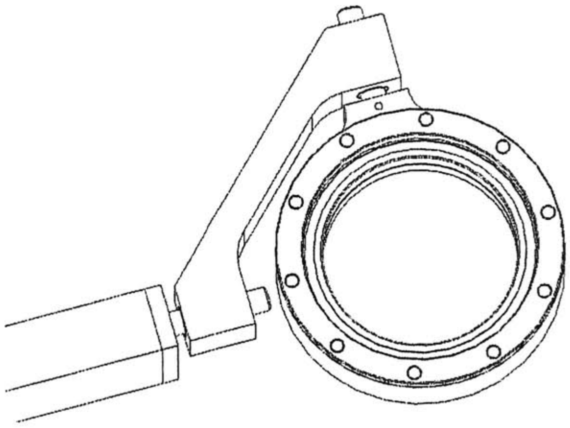

Figure 4.2-3: Four-degree-of-freedom gimbal mechanism

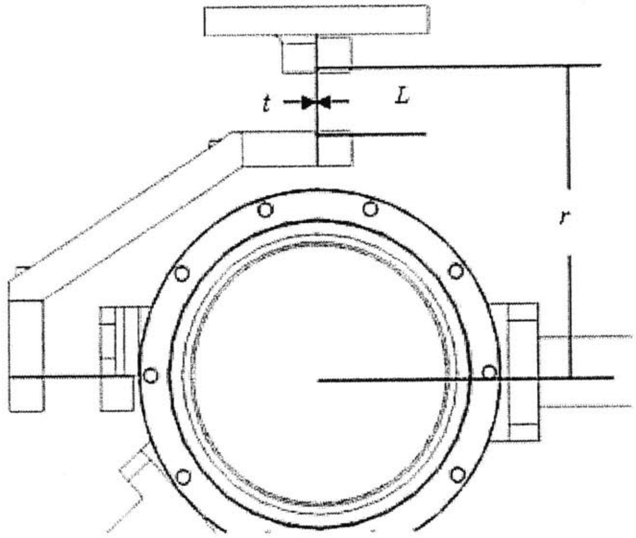

Figure 4.2-4: Four-degree-of-freedom flexure mechanism

A tensioned cable can act in a similar way to a flexural bearing. A small cable can hold large loads in tension but has negligible stiffness in any other direction. Two vertical pretensioned cables would provide bi-directional force along the vertical axis only. This approach would only be applicable to the connection from the vertical actuator to the load-bearing spline because of the cable length needed. The cables would connect to a mounting tab that extends out from the structure around the large spline nut. The connection method makes for a short moment arm for the linear actuator bearings so that they are not subjected to large moment loads, but the resulting long moment arm to the spline nut creates a sine error on tilting misalignments: tilting the spline nut would cause vertical motion of the linear actuator. While this cable design is promising, it was found to be feasible late in the design of this robot. It is therefore not pursued in this thesis, though a future implementation of the device could incorporate this design.

The decision between the plain and flexural bearings requires analysis of the displacement achievable with flexures and the comparison of achievable displacements with expected misalignment. This process is carried out in section 6.8.

4.2.5 Source of body-weight support forces

The next step in the conceptual design of the four-degree-of-freedom mechanism is to select the source of vertical forces. As dictated by the specifications, these forces can be as large as 620 N or 140 lbs. Because body-weight support forces are mostly constant, a passive mechanical element can be considered as a possible force source. Since the force must be applied to a prismatic joint, any linear energy storage element would fit, including counterweights, coil springs, constant force springs, charged gas springs, and surgical tubing springs. In addition, the use of actuators to generate vertical forces is also a possibility. These actuators can take the form of direct-drive linear motors, motors with a transmission such as a ball-screw, and actively controlled air pressure cylinders. Moreover, combinations of any two or more elements are also viable alternatives.

The counterweight can immediately be eliminated as a possibility. While in static conditions it provides a constant force, in dynamic operation the inertia of the counterweight alters the force output of the device.

Coil springs are available off-the-shelf in a variety of lengths and load ratings, and can also be custom wound. Because they are generally made out of steel, however, their maximum deflection is limited: the high elastic modulus of steel converts even modest strains into large stresses. Steel is also heavy, and coil springs have an inherent natural frequency that depends on their weight and stiffness.

Another type of metal springs is the constant force spring in Figure 4.2-5. As its name implies, this spring maintains a near-constant tension throughout its travel. This type of spring is ideal for supporting static weight, such as the weight of the linkage in this robot. For dynamic applications, however, the low fatigue life of these springs severely limits their use. Generally constant force springs are rated for 2,500 - 20,000 cycles although some are designed for as many as 10^6 cycles [62]. Also, the only way to adjust force is to attach and detach springs.

Charged gas springs store their energy in the form of pressure in an enclosed volume. As shown in Figure 4.2-6, hydrostatic pressure acting on the two surfaces of the piston in a charged gas spring generates a force. Gas springs have low spring constants because the only change in force is due to the increase in pressure that occurs when the piston rod enters the spring and reduces the volume. While charged gas springs can have a large range of motion and can be easily mounted, they suffer from relatively high friction and from a relative dearth of detailed force-length data.

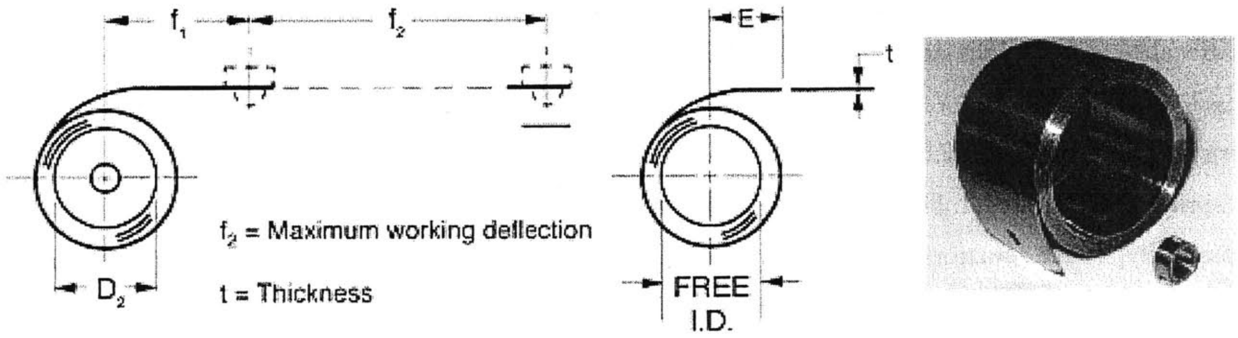

Figure 4.2-5: Constant force spring [62]

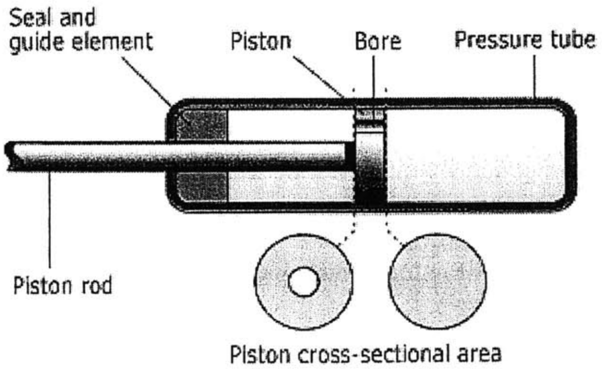

Figure 4.2-6: Operating principles of a gas spring [59]

The final category of mechanical spring mentioned above is the surgical tubing spring. Springs made of this material have a hollow cylinder cross-section and the compliance originates from the inherent properties of the material. The simple cross-section allows surgical tubing springs to be wrapped around pulleys even while under tension. Also, the material used for these springs can withstand very large strains, so surgical tubing springs can safely stretch up to three times their original length [37].

It is also possible to generate vertical forces with an actuator instead of with an energy storage element. Linear actuators are available as direct drive or with a transmission. Linear motors from Copley are direct drive actuators with high force output and low inertia, as shown in Table 4.2-1. Still, even the most powerful linear motor in the Copley line, the 3810, only produces 35% of the force required for body-weight support in this device. If these motors could output the required 624 N of force with their typical friction of only about 2-3 N, they would be the ideal actuators for this application. Such an arrangement would require three 3810 motors, which would add 15 kg to the vertical inertia of the robot. Since a direct drive electromechanical linear actuator cannot provide the necessary force without adding too much inertia, it is not likely that an actuator with a transmission can be used instead.

Table 4.2-1: Copley linear motor specifications

	3804	3806	3808	3810	Units
Continuous Stall Force	101	142	180	217	N
Continuous Stall Current	2.03	1.90	1.81	1.74	A_{rms}
Forcer Mass	2.15	3.15	4.15	5.15	kg
Forcer Length	167	238	309	380	mm

An actively controlled air pressure system could be used instead of an electromechanical actuator. The WARD, or Walking Assistance Rehabilitation Device, is a device that provides body-weight support forces based on this approach [18]. While systems that generate forces from air pressure can generally both produce high forces and possess desirable output impedance characteristics, the entire system would have to be designed from scratch. Using a pneumatic actuator remains a possibility for a future version of this robot.

Each of the mechanical elements available to provide body-weight support forces has its benefits and drawbacks, so a combination of elements can be used for the design of this module. Additional calculations, and the final selection of the components that will generate the body-weight support forces, are covered in section 6.9.

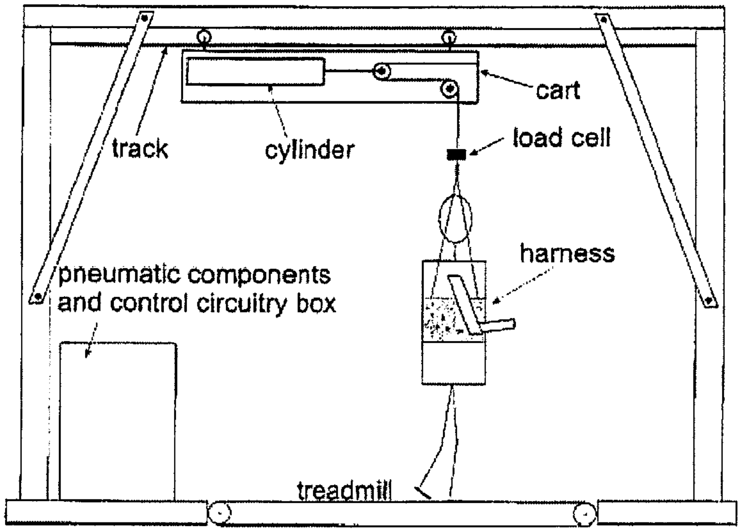

Figure 4.2-7: WARD body-weight support device [18]

4.2.6 Chassis construction

The chassis is the structure that connects all the elements of the pelvis actuation module into a single unit. These elements include the actuators, the spline shafts, the planar linkage and the associated vertical connection sub-assembly, and the source for body-weight support forces. This chassis must support large loads, so possible methods of constructing it include using closed thin-walled sheet metal sections, bolting or brazing plates into the desired shape, casting the desired shape with post-machining to ensure proper tolerances on mating surfaces, and assembling the chassis out of 80/20-brand aluminum extrusion.

Sheet metal construction is attractive because thin-walled sections are lightweight. The chassis will be mounted on a moving base, and so saving weight on it will reduce the power requirements of the overground propulsion motors. Building the chassis out of sheet metal is not feasible for two reasons: first, the thickness and flatness tolerances for sheet metal are poor; and second, while thin-walled sections are globally stiff they are locally flimsy. In other words, the stiffness is high when their cross-sections are assumed to stay plane, but concentrated loads can easily warp the cross-sections.

Thicker sections can be machined and either bolted or brazed together. Thick-walled sections are less susceptible to local warping due to concentrated loads than are thin-walled sections. Still, even thicker sections are much less stiff than the overall structure they form, so a perfectly strait bar will not be perfectly straight once it is assembled into a multi-part structure.

A different approach is to sand-cast the chassis as shown in Figure 4.2-8; the process allows for the inclusion of some complicated stiffening ribs and mounting surfaces into the mold. Once the casting is complete its mating surfaces can be machined flat and parallel. Sand casting is not a simple solution because the mold has to be designed to minimize defects that form due to shrinkage as the material cools. Also, post-machining requires the part to be aligned, fixtured, and machined even though it has no straight edges or right angles.

The final possibility is to build up the chassis out of 80/20-brand aluminum extrusion, as shown in Figure 4.2-9. This extrusion has slots along its length to allow for infinite location of attachments without the need for drilling holes. The assemblies use a plethora of small fasteners instead of few large ones. Furthermore, the slots are tapered so that tightening bolts preloads them and prevents them from vibrating loose. The extrusion conforms to moderately good tolerances. A chassis built out of 80/20 will weigh roughly 30% more than a comparable cast chassis, based on solid models of each approach. In addition, construction with 80/20 requires careful design to ensure alignment surfaces are available for each joint.

Both the cast and 80/20 chassis options are feasible. At this time, the chassis has not been designed so a concept has not been selected.

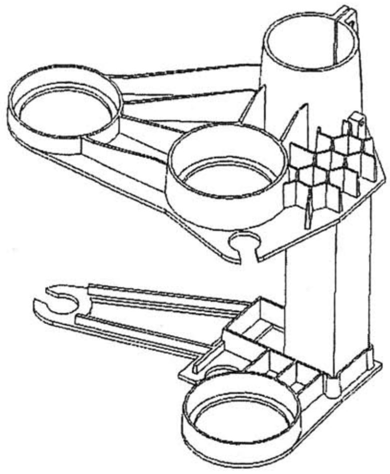

Figure 4.2-8: Bottom view of a three-piece cast aluminum chassis for the pelvic actuation module

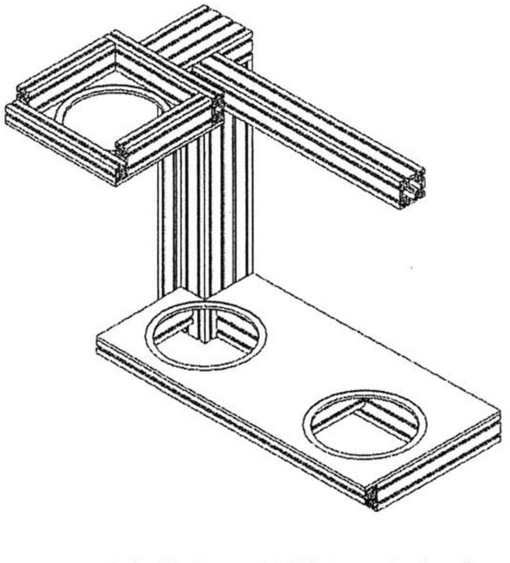

Figure 4.2-9: Chassis built from 80/20-brand aluminum extrusion

Chapter 5: Mockup Design and Testing

Because this gait trainer is a revolutionary and complex machine, its performance is difficult to predict. A mockup is constructed to evaluate concepts for the pelvis actuation module, the body-weight support system, the patient attachment, and the overground propulsion module. Qualitative and quantitative lessons from the mockup are then applied to the design of the alpha prototype.

5.1 Mockup design

Recall from section 4.1.3 that the pelvis actuation module will be a three-degree-of-freedom SCARA linkage with a prismatic vertical degree of freedom. The mockup has the same configuration and is intended to demonstrate the concept's effect on gait, both qualitatively and quantitatively.

The mockup includes an aluminum structure that supports its components. A medium-stiffness spring provides body-weight support and transmits the vertical forces to the subject through the four-DOF mechanism. Both vertical force and compliance are adjustable. A patient attachment method fitted to the four-DOF mechanism shows the subject's tolerance to applied vertical forces. Finally, steerable casters support the mockup structure so the subject can walk overground while an assistant pushes the device.

5.1.1 Four-degree-of-freedom mechanism

The four-degree-of-freedom pelvis mechanism is a mockup of the pelvis actuation module. It has the same configuration that will be used for the alpha prototype, though the mockup lacks motors and has a different linkage design. As shown in Figure 5.1-1, the pelvis mechanism has seven arms; six are 12 inches long and one is 6-inches long from joint to joint. The arms have 3 inch by 2 inch by 0.25-inch hollow rectangular aluminum cross-sections. The arm on the right side of the linkage has three joints and each space between joints measures 6 inches. Each joint has a 0.75 inch steel shaft, a radial ball bearing, and a tapered roller bearing held in place by two retaining rings.

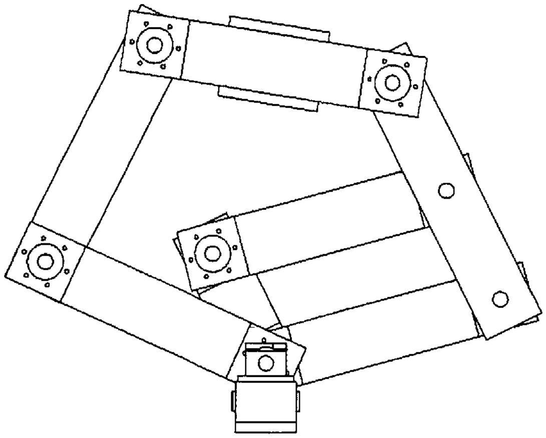

Figure 5.1-1: Plan view of the mockup linkage

The three joints at the base are coaxial so all six joint bearings mount to the same 30-inch long by 0.75-inch diameter hardened steel shaft. The shaft is supported by two linear ball bearings and has 5.5 inches of vertical travel. A backing plate bolts to the ball bearing pillow blocks, and four constant force springs provide 40 pounds of vertical force to support most of the mechanism's weight. The position of the linkage is measured with one linear and three rotary potentiometers connected to a data acquisition card.

A solid model was used to estimate the inertial parameters of each link to calculate the inertia of the mechanism; Table 5.1-1 shows the resulting estimated values. The mockup has acceptable inertia in the vertical direction and low inertia in planar translation, but the transverse rotation inertia is 65% greater than the target value.

Table 5.1-1: Calculated mockup inertia

Relevant Body Segment	DOF	Target	Mockup	*Units*
Head, neck, and torso	z	22.9	20-23	*kg*
Pelvis and lumbar	x, y	11.9	5.2 / 8.4	*kg*
Pelvis and lumbar	Φ	0.1243	0.2060	*kg-m²*

5.1.2 Support structure and body-weight support spring

The pelvis mechanism mounts to an aluminum structure made of 80/20-brand extrusion. As shown in Figure 5.1-2, the mockup structure is includes a vertical column, a lateral beam below the column, and two beams oriented front to back at the end of the horizontal beam. The cross section of the vertical column measures 6 inches by 3 inches with the longer dimension running front-to-back. This column is mounted to the lateral beam by endplates and anchor fasteners specially designed for this material. The lateral beam has three pieces that can be unclamped and extended to vary the width of the device from 32 to 42 inches; all three parts have 6 by 3-inch cross-sections. Two 3 x 3 inch by 45-inch long beams are mounted at the end of the lateral beams to provide the base of support. An 18-inch long beam is also mounted at the base of the column and extends rearwards to serve as a mount for the spring adjustment winch.

The pelvis mechanism connects to the column with two plastic bearing blocks that slide over the slots in the 80/20 sections. For added safety, wing nuts clamp the bearing blocks in place. The bearings allow the pelvis mechanism to move vertically to adapt to any size subject.

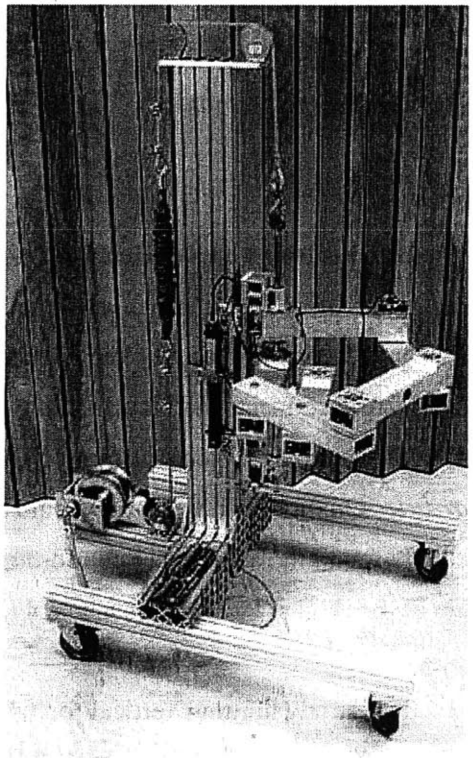

Figure 5.1-2: Mockup without subject attachment

A 12-inch long surgical tube extension spring capable of exerting up to 343 N (77 lbs) of force is attached to the structure and provides body-weight support. The spring is held between two sections of 0.25-inch wire rope; the rope on one side connects to the 30-inch vertical shaft of the pelvis mechanism and the rope on the other side winds around a hand-operated winch equipped with a ratchet to prevent backdriving. One spring with a 560 N/m (3.2 lb/in) spring constant was used for most trials, but two such springs were fitted in parallel when larger forces were needed. Spring tension is adjusted by increasing spring length with the winch.

5.1.3 Subject attachment

Two patient attachments were tested with the mockup: a rock-climbing harness and a bicycle seat. Figure 5.1-3 shows the climbing harness attachment. The subject wears the harness and stands in front of the mockup; webbing wraps around the front link of the mockup and the leg straps of the harness. The harness has a waistband and two leg straps that connect only on the front side. The weak connection between the straps allowed them to shift relative to the body and to each other and resulted in a poor connection to the subject. Attempts to improve the connection by tightening the harness caused discomfort. Also, upward force is transferred to the subject at the rear of the leg straps, so vertical forces generate a moment relative to the subject's center of gravity. This moment tends to tilt the pelvis forward, noticeably (and somewhat comically) altering the gait pattern. The climbing harness is an entirely unsatisfactory subject attachment.

The other subject attachment tested is based on a device for simulated reduced gravity experiments [17]. The subject stands over a bicycle seat and is restrained against the front link of the mechanism with webbing wrapped around the waist. The mockup of this attachment is shown in Figure 5.1-4; an adjustable aluminum pipe structure connects the bicycle seat to the front link of the mechanism. Tests with the bicycle seat attachment showed that subjects were much more tolerant of upward forces than they were with the climbing harness. Qualitative observation could neither see nor feel alterations in the gait pattern. Persons of both genders found the attachment comfortable, though initially the seat mounting structure chafed the inside of the thighs. Padding the area solved the problem.

While the bicycle seat is excellent at transmitting vertical forces it does not transmit horizontal forces well. The waist strap secures the subject in the presence of fore/aft forces but does not strongly resist lateral forces or torques about the vertical axis. The patient attachment method needs to be refined to improve force transfer in the horizontal plane. Furthermore, the bicycle seat location is adjustable, but it cannot be changed while the subject is attached to the device. The alpha prototype should have a patient attachment method that can be adjusted during use and that does not require tools to adjust.

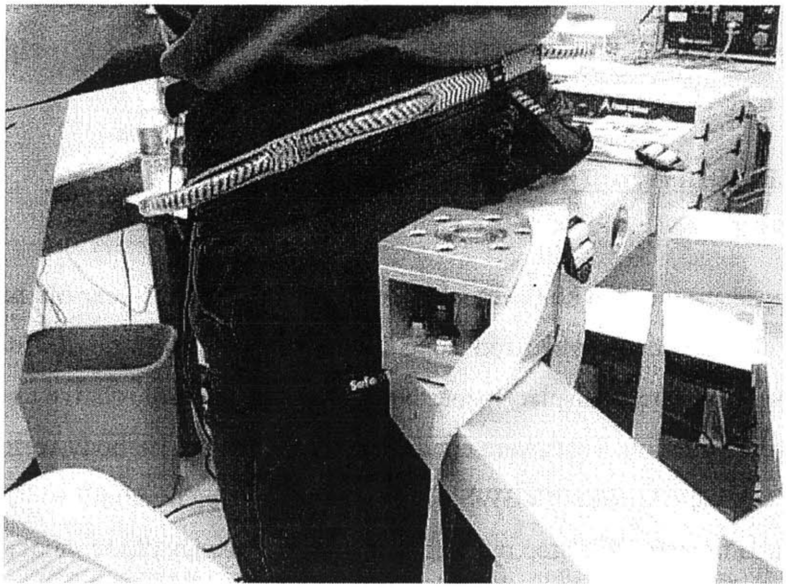

Figure 5.1-3: Attachment method using a climbing harness

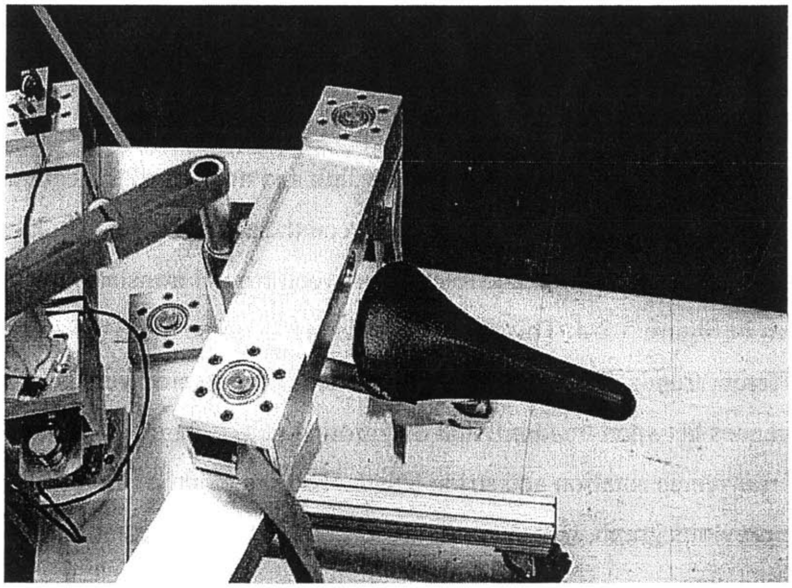

Figure 5.1-4: Attachment method using a bicycle seat

5.2 Mockup testing and results

Three types of tests were conducted with the mockup: treadmill walking, step-up onto a platform, and walking overground. The treadmill test used potentiometers on the device to measure the pelvis position in four degrees of freedom. The other two tests used infrared gait analysis equipment that measured the position and orientation of eleven body segments[1].

5.2.1 Mockup treadmill testing

The first gait measurements with the mockup were made while a 22-year-old healthy male subject walked on a treadmill. The subject was secured using the climbing harness. The measured motions were the vertical displacement, the lateral displacement, the frontal displacement relative to average forward motion, and the transverse rotation. Tests were conducted with 0% and 15% body-weight support. Figure 5.2-1 shows an average gait cycle with 0% BWS. Data collected during treadmill walking was then compared with published figures [26]. Step rate is given by the frequency of the mockup data while step length was calculated from the step rate and the treadmill's speed readout.

Figure 5.2-2 shows that mockup treadmill gait follows the published trend of increasing vertical center of gravity (Cg) displacement with increasing step length. In Figure 5.2-3, however, the lateral excursion of the pelvis during mockup treadmill gait does not follow the trend in published data: the magnitude of motion increases with step rate instead of decreases. The discrepancy occurs because the data output by the mockup shows the position of its front link and not that of the center of gravity of the subject. Transverse rotations thus create a difference between the actual subject Cg lateral position and the mockup's lateral position output value. The relation between frontal translation of the pelvis and walking speed is shown in Figure 5.2-4. This data is ambiguous because the BWS curve and the non-BWS curve follow different trends. The bulk of the differences in measured versus published results are likely due to the differences between treadmill and overground gait. Figure 5.2-5 shows the relation between amplitude of transverse rotation and stride length. The same outlying point found in Figure 5.2-4 appears. Unlike in the previous graph, however, the trend in the transverse rotation of the pelvis follows the trend of the published data.

---

[1] The author would like to thank Dr. David Krebs and Dov Goldvasser from the Biomotion Laboratory at the Massachusetts General Hospital for conducting the gait analysis presented in this section.

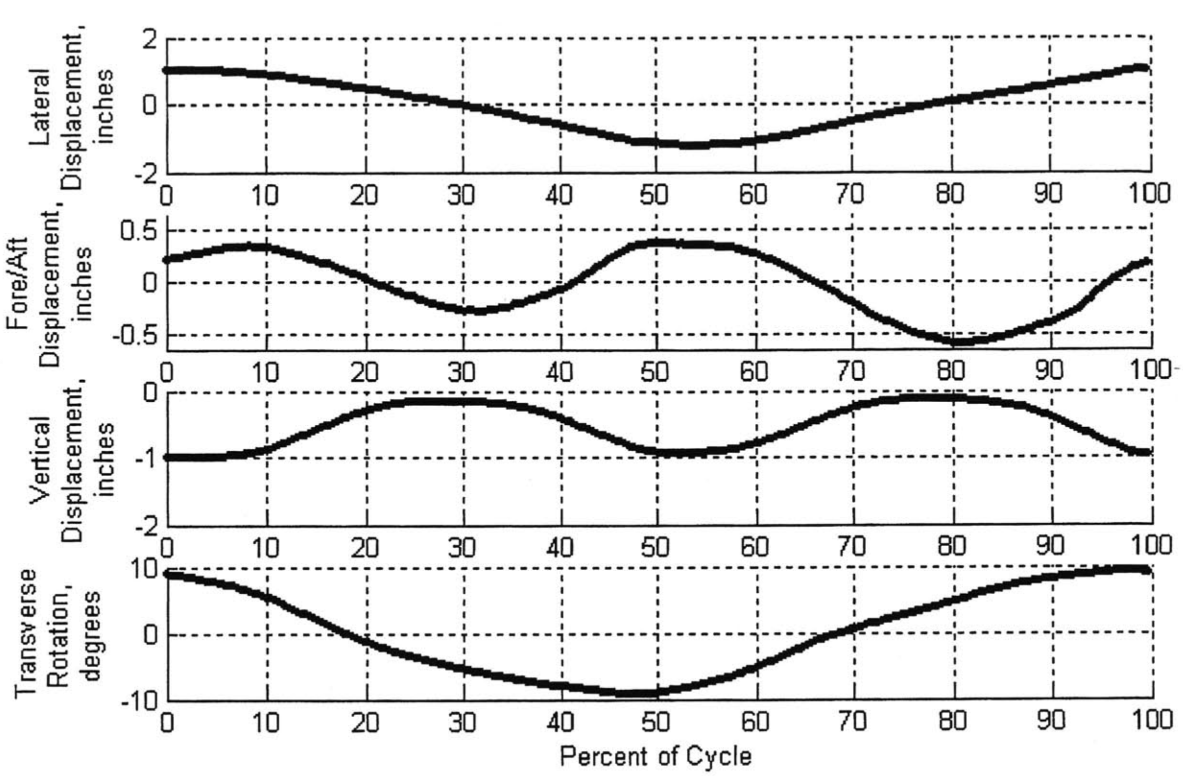

Figure 5.2-1: Pelvis motions measured by the mockup during treadmill walking

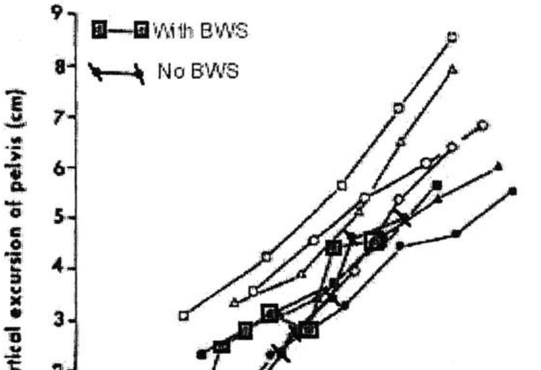

Figure 5.2-2: Step length versus vertical excursion of the pelvis, mockup treadmill results superimposed on published data [18]

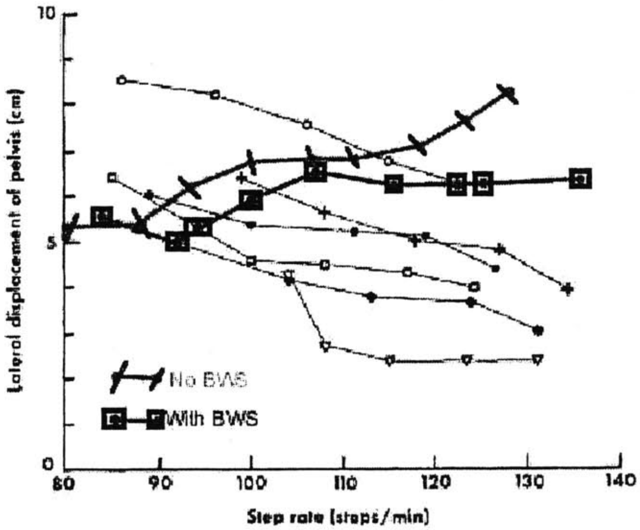

Figure 5.2-3: Step rate versus lateral excursion of the pelvis, mockup treadmill results superimposed on published data [26]

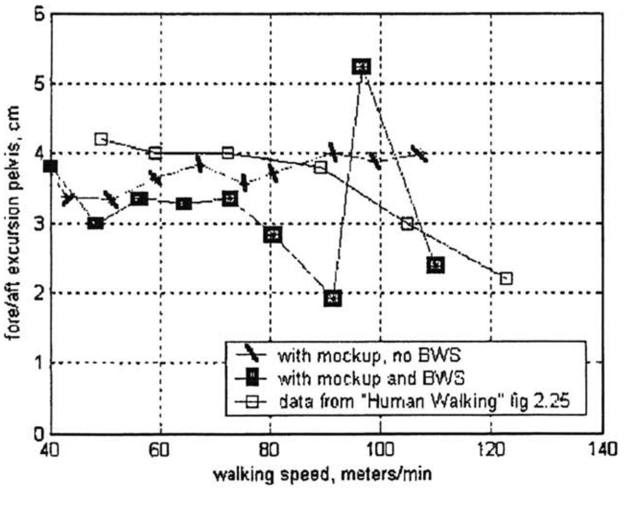

Figure 5.2-4: Walking speed versus fore/aft excursion of the pelvis, mockup treadmill results superimposed on published data [18]

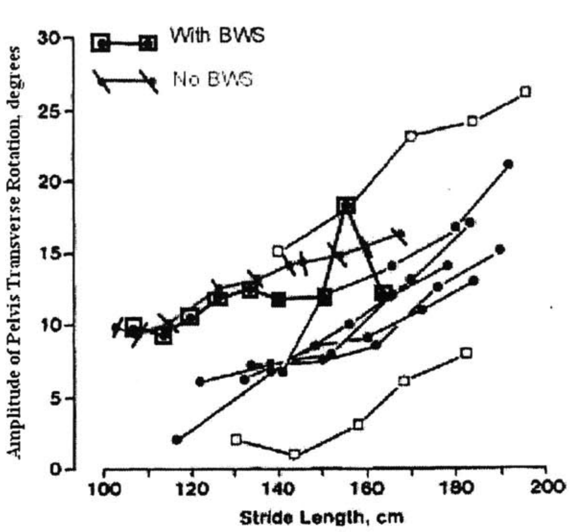

Figure 5.2-5: Stride length versus amplitude of transverse rotation of the pelvis, mockup treadmill results superimposed on published data [26]

Treadmill tests with the mockup were a starting point to evaluate feasibility and tolerance of the testing. These tests showed the need for a new attachment method as discussed in section 5.1.3 and the need to alter the data output of the mockup to estimate the position of the subject's center instead of the position of the linkage end effector.

5.2.2 Gait analysis: step-up task

The first task analyzed at the Massachusetts General Hospital Biomotion Lab was a step-up task [25]. Two healthy male subjects took part in the gait analysis. The task consists of stepping on and off a 3-inch tall platform in an up-up-down-down pattern. Each subject performed under four conditions: unrestrained, using the mockup but with no body-weight support, and using the mockup with approximately 15% BWS and 30% BWS. Zero- and fifteen-percent body-weight support were implemented with one spring while 30% BWS used two springs. The task was paced at 100 steps per minute using a metronome.

Gait analysis equipment in the Biomotion Lab measures the position and orientation of eleven body segments. The potentiometers attached to the pelvis mechanism were not used in these trials. The gait analysis equipment relies on infrared-emitting LED arrays that are fastened to the body with Velcro straps as shown in Figure 5.2-6. Infrared cameras placed in calibrated frames detect these LEDs. Prior to testing, a calibration routine is required that measures the location of the subject's joints.

Plots for anterior/posterior motion of the subject center of gravity (Cg) are shown in Figure 5.2-7. The data is shown in phase plot format, or velocity versus position. The mockup was designed to have enough travel for walking, but the step-up task was not considered in the design. Comparing the frontal Cg phase plot for subject B in unconstrained versus 0% BWS stepping shows that motion was reduced by about 30%. Qualitatively, frontal travel was insufficient to allow the entire foot to be placed on the platform. Subjects could only place the front half of the foot on the platform and had to support weight on the balls of the feet. The mechanism had sufficient range of motion in the other directions so as to not impact stepping.

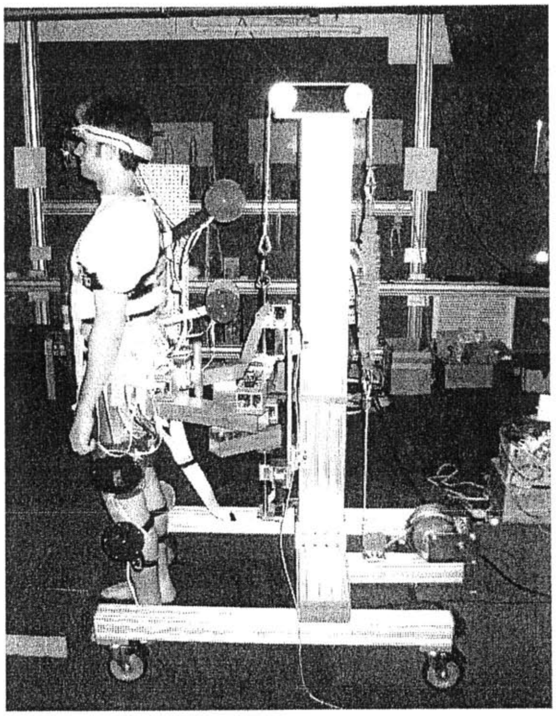

Figure 5.2-6: Subject A ready to perform the step-up task in gait analysis laboratory

Figure 5.2-8 shows the lateral position of the center of gravity during the step-up task for both subjects. The lateral position data is also re-centered at each cycle to show the lateral drift between cycles. Starting with the data in Figure 5.2-8 and plotting the lateral excursion of each cycle yields the graphs in Figure 5.2-9. The two subjects show very similar results for the three mockup tests, both in the trends and in the magnitude of the lateral excursion. In free stepping, however, the two subjects show a different magnitude of lateral excursion. Figure 5.2-8 shows a more uneven cyclic pattern in the unconstrained condition of subject B relative to the other plots, whereas the unconstrained plot for subject A shows a more constant cyclic pattern. Thus, the data suggests that the data point belonging to subject B is the outlier and that the trend is towards decreasing lateral excursion with increasing body-weight support. No conclusion should be drawn regarding the difference between unconstrained stepping and 0% BWS stepping due to the small sample size.

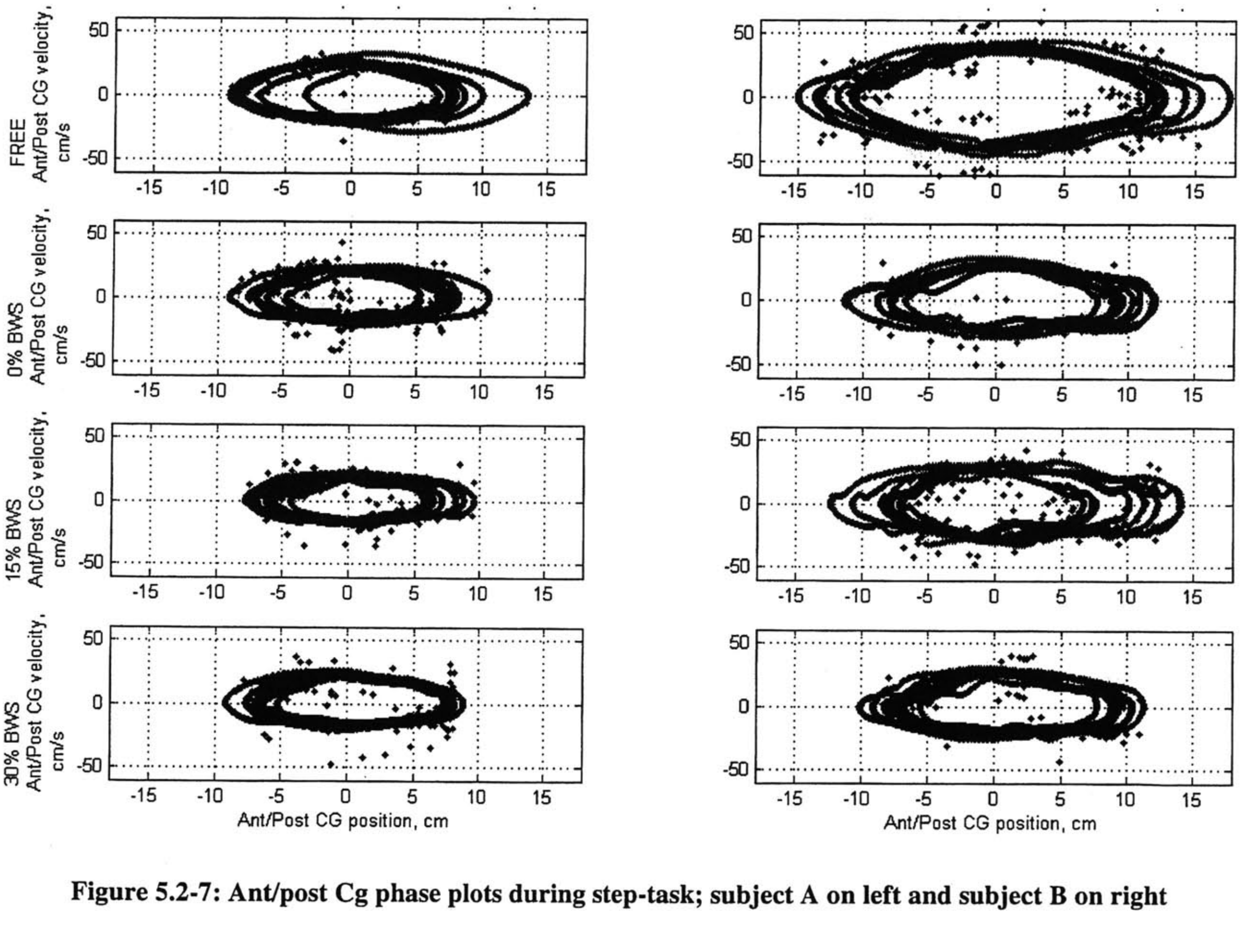

Figure 5.2-7: Ant/post Cg phase plots during step-task; subject A on left and subject B on right

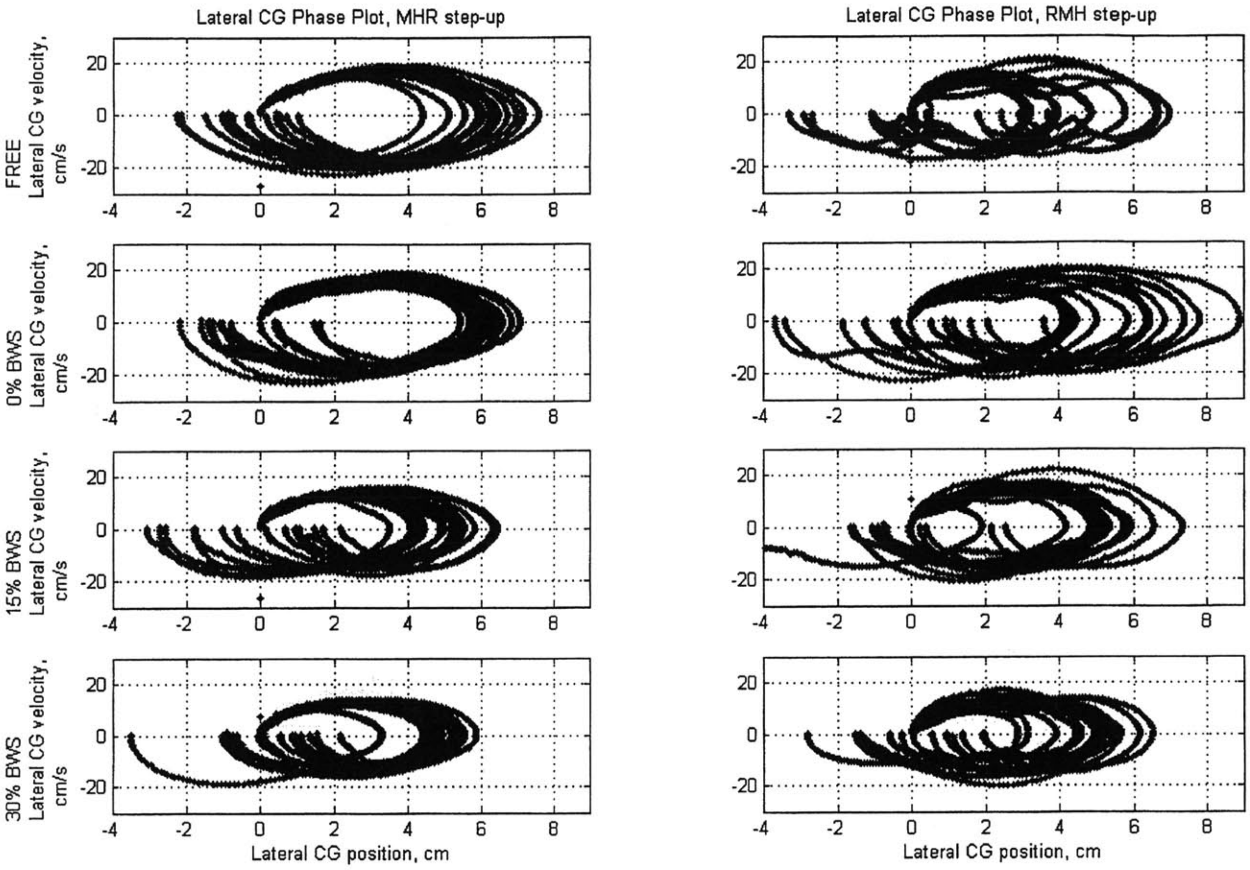

Figure 5.2-8: Lateral Cg phase plots during step-task for subject A on left and subject B on right

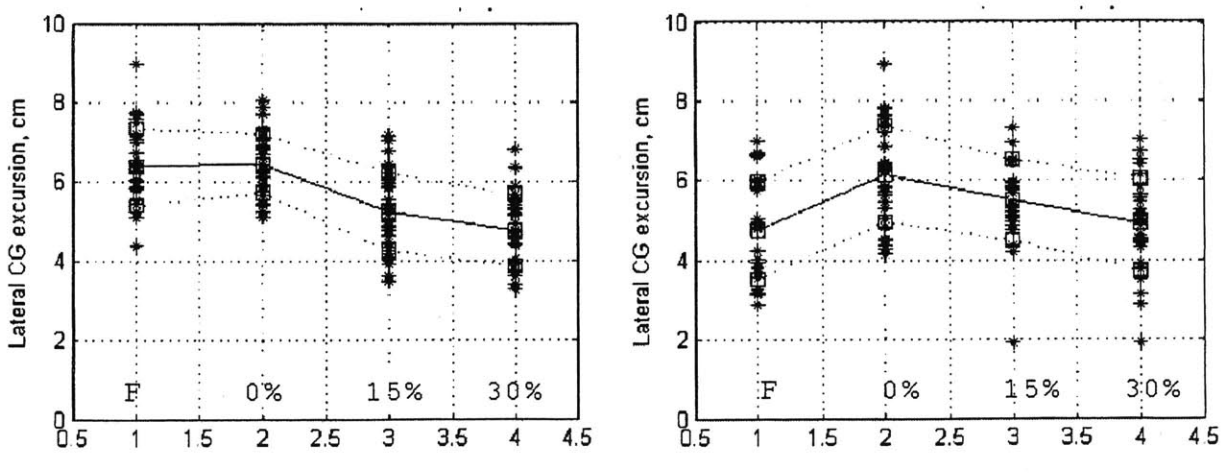

Figure 5.2-9: Lateral excursion of Cg during step-up vs. body-weight support for subject A on left and subject B on right.

5.2.3 Gait analysis: overground walking

Overground gait data was collected from the same two subjects tested in the previous section. Walking was analyzed in unconstrained as well as 0%, 15%, and 30% body-weight support conditions. In addition, subjects walked at both self-paced cadence and at 60 steps per minute. Gait data is only collected directly in front of the cameras so each pass contains one to two gait cycles.

Table 5.2-1, Table 5.2-2, Table 5.2-3, and Table 5.2-4 show the step length and cadence for each condition for both subjects. Only subject B's paced walk, in Table 5.2-4, has a similar step lengths in the unconstrained and mockup conditions. The other test shows a 15 to 30% reduction in step length when walking with the mockup compared to unconstrained walking. Self-paced trials also show a 10-20% reduction in cadence when walking with the mockup.

The mass of the mockup, the small linkage travel in the frontal direction, and the limited space for acceleration and deceleration in the gait analysis facility all probably contributed to the reduction in speed when walking with the mockup. Further decrease in step length can also be attributed to the presence of the mockup structure's lateral beam behind the subject.

Table 5.2-1: Subject A self-paced overground walk

Condition	Step Length, cm	Cadence, steps/min
Unconstrained	151	114.0
0% BWS	110	99.7
15% BWS	115	103.6
30% BWS	113	94.4

Table 5.2-2: Subject B self-paced overground walk

Condition	Step Length, cm	Cadence, steps/min
Unconstrained	151	101.3
0% BWS	133	92.6
15% BWS	126	86.4
30% BWS	128	89.0

Table 5.2-3: Subject A paced overground walk

Condition	Step Length, cm	Cadence, steps/min
Unconstrained	102	57.0
0% BWS	75	57.4
15% BWS	84	58.5
30% BWS	76	58.3

Table 5.2-4: Subject B paced overground walk

Condition	Step Length, cm	Cadence, steps/min
Unconstrained	118	56.5
0% BWS	109	65.4
15% BWS	107	65.1
30% BWS	110	54.0

Selected gait data from subject B's paced walk is shown in Figure 5.2-10, including center of gravity vertical position, left hip flexion, pelvis rotation in the coronal plane, and pelvis rotation in the transverse plane. As expected from the fact that all four conditions had similar step length and cadence, minimal differences in vertical Cg amplitude are observed.

There is a small decrease in hip extension in mockup walking as compared to unconstrained walking. The fact that the other three conditions have almost identical hip extension patterns makes this difference significant. Interestingly, there was a reduction in hip flexion when walking with 30% BWS. There is a difference in transverse pelvis rotation but it is probably not significant due to the fact that the trajectories in the unconstrained and in the 15% BWS conditions were identical. Coronal pelvis rotations shown in Figure 5.2-10 reveal no discernable effect on that motion from the constraints of the bicycle seat attachment.

Selected gait data for subject A's paced overground walking is shown in Figure 5.2-11. The vertical Cg translation has larger amplitude for unconstrained walking than for walking with the mockup, and Table 5.2-3 shows a corresponding 20-25% difference in step length between the two conditions. Data in Figure 5.2-2 on page 87 suggests that this increase in vertical Cg excursion is explained by the change in step length and is not due to the influence of the mockup.

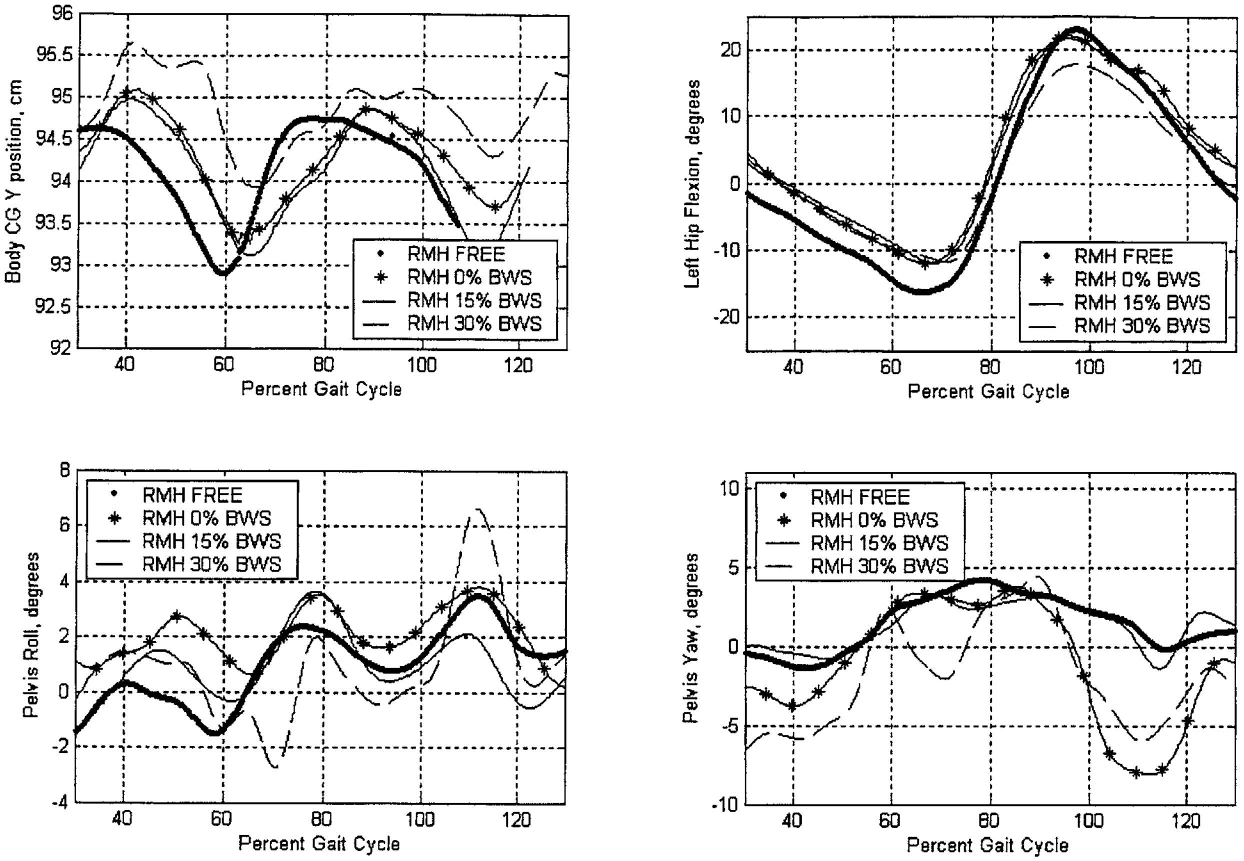

Figure 5.2-10: Displacement of the body center of gravity (CG) in the vertical direction (y), left hip flexion, pelvis coronal rotation (roll), and pelvis transverse rotation (yaw) for subject B during the paced-walk task.

Both hip flexion and extension are reduced in mockup walking relative to unconstrained walking, but the change could be a reflection of the shorter steps taken with the mockup. Transverse rotation of the pelvis had no change in amplitude between the four conditions. Coronal rotation of the pelvis was not reduced by the mockup attachment; in fact the amplitude of motion was increased in mockup walking, but the data is too noisy to be conclusive.

The gait analysis described in this chapter was a useful process for evaluating the concepts selected for the alpha prototype robot. While the data collected was not extensive enough to conclude that the differences in gait caused by the mockup were negligible, the data and qualitative observations together point to the viability of both the four-degree-of-freedom pelvis actuation concept and the bicycle seat attachment concept.

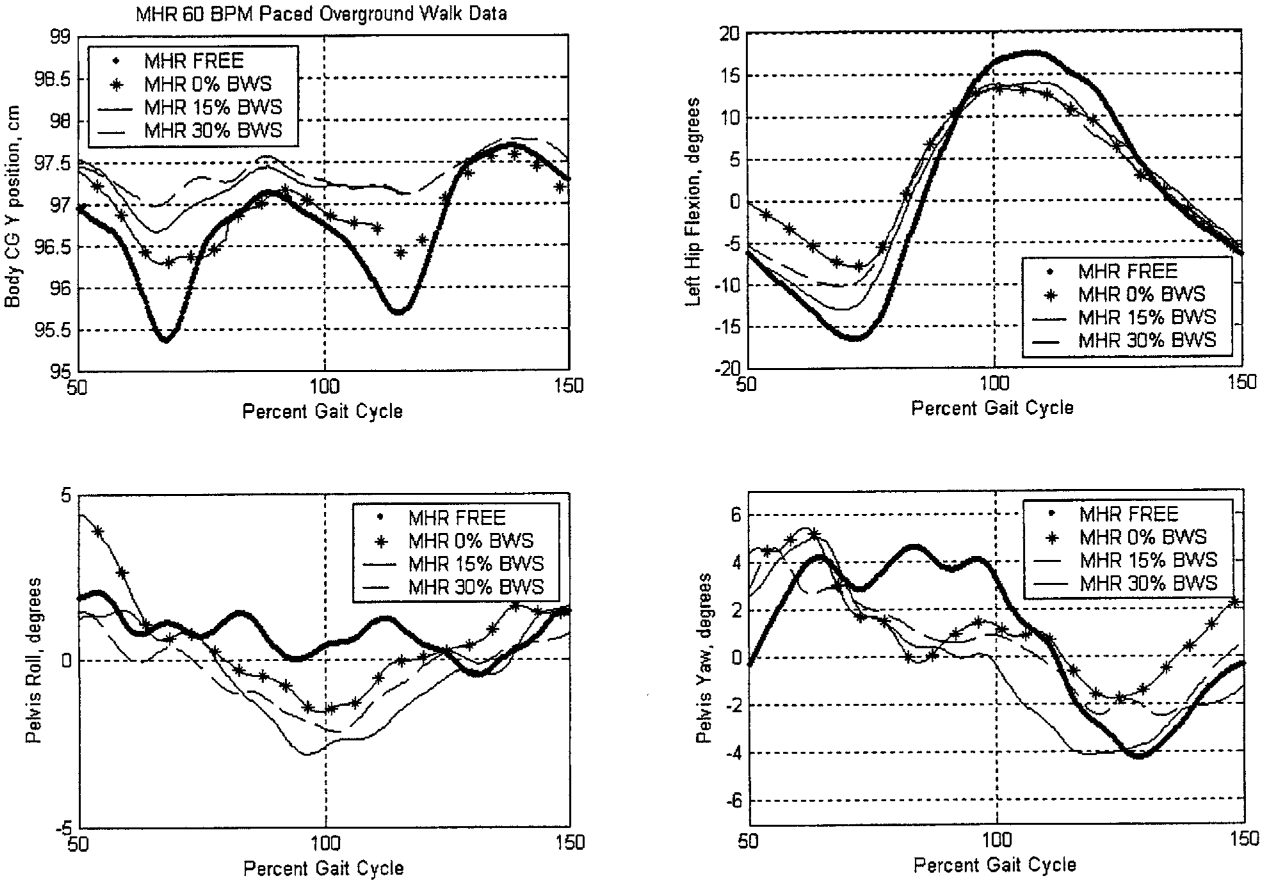

Figure 5.2-11: Displacement of the body center of gravity (CG) in the vertical direction, left hip flexion, pelvis roll, and pelvis yaw for subject A during the paced-walk task.

Chapter 6: Design Analysis

This chapter contains the calculations for the main aspects of the pelvis actuation module. These include the linkage design, spline selection, actuator selection, bearing selection, robot arm cross-section selection, L_1-L_4 shaft bolted joint analysis, L_1-L_4 joint stiffness analysis, vertical connection sub-module design, and body-weight support sub-module design.

6.1 Linkage design

This section contains a detailed analysis of the three-degree-of-freedom planar linkage for the alpha prototype pelvis actuation module. The overall arrangement of the links is established first, followed by calculations to determine optimal lengths for each link.

6.1.1 Overall linkage layout

The planar linkage connects three rotary motors to the patient's pelvis to actuate the frontal and lateral translations as well as the transverse rotation. It also transmits vertical loads to the patient. The geometry of the linkage relates motor torque, motion, and output impedance to force, motion, and impedance at the robot endpoint. Thus, the linkage geometry must be defined before the specifications for endpoint properties can be converted to motor specifications. The linkage and actuator combination must have a range of motion larger than the workspace and must meet endpoint impedance specifications within the workspace. The linkage should not cause large endpoint impedance variations within the workspace, and it should have similar friction and inertia in the two planar DOFs if possible. In meeting these requirements the linkage should have the shortest links possible and should not have any singularities in or near the workspace. The shorter the links the less stiff they must be and the less moment loads they will be subjected to in the vertical direction.

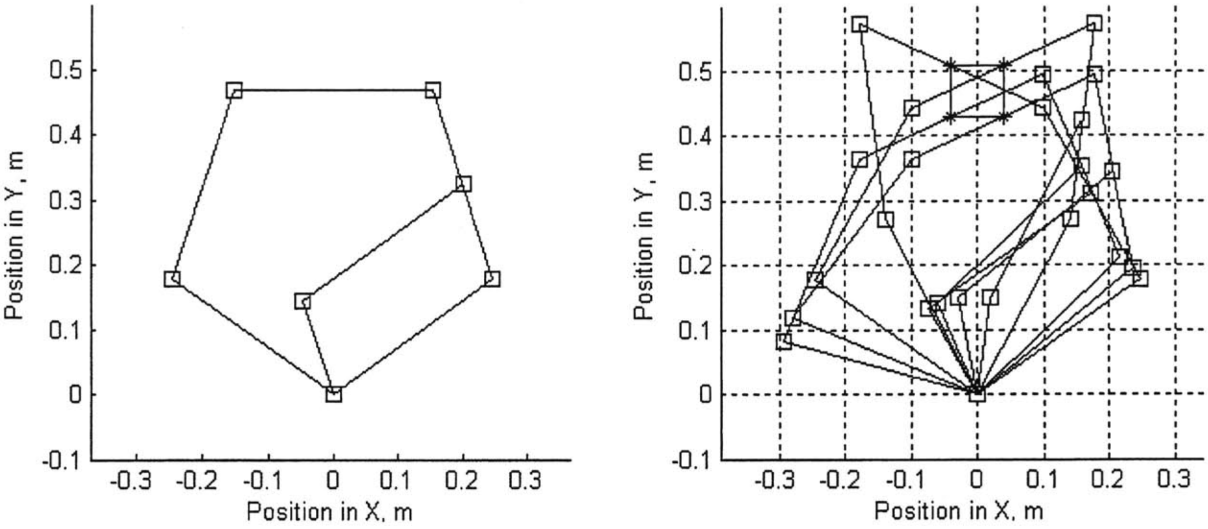

Figure 6.1-1: Mockup linkage configuration and workspace size

Figure 6.1-1 shows the mockup linkage configuration. The approximate workspace size is 8 cm by 8 cm in the planar translations. As shown in the figure the linkage approaches singularities at the edges of the workspace. A better arrangement of links is desired to improve the relative workspace size.

Simple mathematical tools allow for the analysis of existing linkages but do not help in linkage design. Therefore, the three-degree-of-freedom linkage must first be divided into modules. Two frontal translation modules combine for fore/aft and transverse rotation and additional module provides lateral translation. The proposed translation module is the crank shown in Figure 6.1-2. The crank consists of two links and one prismatic joint to guide the endpoint. Torque about the first link is converted into linear force along the prismatic joint F_L and perpendicular force F_P. The position of the crank can be described by either the angle of the first link θ or the position of the slider x. The physical dimensions of the crank are the link lengths L_1 and L_2 and the distance d between the origin and the slider. Detailed equations describing cranks are contained in *Appendix A: Supplementary Calculations*.

Cranks are of interest because they allow the analysis of each degree of freedom independently. Meaningful information about the likely interaction between degrees of freedom can also be derived from the values of d and F_P; length d represents the perpendicular motion imposed on the crank while force F_P represents the force that must be imparted on the crank to maintain straight motion. The crank equations for linear force, perpendicular force, position, and velocity are

6.1-1 $$F_L = \frac{\tau \sin\alpha}{L_1 \sin(\alpha - \theta)}$$

6.1-2 $$F_P = \frac{\tau \cos\alpha}{L_1 \sin(\alpha - \theta)}$$

6.1-3 $$x = L_1 \sin\theta + L_2 \sin\alpha$$

6.1-4 $$\dot{x} = \dot{\theta} L_1 \frac{\sin(\alpha - \theta)}{\sin\alpha}$$

where all dimensions are according to Figure 6.1-2 and the angle of the second link relative to horizontal is

6.1-5 $$\alpha = \cos^{-1}\left(\frac{d - L_1 \cos\theta}{L_2}\right)$$

Figure 6.1-3 shows the output force of a crank with dimensions $L_1 = 1$, $L_2 = 2$, and $d = 1$. Note that the crank angle is zero at $x = 2$. These figures show that the crank force characteristics are close to uniform near zero angle but diverge rapidly for both large positive and large negative angles. A linkage composed of cranks should allow motion in both directions to maximize workspace size relative to link length

To achieve the three planar degrees of freedom, three cranks are arranged as shown in Figure 6.1-4. The workspace of the linkage includes positive and negative crank angles, and the lateral linkage is perpendicular to the two frontal linkages. The dimensions of the overall linkage are link lengths L_1 through L_8 as well as the positions of the three motors. The patient attaches to this linkage at the end effector link L_7. In the sections that follow, each link is sized according to the constraints and specifications that affect it.

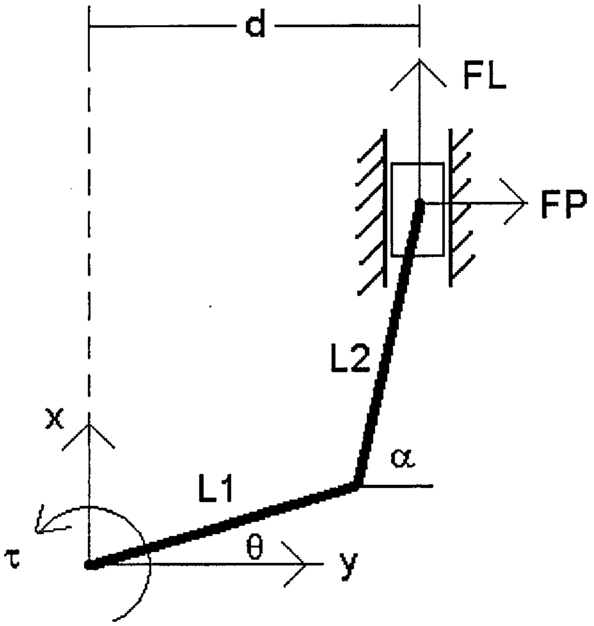

Figure 6.1-2: One-degree-of-freedom crank mechanism

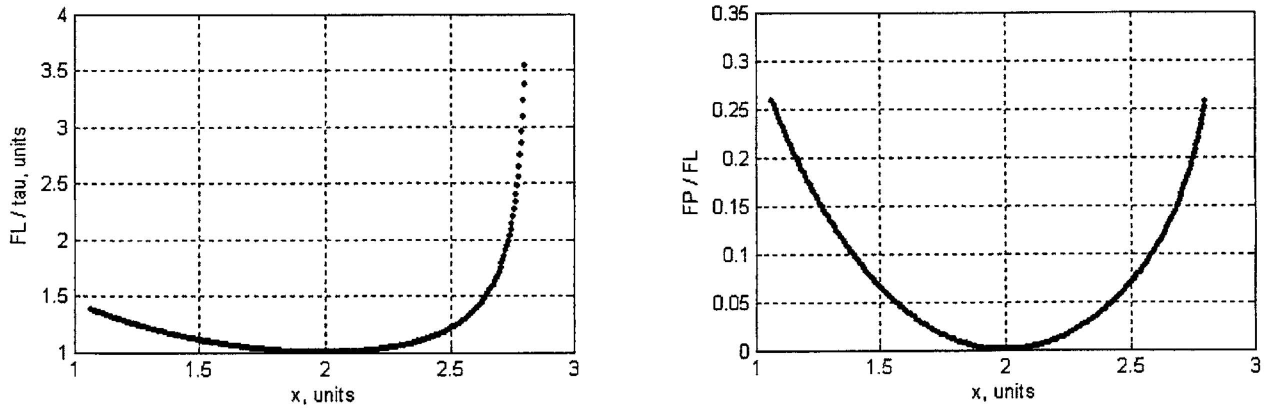

Figure 6.1-3: Force output of crank versus travel; $L_1 = 1$, $L_2 = 2$, $d = 1$

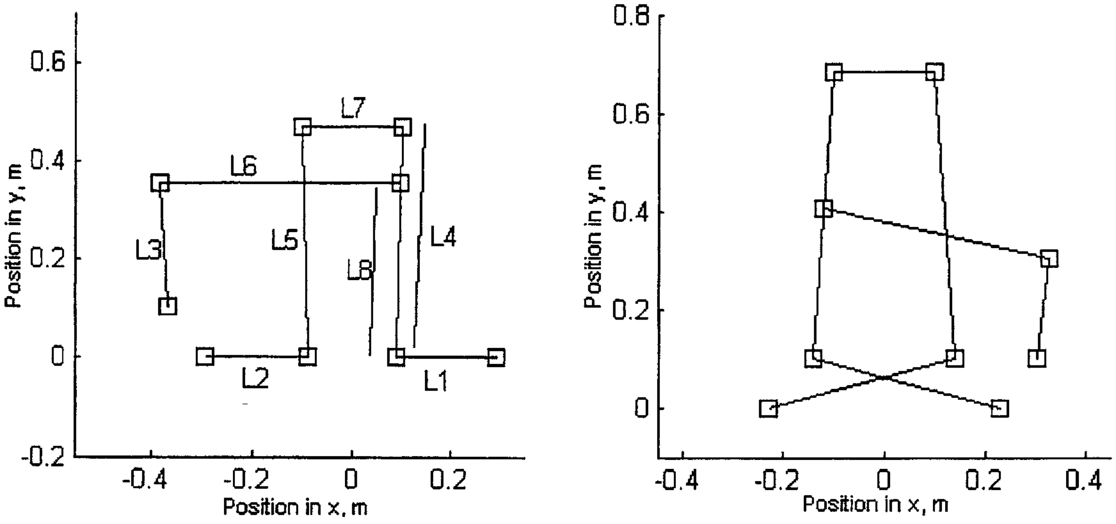

Figure 6.1-4: Three degree-of-freedom planar linkages composed of three cranks

6.1.2 Sizing L_7

The first step in sizing the linkage is choosing the length of L_7, the end effector link. As discussed in section 3.2.3, the maximum allowable inertia of the mechanism is the inertia of a person in the direction of travel. The ratios between the inertias in the linkage degrees of freedom should be the same as the ratios between the inertias of a person's degrees of freedom.

Figure 6.1-5 shows how the preceding principle can be applied to link L_7. Two mechanisms are used to move the hips in the fore/aft direction; they move in unison to translate the body and move in opposite directions to rotate the body. If each mechanism has inertia M, and if the mechanisms are a distance d apart, the inertia in the fore/aft direction is

6.1-6
$$I_{mech,f/a} = 2M$$

and the inertia of rotation about the middle of the line d is

6.1-7 $$I_{mech,r} = \frac{1}{2} d^2 M$$

The ratio of I_{rotate} to $I_{fore/aft}$ should be the same as that of the human body. Section 3.2.3 states that the fore/aft inertia of a human is 11.9 kg and the rotational inertia is 0.1243 kg-m^2. Therefore,

6.1-8 $$\frac{I_{mech,r}}{I_{mech,f/a}} = \frac{\frac{1}{2} d^2 M}{2M} = \frac{1}{4} d^2$$

6.1-9 $$d = \sqrt{4 \cdot \frac{I_{body,r}}{I_{body,f/a}}} = \sqrt{4 \cdot \frac{0.1243}{11.9}} = 204mm = 8.0in$$

The distance between the mechanisms that move the hips in the fore/aft direction should be 8 inches apart. Because the machine is designed in inch units, this length is rounded to 8 inches exactly, or 203 mm.

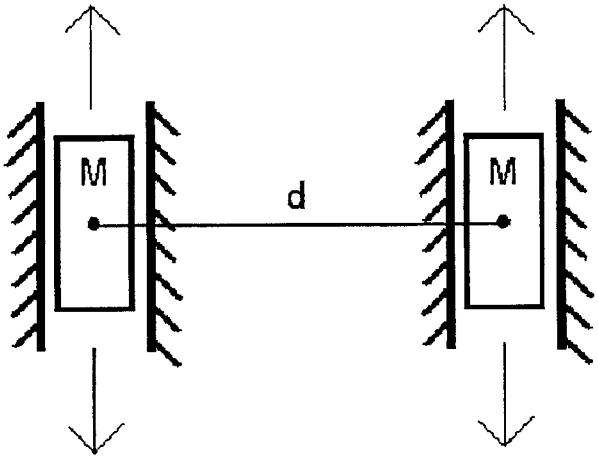

Figure 6.1-5: Two mechanisms that push each hip in the fore/aft direction represented as masses *M* separated by distance *d*

6.1.3 Frontal workspace

Once the length of L_7 is known, the specifications for fore/aft and rotational workspace can be converted into fore/aft translations at each hip. Section 3.2.1 specifies that the robot workspace must be $y_{WS} = 400$ mm in the frontal direction and $\Phi_{WS} = +/- 25$ degrees in the transverse rotation. The total frontal translation at each hip for this workspace size is therefore

6.1-10 $$WS = y_{WS} + L_7 \sin\Phi_{WS} = 400 + 203\sin(25°) = 486mm = 19.1in$$

The crank linkages that move each hip in the frontal direction should have a 486 mm (19.1 inch) workspace.

6.1.4 Sizing *L₄*, *L₅*

The mechanism must provide enough clearance behind the leg of the patient. At the same time, the mechanism must be as compact as possible to shorten the lever arms for both vertical and lateral forces. As shown in Figure 6.1-6, the links L_4 and L_5 should only be long enough to ensure leg clearance *CL*, provide room for the motor diameter D_{motor}, and allow linkage workspace travel *WS*:

6.1-11 $$L_{4,5} = CL + \frac{1}{2}D_{motor} + \frac{1}{2}WS = 200mm + 140mm + 243mm = 583mm$$

This equation assumes a motor diameter of 280 mm and a minimum clearance of 200 mm. Clearance was increased by 50% relative to the minimum value from the specifications in case the patient moves rearward out of the workspace. The length of the L_4 and L_5 arms should be 583 mm or 23 inches.

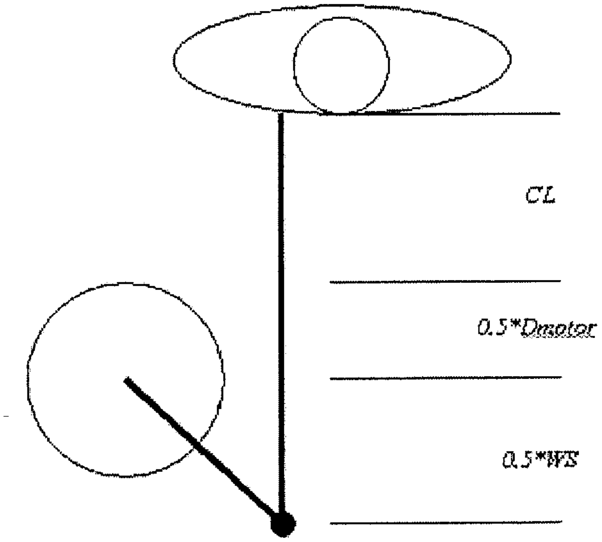

Figure 6.1-6: Required length of L_4 and L_5

6.1.5 Sizing L_1, L_2

Next, the length of the lever arms for the two fore/aft motors is determined. These two lengths are labeled L_1 and L_2 in Figure 6.1-4, and are connected to the links labeled L_4 and L_5, respectively. Because these links are symmetric, L_1 is used to refer collectively to L_1 and L_2 and L_4 is used for both L_4 and L_5. The effect of changing the length of L_1 is explored in Figure 6.1-7 and Figure 6.1-8. Both figures are computed for a workspace measuring 20 cm laterally, 40 cm frontally, and +/- 25 degrees rotationally. In addition, a d_0 value of $d_0 = L_1 - 0.019/L_1$ is used for all points, and L_4 is 583 mm as defined above.

As shown in Figure 6.1-3, the parasitic force is at a maximum at the extremes of the workspace and at a minimum at the workspace center. Figure 6.1-7 plots these maximum and minimum values of the parasitic force F_P/F_L for a range of values of L_1. It is desired that the maximum and minimum values have the same magnitude and opposite direction so that neither force will dominate the properties of the linkage. Figure 6.1-3 shows that this aim is achieved for a range of L_1 by making $d_0 = L_1 - 0.019/L_1$.

Another property of the crank shown in Figure 6.1-3 is that the ratio between input torque and output force is not constant. Curves showing the maximum and minimum values of F_L/τ in the workspace are plotted in Figure 6.1-8 for all values of L_1. The curves in the figure take into account frontal as well as lateral motion of the crank. The minimum value of F_L/τ determines the torque required to meet output force specifications. The maximum value dictates the maximum static friction force at the output for a given static friction torque at the motor.

To select the length of L_1, the force and friction at the endpoint must be calculated using both Figure 6.1-8 and the specifications of available motors. These values must then be compared to the desired machine specifications to choose an acceptable solution. Furthermore, other aspects of the design must be considered when selecting L_1, including the overall machine width and the clearance between moving components.

Figure 6.1-8 shows that a reasonable L_1 would be above 0.35 m to give adequate friction properties. The fact that L_1 will be at least that long makes it possible to consider a linkage in which L_1 and L_2 cross, as shown in Figure 6.1-4. This arrangement allows for a narrower machine while using the same link lengths. For a crossed link design, there must be clearance between the spline shaft and the joints so that the parts will not interfere and so that a person cannot get his or her fingers caught between the moving parts. The joints are estimated to have 2-inch diameters while the spline shaft and spline nut are estimated to have a 4-inch diameter. Thus the minimum distance between joint and shaft is 3 inches, plus 1 inch for finger clearance. The resulting L_1 is 16 inches or 0.406 m, and the resulting spline shaft spacing is 20 inches or 0.508 m.

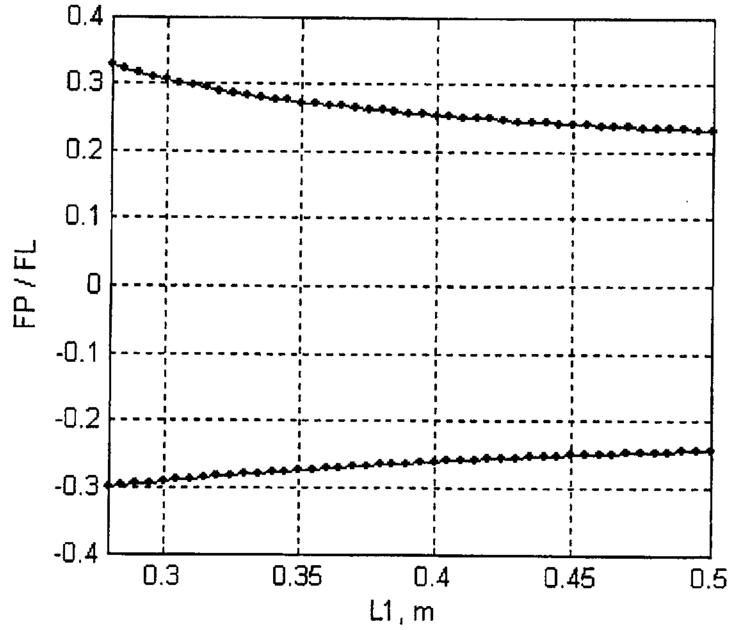

Figure 6.1-7: Maximum parasitic force F_P/F_L in each direction versus L_1

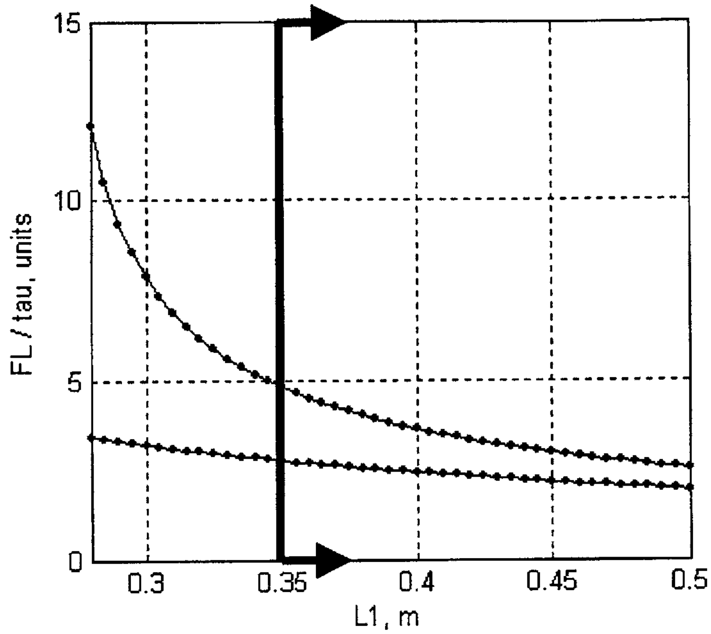

Figure 6.1-8: Maximum and minimum FL/t in the workspace versus L_1 in m

6.1.6 Lateral crank: sizing L_3, L_6

The lateral crank must produce a torque about L_4 to create lateral force at the endpoint. Since the force required is 167 N and the link length is 0.583 m, the torque required is approximately

6.1-12 $$\tau = F \cdot L = 167N \cdot 0.583m = 97N - m$$

where F is force and L is the link length.

Figure 6.1-9 shows a method for reducing the motor torque required to produce torque about L_4 by changing the relative link lengths. Link L_3 is shortened so that it is half the length of L_8. As shown in Figure 6.1-10, link L_6 and link L_1 remain nearly parallel throughout the workspace so the torque required from the lateral motor is not strongly dependent on frontal position.

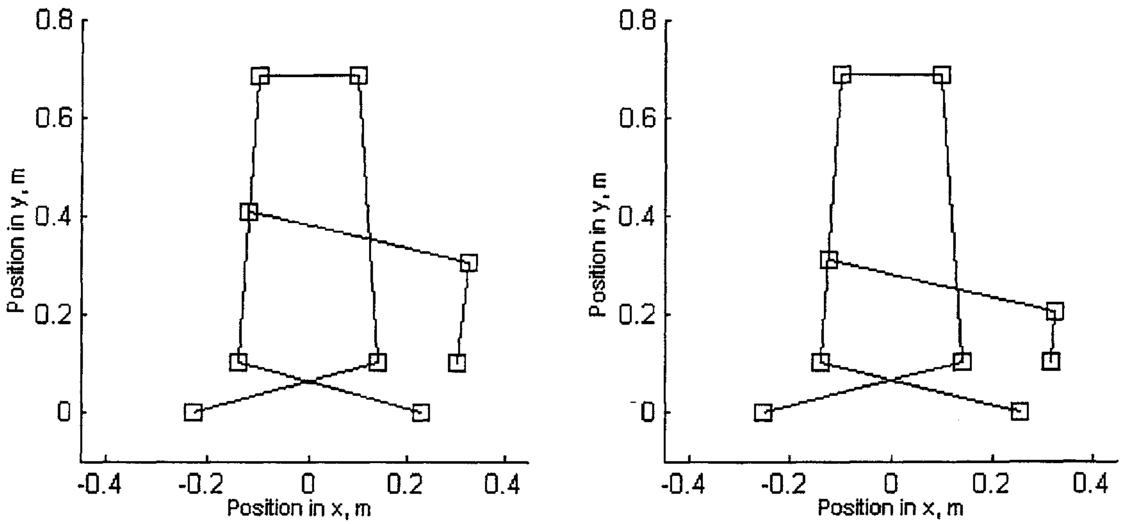

Figure 6.1-9: Changing the link lengths to reduce the torque requirement for lateral motion

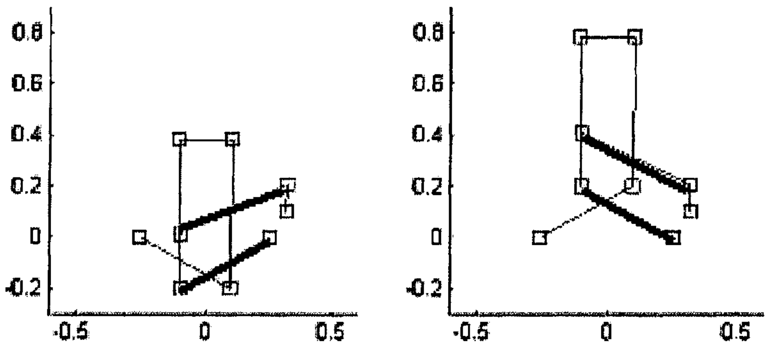

Figure 6.1-10: Lateral link L_6 (bold) remains nearly parallel to L_1 throughout frontal range of motion

The best combination of parameters were found to be $L_4 = 5.5$ inches, $L_8 = 11$ inches, and $L_6 = 21.5$ inches, with the lateral motor (motor 3) located 6 inches to the right of and 5.5 inches in front of the right frontal motor (motor 1).

6.1.7 Linkage summary

This section describes the procedure for sizing the planar linkage. Table 6.1-1 and Table 6.1-2 show the linkage dimensions arrived at through this process and the resulting linkage performance.

Table 6.1-1: Linkage dimensions

	Symbol	Value	Units
Spline Shaft 1 Position	x_1	10	*in*
	y_1	0	*in*
Spline Shaft 2 Position	x_2	-10	*in*
	y_2	0	*in*
Spline Shaft 3 Position	x_3	16	*in*
	y_3	5.5	*in*
Frontal Motor Lever Arms	L_1	16	*in*
	L_2	16	*in*
Lateral Motor Lever Arm	L_3	5.5	*in*
Fore/Aft Connecting Links	L_4	23	*in*
	L_5	23	*in*
Lateral Connecting Link	L_6	21.5	*in*
Patient Attachment Link	L_7	8	*in*
Lateral Link Joint	L_8	11	*in*

Table 6.1-2: Linkage performance

	Value	Units
Lateral Static Friction	5.4	*N / N-m*
Frontal Static Friction	6.7	*N / N-m*
Rotational Static Friction	0.80	*N-m / N-m*
Shaft 1 Torque	37.1	*N-m*
Shaft 2 Torque	37.9	*N-m*
Shaft 3 Torque	50.7	*N-m*
Shaft 1 Stiffness	218	*N-m / rad*
Shaft 2 Stiffness	216	*N-m / rad*
Shaft 3 Stiffness	385	*N-m / rad*
L4, L5 Axial Load	604	*N*
L6 Axial Load	1715	*N*

6.2 Spline selection and loading

This section shows the process of selecting spline shafts. The loads on the nuts are determined, then the moment on the shaft is found; the loads are used to size the spline shaft. Finally, a method for connecting the spline shafts to the motors is designed.

6.2.1 Radial load on spline nuts

The gait-training device will provide partial body weight support and will impart horizontal forces on the patient. These forces will be transmitted through the linkage to the splines. Two of the splines will support radial loads only, while one spline will support radial load and body-weight loads. Figure 6.2-1 shows a diagram of the latter spline, and illustrates how the forces at the endpoint are transferred to radial forces on the two spline-nuts.

The radial force F_r and body weight force F_w are known from the specifications of the machine. Also, the length of the longest possible moment arm L_a is known from the dimensions of the linkage. What is left is to relate the spline nut spacing d to the radial loads at the spline nuts P_1 and P_2. In terms of the values defined above, the equations are

6.2-1
$$P_1 = \frac{F_w L_a}{d} + \tfrac{1}{2} F_r$$

6.2-2
$$P_2 = -\frac{F_w L_a}{d} + \tfrac{1}{2} F_r$$

These values can be used in a beam-bending calculation to find the loading on the shaft along its length. Also, the radial loads on the spline nuts are important for calculating spline life.

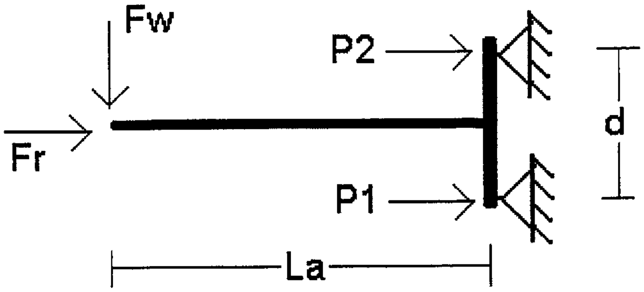

Figure 6.2-1: Radial forces at the spline nuts and endpoint forces on the robot arm

6.2.2 Maximum moment on spline

The spline that supports the vertical loads will have two nuts, will be fixed at the motor end, and will be simply supported at the opposite end. Figure 6.2-2 shows a diagram of the loading condition.

The maximum moments on the spline shaft can be found through beam bending equations. Using singularity functions, the loading condition of the shaft is expressed by

6.2-3 $$q(x) = M_1\langle x\rangle_{-2} + F_1\langle x\rangle_{-1} + P_1\langle x-a\rangle_{-1} + P_2\langle x-b\rangle_{-1} + F_2\langle x-L\rangle_{-1}$$

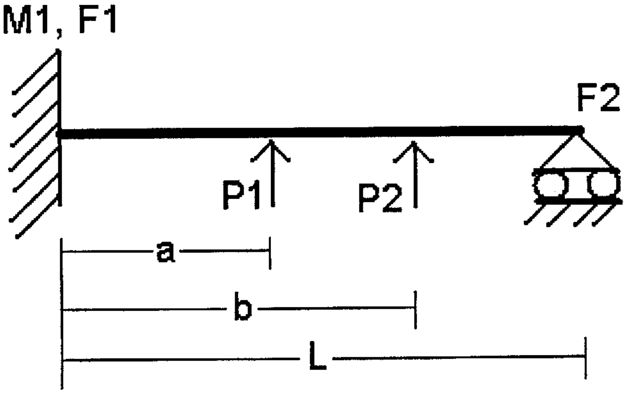

Figure 6.2-2: Loads on the spline shaft

The spline nut forces P_1 and P_2 were calculated in the previous section and the support loads F_1, M_1, and F_2 are unknown. For a review of singularity functions refer to *Appendix A: Supplementary Calculations.* Equation 6.2-3 can be integrated four times to find the shear, moment, angle, and displacement of the beam:

6.2-4 $$V(x) = \int -q(x)dx = -M_1\langle x\rangle_{-1} - F_1\langle x\rangle^0 - P_1\langle x-a\rangle^0 - P_2\langle x-b\rangle^0 - F_2\langle x-L\rangle^0 - C_1$$

6.2-5 $$M(x) = \int -V(x)dx = M_1\langle x\rangle^0 + F_1\langle x\rangle^1 + P_1\langle x-a\rangle^1 + P_2\langle x-b\rangle^1 + F_2\langle x-L\rangle^1 + C_1x + C_2$$

6.2-6 $$\begin{gathered} EIv'(x) = \int M(x)dx = \\ M_1\langle x\rangle^1 + \frac{1}{2}F_1\langle x\rangle^2 + \frac{1}{2}P_1\langle x-a\rangle^2 + \frac{1}{2}P_2\langle x-b\rangle^2 + \frac{1}{2}F_2\langle x-L\rangle^2 + \frac{1}{2}C_1x^2 + C_2x + C_3 \end{gathered}$$

6.2-7 $$\begin{gathered} EIv(x) = \int EIv'(x)dx = \\ \frac{1}{2}M_1\langle x\rangle^2 + \frac{1}{6}F_1\langle x\rangle^3 + \frac{1}{6}P_1\langle x-a\rangle^3 + \frac{1}{6}P_2\langle x-b\rangle^3 + \frac{1}{6}F_2\langle x-L\rangle^3 + \frac{1}{6}C_1x^3 + \frac{1}{2}C_2x^2 + C_3x + C_4 \end{gathered}$$

The integrations require the definition of constants of integration C_1, C_2, C_3, and C_4. Boundary conditions are needed to solve for these values.

The first boundary condition is that the moment of the shaft at the cantilevered end is equal to M_1. Thus,

6.2-8 $$M(x=0) = M_1 + C_2 = M_1$$

6.2-9 $$C_2 = 0$$

Next, because the cantilevered end is held fixed it cannot rotate, so $v'(x = 0) = 0$. The only variable left on the right side of the equation for $v'(x = 0)$ is C_3, so

6.2-10 $$C_3 = 0$$

Another consequence of the cantilevered condition is the fact that that end must have zero displacement. Setting $x = 0$, the only variable left on the right side of the equation for v is C_4.

6.2-11
$$C_4 = 0$$

Unlike at the cantilevered end, the boundary conditions stipulate that the moment at the simply supported end of the shaft is zero. Therefore,

6.2-12
$$M(x = L) = M_1 + F_1 L + P_1(L - a) + P_2(L - b) + C_1 L = 0$$

The final boundary condition is that the displacement at the simply supported end must be zero. The equation for this condition is

6.2-13
$$EIv(x = L) = \frac{1}{2} M_1 L^2 + \frac{1}{6} F_1 L^3 + \frac{1}{6} P_1 (L - a)^3 + \frac{1}{6} P_2 (L - b)^3 + \frac{1}{6} C_1 L^3 = 0$$

The unknowns left are C_1, F_1, M_1, and F_2. The final two equations required are that the sum of the forces and the sum of the moments on the beam are zero.

6.2-14
$$\sum F = F_1 + P_1 + P_2 + F_2 = 0$$

6.2-15
$$\sum M = M_1 + P_1 a + P_2 b + F_2 L = 0$$

Solving these equations in terms of P_1 and P_2 and the dimensions of the beam yield the following results:

6.2-16

$$M_1 = \frac{1}{2L^2}\left[P_1L^2(L-a)+P_2L^2(L-b)-P_1(L-a)^3-P_2(L-b)^3\right]$$

6.2-17

$$F_1 = \frac{1}{L}\left[M_1 - P_1(L-a) - P_2(L-b)\right]$$

6.2-18

$$F_2 = -F_1 - P_1 - P_2$$

6.2-19

$$C_1 = -\frac{2M_1}{L}$$

Using these values, the moment on the beam as well as the angle and deflection can be calculated along its entire length.

6.2.3 Size spline shaft

The equations presented in the preceding section solve for the bending moments, angles, and deflections in the spline shaft. By combining those equations with the required load-carrying capability and the specifications of the ball-splines available the correct spline size can be chosen. Table 6.2-1 shows the relevant specifications.

THK splines were chosen for this design. The LT line of splines was chosen because they perform better when subjected to bending moments than the LS line. Table 6.2-2 shows the specifications for three sizes of spline that may be suitable for this machine.

Table 6.2-1: Spline specifications

	Max	Units
Vertical workspace	300	*mm*
Body weight support loads	628	*N*
Fall support loads	6280	*N*
Planar Force Produced	166	*N*
Static Friction	8.3	*N*
Maximum Moment Arm	1194	*mm*

While the required travel is known, the spacing between the two load-bearing spline nuts is not. Figure 6.2-3 plots the maximum moment in the spline shaft as the nut spacing is changed. The values plotted are the maximum moment reached for all points along the vertical travel. Figure 6.2-3 shows that the minimum desirable spline nut spacing is slightly over 0.2 m.

At any given position of the spline nuts, the maximum moment can be at either the cantilevered motor bearing supports or at one of the spline nuts. As shown in Figure 6.2-4, when the nuts are near the top of their travel the maximum moment is found at the cantilevered base. Figure 6.2-5 shows the maximum moment at any point in the shaft as the spline nuts move throughout their travel.

Table 6.2-2: Spline parameters [65]

	LT30	LT40	LT50	Units
Nominal Diameter	30	40	50	*mm*
Spline Nut Mass	375	1000	1950	*g*
Spline Nut Length	80	100	125	*mm*
Spline Nut Diameter	47	64	80	*mm*
Basic Load Rating	20.5	37.8	60.9	*kN*
Basic Torque Rating	148	377	769	*N-m*
Maximum Allowable Moment	253	602	1176	*N-m*
Static Friction	2.45*	4.90*	7.84*	*N*

* - Friction values for CL-spec nut preload

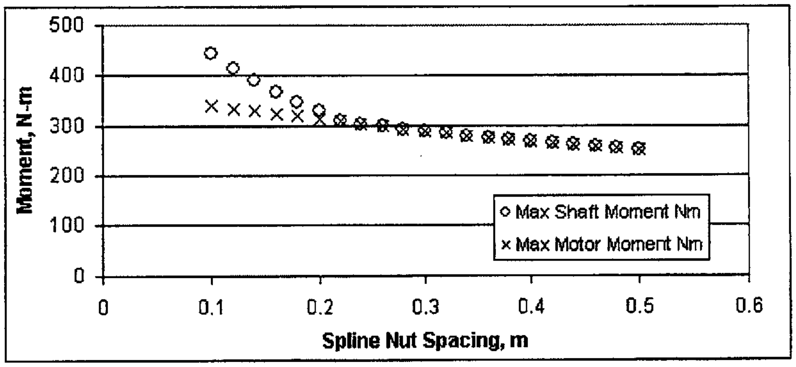

Figure 6.2-3: Maximum moment in the shaft and the maximum moment at the motor bearing supports for spline nut spacing 0.1 m to 0.5 m

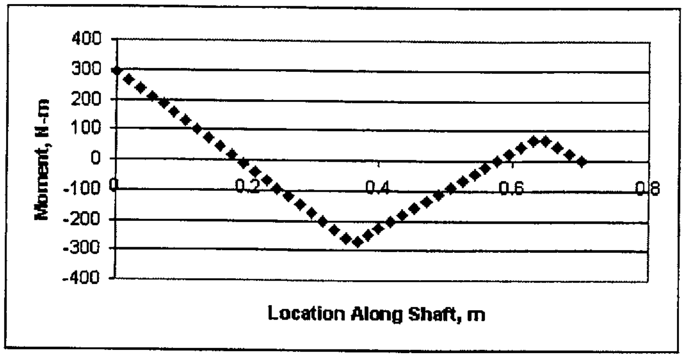

Figure 6.2-4: Moment in the shaft for nut spacing of 0.3 m and the nuts at the top of their travel

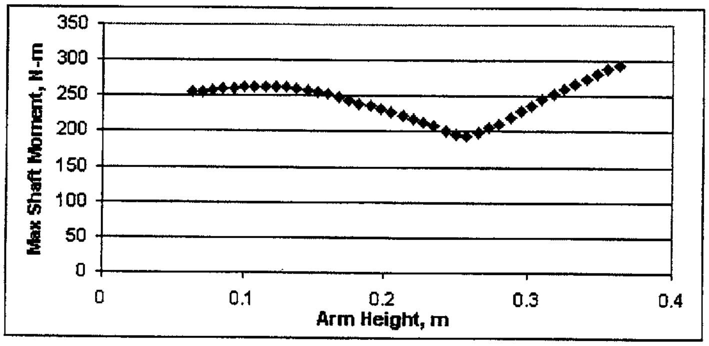

Figure 6.2-5: Maximum moment in the loaded shaft versus vertical position

Another important characteristic to evaluate is the expected life of the spline nuts. To calculate this value, an equivalent radial load must first be found from the torque and radial loads by the equation [65]

6.2-20
$$P_E = P_C + \frac{4 \cdot T_C \times 10^3}{i \cdot dp \cdot \cos\alpha}$$

where P_C and T_C are the applied radial and torque loads, respectively, and i is the number of ball trains in the spline nut, α is the contact angle of the balls, and dp is the ball center-to-center diameter. This equivalent radial load is then entered into the nominal life equation [65]

6.2-21 $$L_{km} = \left(\frac{f_T \cdot f_C}{f_W} \cdot \frac{C}{P_E} \right)^3 \times 50$$

where L_{km} is the nominal life in kilometers, C is the basic dynamic load rating, and f_T, f_C, and f_W are the temperature, contact, and load factors, respectively. The temperature factor is less than unity if the temperature is above 100 Celsius, so it is not relevant for this design. The contact factor is unity if there is one nut on a shaft but drops to 0.81 for two nuts. Finally, the load factor represents the vibration and impact encountered by the machine; for the spline bearing vertical loads this was set to 2 (medium to heavy shock loads) while for the other two splines this factor was 1.5 (light to medium shock loads) [65].

Converting the average life in km to an approximate value in time units requires an average velocity. The step rate and the vertical amplitude multiplied together is the upper bound,

6.2-22 $$v_{avg} = 4 \cdot SR \cdot A_{vert} = 0.3864 m/s$$

with a multiplier of four to account for the fact that each step raises and then lowers the center of gravity by twice the amplitude. To compute the life of the spline in weeks, assume forty hours of use per week and match the units:

6.2-23 $$L_{wks} = \frac{L_{dist}}{v_{avg}} = \frac{L_{km}}{55.64} weeks$$

Table 6.2-3 shows the results for the spline loading calculations including the moment in the shaft, deflection, angle, and life. Based on the data in Table 6.2-3, the 50 mm spline shaft was chosen to bear vertical loads while 40 mm spline shafts will be used for the other two degrees of freedom. This combination of shafts has long life, high stiffness, and adequate safety factor. Of particular concern is added stress on the load-bearing spline caused by stress concentrations at the supports. The principal drawback of using these splines is the high friction: total vertical friction is 25.5 N, over three times the specified desired amount in Table 6.2-1. The spline nuts will be specified with CL preload. This is a light preload that allows for alternating torques without backlash, high stiffness and low friction [65]

Table 6.2-3: Spline loading

	Load	Load	No Load	No Load	Units
Shaft Diameter	50	40	40	30	*mm*
Spline Nut Spacing	0.275	0.3	*N/A**	*N/A**	*m*
Moment	294.2	290.7	45.9	45.9	*N-m*
Moment Safety Factor	4.0	2.1	13.1	5.5	
Deflection	0.123	0.29	0.091	0.29	*mm*
Angle	0.00053	0.0013	0.00049	0.0012	*rad*
Nut Radial Load	2879	2653	341	341	*N*
Motor Moment Load	294.2	290.7	45.9	45.9	*N-m*
Motor Radial Load	1565	1571	294	303	*N*
Support Radial Load	1224	1231	328	331	*N*
Nominal Life, distance	2811	502	7300	521	*km*
Nominal Life, time	50.5	9.02	131	9.36	*weeks*

*- *Not applicable*

6.2.4 Spline shaft to motor connection

The connection between the spline shafts and the motors is critical. The most important connection is for the load-bearing spline. This connection must accurately locate the shaft, transmit torque loads, transmit bending moments, and must be removable. The connection for the other two shafts has the same requirements but with much lower bending moments.

A design such as the one shown in Figure 6.2-6 was chosen for this connection. A taper and a groove will be machined into the end of the shaft so that a collar can clamp the shaft into a matching taper in the motor bore. Because the spline shafts for the load-bearing and non load-bearing shafts have different-sized tapers, motors with two different shafts must be manufactured.

Morse standard tapers were chosen because they have a long, shallow taper that increases the effective clamping pressure on the interface [44]. To find the amount of pressure at the interface needed to transmit the torque and bending moments, equations from Slocum's Precision Machine Design were used [56]. The first equation relates the minimum pressure to the torque,

$$P_{\min,torque} = \frac{2T}{\mu \pi D^2 L} \tag{6.2-24}$$

where $P_{min,torque}$ is the minimum pressure required to transmit a desired torque T, μ is the coefficient of friction, D is the interface diameter and L is the interface length. This calculation is for a cylinder so the small end of the taper is used as the diameter and the result is conservative. To resist bending moments, the pressure times the coefficient of friction has to be at least equal to the maximum stress in the shaft [56], or

$$P_{\min,bend} = \frac{\sigma_{\max}}{\mu} \tag{6.2-25}$$

where $P_{min,bend}$ is the minimum pressure to resist bending and σ_{max} is the highest compression or extension stress at the surface of the beam. This stress is given by

$$\sigma_{\max} = \frac{M_{\max} c}{I} \tag{6.2-26}$$

where M_{max} is the shaft support bending moment calculated from the equations in the previous section, c is the distance from the section centerline or half the diameter, and I is the section modulus or $\pi d^4/64$ for a shaft of diameter d. In this case the diameter used is for the largest diameter of the taper.

Shear loads on the shaft can cause it to deform, lessening the contact pressure. This pressure decrease can be expressed as

$$P_{\min,shear} = \frac{V}{DL} \tag{6.2-27}$$

where V is the shear load. Slocum states that this is a lower bound on the value of $P_{min,shear}$, but at least the equation gives an estimate of the magnitude [56].

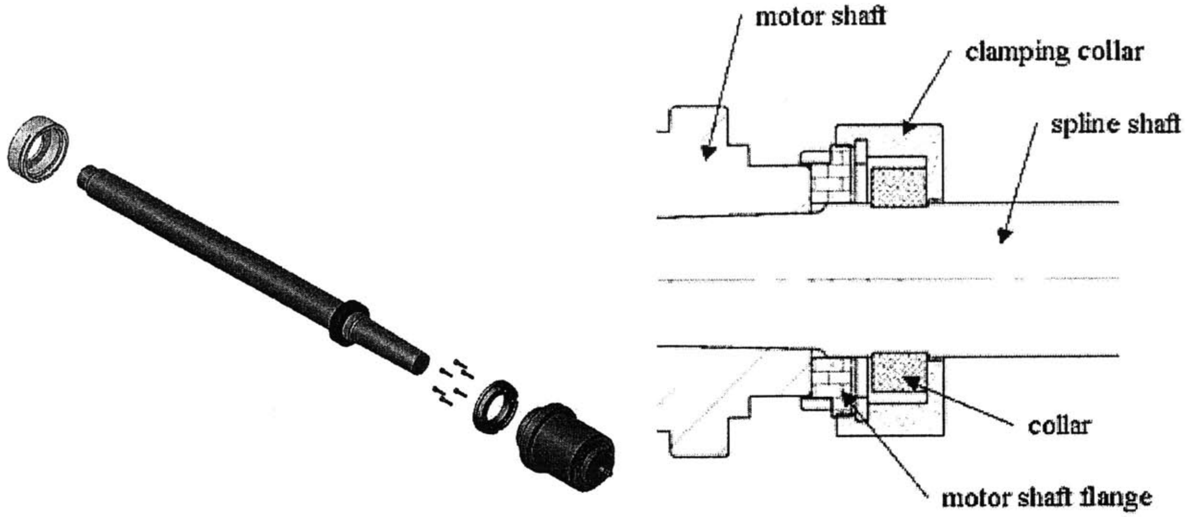

Figure 6.2-6: Spline shaft mounting design

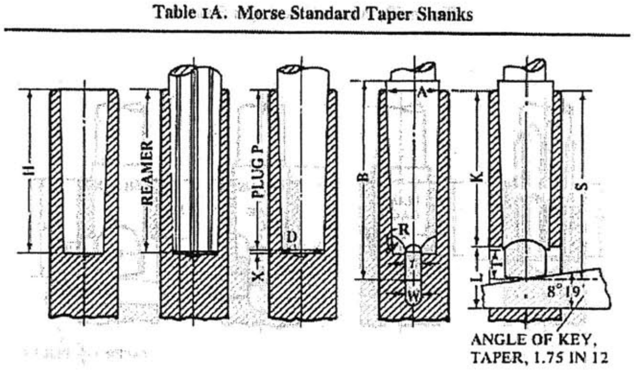

Figure 6.2-7: Standard taper dimensions [44]

Finally, the geometry of the tapered joint must be used to relate the clamping force pushing the shaft into the bore to the resultant pressure at the interface between the two parts. This relation can be expressed as

6.2-28
$$F_C = P \cdot \sin\theta \cdot \frac{1}{4}\pi\left(D_1^{\,2} - D_2^{\,2}\right)$$

where F_C is the clamping force, P is the resultant pressure, and D_1 and D_2 are the diameters of the large and the small ends of the taper, respectively. The sine of the angle of the taper, $\sin\theta$, can be expressed more easily in terms of the dimensions of the parts as

6.2-29

$$\sin\theta = \frac{D_1 - D_2}{2L}$$

Using these equations, the minimum pressure required to resist the necessary torsional, bending, and shear loads can be summed to find the total required pressure, and then the geometry of the taper can be used to convert this required pressure into a clamping force. To make the calculation of pressure conservative, a safety factor of two is used for the torque load, the bending stress and the shear load. Also, μ is set to either 0.2 or 0.3, an approximate value for steel on steel [56].

Table 6.2-4: Spline shaft coupling calculations

	Label	Load	No Load	Units
Shaft Diameter	D_{shaft}	50	40	*mm*
Rated Torque	T	160	160	*N-m*
Max Bending Moment	M	294	45.9	*N-m*
Shear Load	V	1564	303	*N*
Safety Factor	SF	2	2	
Coefficient of Friction	μ	0.2	0.2	
Large Taper Diameter	D_1	0.04440	0.03127	*m*
Small Taper Diameter	D_2	0.03747	0.02632	*m*
Taper Length	L	0.1318	0.09621	*m*
Sine of Taper Angle	$\sin\theta$	0.02631	0.02569	
Moment of Area	I	$1.908\text{x}10^{-7}$	$4.692\text{x}10^{-8}$	m^4
Distance From Centerline	c	0.02220	0.01563	*m*
Max Stress	σ_{max}	34.22	15.29	*MPa*
Torsion Pressure	$P_{min,torque}$	5.508	15.28	*MPa*
Bending Pressure	$P_{min,bend}$	342.2	152.9	*MPa*
Shear Pressure	$P_{min,shear}$	0.6341	0.232	*MPa*
Total Pressure	P	348.3	168.5	*MPa*
Clamping Force	F_C	4086	967.4	*N*

6.3 Actuator and sensor selection

This section explores the selection of rotary motors for the planar linkage, a linear motor for the vertical degree of freedom, and a six-degree-of-freedom force transducer for the robot endpoint.

6.3.1 Rotary motors

Selecting rotary motors for this application is an involved process. From section 4.2.1 it is known that direct drive rotary actuators will be used. The next step in the specification process is to select motor type and brand. Brushless servomotors are used for this robot instead of brushed motors because brushless motors are smoother and last longer with less maintenance. In particular, Kollmorgen direct drive rotary (DDR) motors are chosen because of their high torque, low cogging, and relatively low inertia [14].

Table 6.3-1 shows the properties of some Kollmorgen DDR housed motors with suitable continuous stall torque. Recall from Table 6.1-2 that the minimum continuous torque is 38 N-m for the two fore/aft motors and 51 N-m for the lateral motor. The D101 is strong enough for the fore/aft motors while the D083 and the D102 meet the lateral motor requirements. The D083 is the better-suited motor for both applications: its weight and rotary inertia are significantly lower than the D101 and the D102 [14].

Table 6.3-1: Properties of some Kollmorgen DDR housed motors [14]

	D082	**D083**	**D101**	**D102**	***Units***
Continuous Stall Torque	28.7	56.0	40.7	74.6	*N-m*
Continuous Stall Current	4.59	4.68	4.50	4.77	A_{rms}
Peak Torque	92.2	160	129	210	*N-m*
Maximum Speed	300	250	300	200	*rpm*
Weight	21.5	28.8	31.5	43.8	*kg*
Inertia	0.0194	0.0301	0.0693	0.0992	*kg-m*^{2}
Diameter	217	217	280	280	*mm*
Length	169	209	188	251	*mm*
Maximum Moment Load	70.9	53.3	192.4	146	*N-m*

The housed D083 motor faces some problems. From Table 6.2-3 on page 117, the expected maximum moment loads are 294 N-m for the motor driving the load-bearing spline and 46 N-m for the locating link motors. As shown in Table 6.3-1, the housed D083 cannot support the load-bearing spline in a direct-drive arrangement. Also, the housed DDR motors are assembled either with resolvers or with sine encoders. Both of these sensors are designed to work with the Kollmorgen servo amplifiers, but Copley servo amplifiers are preferred because they are less expensive, easier to use, and can be mounted on a 4-card chassis for a compact design [11]. Another problem with the housed DDR motors is that they have static friction on the order of 1-1.2 N-m, according to the distributor; this value is at the limit allowed by the specifications as discussed earlier in this section. Finally, the housed motor would not be able to connect to the taper at the end of the spline shaft as discussed in Section 6.2.4.

The use of frameless motors solves the above problems. Therefore, the frameless version of the D083 DDR, called the F5732, will be used for all three rotary motors. The housing for the motor will be custom-made[2] so that its bearings (paired deep-groove ball bearings) can withstand the maximum applied moment loads and so that an encoder that is compatible with Copley servo amplifiers can be used. The servo amplifier should have at least 4.7 A_{rms} continuous current output, as shown in Table 6.3-1. A suitable model is the Accelus ASC-055-18 with 6 A_{rms} continuous current and 18 A_{rms} peak current [11].

If possible, the encoder used should have a resolution higher than the highest useful value. The highest useful encoder resolution is that for which, at the maximum motor stiffness, moving the motor one count of resolution produces one bit to change in the command torque. The same stiffness can be achieved with a lower resolution by incrementing the command torque by more than one bit per count of displacement, but smoothness will suffer. Likewise, the same stiffness is achievable with higher resolution by only incrementing torque every other count of displacement, but there will be no performance gains for the higher resolution.

Therefore, the highest useful encoder resolution R_{ENC} in counts/revolution is

---

[2] The author would like to thank Mike Sandman at Interactive Motion Technologies for designing the housings for the rotary motors.

6.3-1
$$R_{ENC} = 2\pi \frac{K_\theta R_{OUT}}{2\tau_{PEAK}}$$

where K_θ is the maximum motor stiffness in N/radian, R_{OUT} is the resolution of the command torque in counts from *-PEAK* to *+PEAK*, and $2\tau_{PEAK}$ is twice the peak motor torque in N/m, or the total range of possible command torques. The values for equation 6.3-1 are the highest value of K_θ from Table 6.1-2 of 385 N-m/rad, peak torque of 160 N-m from Table 6.3-1, and the R_{OUT} that the Copley Accelus amplifier accepts of 12-bits. Entering those values into equation 6.3-1 yields a highest useful encoder resolution of R_{ENC} =31000 counts or 14.9 bits.

Based on the analysis above, a 16-bit encoder is selected. The higher resolution should increase smoothness for slow movements and help to improve the stability of the robot. The encoder specified is the Gurley Vx20 virtual absolute encoder with VB interpolator that yields 16 bits of total resolution. The 'virtual absolute' encoder uses a random sequence of bits on the outer ring to be able to determine its position absolutely once the disc moves about 10 counts. Therefore the motor does not need a homing sequence upon startup [19].

Table 6.3-2: Rotary motor summary data

Quantity	*3*
Transmission	*Direct drive*
Type	*Kollmorgen F-series*
Model	*F5732*
Encoder Type	*Gurley 'virtual absolute' optical*
Interpolator	*Gurley VB*
System Resolution	*16 bits per revolution*
Max. Bearing Moment Loads	*294 N-m*
Max. Static Friction Torque	*1.2 N-m*
Amplifier	*Copley Accelus ASC-055-18*
Continuous Stall Current	*4.68* A_{RMS}

6.3.2 Linear motor

A linear motor is required to drive the robot in the vertical degree of freedom. The steps to specifying this linear motor are to select the motor type and size, choose a servo amplifier to power the motor, check that the linear bearings that come with the motor can carry the required loads, and specify the sensor so that the linear motor can achieve a high enough stiffness for the application.

Past work in this lab has shown that Copley linear motors provide a good combination of force and low friction. Furthermore, Copley linear motors are available as modules that include linear bearings and optical encoders, so all the customer must do is choose the motor size, length, and encoder resolution. Copley also manufactures servo amplifiers; as discussed in Section 6.3.1, the use of Copley servo amplifiers is advantageous because they can be mounted in card slots for compact electronics packaging.

The first step is to size the linear motor. While this motor will not need to produce the body weight support forces, it will need to be strong enough to alter the endpoint impedance of the device. In other words, it must produce enough force to implement a controller that could lower the machine's apparent inertia and friction. Because viscous friction specifications are not available for the ball-screw splines, static friction and inertia are used to estimate the force required. The force due to these two factors is calculated using the worst-case trajectory from the specifications. Then a motor is sized by matching its continuous force output to the maximum force required to move the motor through that trajectory. Values that are useful for this calculation are shown on Table 6.3-3. It includes values for movement amplitude, inertia, stiffness, and step rate.

Table 6.3-3: Vertical DOF specifications

Specification		**Units**
Movement Amplitude	45	*mm*
Inertia	22.9	*kg*
Achievable Stiffness	4150	N/m
Step Rate	2.15	*Hz*
Estimated Static Friction	22.5 - 28.4	*N*

Using the values in Table 6.3-3, the maximum force that the linear motor would need to exert can be estimated. First, assume that vertical motion occurs sinusoidally

6.3-2
$$x = A \sin ft$$

so that the acceleration is

6.3-3
$$a = -Af^2 \sin ft$$

where x is the vertical position, A is the amplitude of motion, f is the frequency of oscillation, t is time, and a is vertical acceleration. The maximum acceleration is therefore Af^2, so the maximum inertial force is

6.3-4
$$F_{inertial} = m \cdot Af^2$$

where m is the vertical inertia of the device.

Friction in the vertical direction has viscous and static components. It is assumed that inertial forces are much greater than viscous frictional forces. Because the maximum inertial force occurs at zero velocity, the viscous friction force at that time is zero, so viscous friction is ignored in the calculation of maximum motor force. While static friction force is zero for zero velocity as well, the static friction force becomes non-zero at an infinitesimal velocity. Due to this fact the static friction force is considered in the calculation of maximum force. The maximum force is

6.3-5
$$F_{\max} = F_{inertial} + F_{staticfriction}$$

The magnitude of this force can be estimated with the values in Table 6.3-3. Movement amplitude is 45 mm, frequency is 2.15 Hz, vertical inertia is 22.9 kg, and static friction is 28.4 N. These figures yield a maximum force of 216 N. According to Table 6.3-4, only the Copley 3810 would be suited to produce the required continuous force [11].

Table 6.3-4: Copley linear motor specifications [11]

	3804	3806	3808	3810	Units
Continuous Stall Force*	101	142	180	217	N
Continuous Stall Current*	2.03	1.90	1.81	1.74	A_{rms}
Forcer Mass	2.15	3.15	4.15	5.15	kg
Forcer Length	167	238	309	380	mm
Module Length	525	575**	675	725	mm

* Without heatsink plate, 25 degree C ambient.

** Actual module length should be 238 + 300 + 40 = 578 but difference rounded down.

Table 6.3-4 also shows the module length required for this design. The module length is the required travel of 300 mm plus the forcer length plus 40 mm for the end supports, rounded to the nearest standard length. Standard lengths for the modules begin at 225 mm and increase in 50 mm increments [11].

The above calculations assume that the vertical inertia of the device is the specified 22.9 kg maximum. It would be mechanically simpler to have the actuators translate vertically as well, so that the vertical inertia would be larger. In particular, if three Kollmorgen D063 motors are added at 13.8 kg each the total vertical inertia rises to 64.3 kg [14]. Using the same formulas as above, the maximum force required to drive this inertia through a 45 mm amplitude sinusoid at 2.15 Hz is 527 N. This figure does not take into account the inertia of the forcer or that of the structure connecting the motors. It also does not take into account static friction. Because of the large forces that would be necessary to accelerate the mass of the motors, the motors are connected to the planar linkage by splines so that they remain stationary.

Once the motor type and size is known, the servo amplifier can be selected from the continuous current the motor can draw. As shown in Table 6.3-4, the Copley 38-series linear motors do not draw more than two amps of continuous stall current. Therefore the Accelus ASC-090-09 model amplifier is ideal; it has 3 amps continuous and 9 amps peak output [11].

Another component that must be sized is the linear bearing. As stated before, Copley linear motors are available as pre-built modules that include a linear bearing, optical encoder, and motor frame. The module comes equipped with a THK SHW-21 linear bearing with a maximum allowable static moment of 80 N-m [11, 65]. If the linear motor is mounted adjacent to the planar motor that drives the weight-bearing spline it will have a moment arm of 0.25 m. Therefore the motor would be able to output 320 N before it overloads the bearings. While this force is higher than the continuous force output of every Copley linear motor it does not allow for intermittent operation at higher loads. THK manufactures a linear bearing of the same type with two bearing blocks on the rail; if a Copley module can be had with such an arrangement it would be preferable, though the single bearing block design is also acceptable.

Finally, an appropriate sensor must be chosen for the linear motor. The Copley modules are available with either magnetic or optical sensors, but optical sensors are specified because of previous experience with that type of sensor. To select the desired resolution of the sensor, match the stiffness of the motor to the maximum desired stiffness. The stiffness performance of the linear motor is

6.3-6 $$K_e = \frac{2F_{PEAK}}{2^{Fbits} RES_{ENCODER}}$$

where K_e is the estimated stiffness based on a one-count force increment to one-count displacement scenario. Twice the peak motor force F_{PEAK} is the force range of the actuator, so that value divided by the number of counts that comprise that range (2^{Fbits}) yields the force increment of the system. Dividing that number by the resolution of the encoder gives the estimated stiffness. Table 6.3-5 shows the force constant, peak force for 9 A_{rms}, input and output resolution, and resultant stiffness for the 38-series Copley actuators. As can be seen from the table, all of these actuators can easily surpass the desired vertical stiffness of 4.15 kN/m even with the standard 5-micron optical encoder. The linear motor is now fully specified. Table 6.3-6 contains a summary of all the decisions that are made in this section.

Table 6.3-5: Copley linear motor stiffness [11]

	3804	3806	3808	3810	Units
Force Constant	49.8	74.7	99.6	124.4	N/A_{rms}
Peak Force*	448.2	672.3	896.4	1119.6	N
Input Resolution	5	5	5	5	μm
Output Counts	2^{12}	2^{12}	2^{12}	2^{12}	counts
Estimated Stiffness	43.8	65.7	87.5	109.3	kN/m

* Peak force under 9 A_{RMS} peak amplifier current

Table 6.3-6: Linear motor specifications

Quantity	1
Type	ThrustTube Module
Forcer	TB3810
System Length	725 mm
Encoder Type	Optical
Encoder Resolution (with quadrature)	5 μm
Linear Bearing	Two Bearing Blocks*
Energy Chain for Cable Routing	Yes
Limit Switches	Yes
Continuous Stall Current	2.00 / 1.74 A_{RMS}**

* Order linear bearing with two bearing blocks if available, otherwise order standard part.

** Higher value for use with 25 x 25 x 2.5 cm heatsink plate, lower value without heatsink, both with 25 degree C ambient temperature.

6.3.3 Force transducer

Force sensing at the robot endpoint is useful for clinical applications and for control. In a clinical trial, force transducer data gives quantitative information about the interaction between the robot and the patient. For control, force sensing allows the compensator to reduce the friction felt at the endpoint. Given that only 8.3 N of static friction are allowed and the spline shafts alone account for 25 N of friction in the vertical direction, a friction compensator could improve the feel of the robot.

Specifications for a force transducer include the maximum overload capability before damage occurs and maximum sensing range. The overload capability dictates the size of the transducer while the sensing range dictates resolution. However, a force transducer that must be large to withstand large overloads may not achieve a high enough resolution for a small sensing range.

Table 6.3-7 shows the sensing range required of the force transducer according to the design specifications. Moreover, the safety factor of the design is four, so the overload capability of the force transducer must be at least four times the values in Table 6.3-7. These overload values are shown in Table 6.3-8.

Table 6.3-7: Force transducer sensing range requirement

Direction	**Maximum**	***Units***
Vertical Force	624	*N*
Frontal Force	166	*N*
Lateral Force	166	*N*
Transverse Rotation Torque	95	*N-m*

Table 6.3-8: Force transducer overload capacity requirements

Direction	**Maximum**	***Units***
Vertical Force	2500	*N*
Frontal Force	664	*N*
Lateral Force	664	*N*
Transverse Rotation Torque	380	*N-m*
Sagittal Rotation Torque	749	*N-m*

The first four values in Table 6.3-8 are simply the values from Table 6.3-7 multiplied by a safety factor of four. The last value for torque about the sagittal plane is derived from multiplying the vertical force by a moment arm of 0.3 m. This moment arm was measured from the bicycle seat body-weight support system on the mockup, with a small amount added for increased safety.

The force transducer selected for this design is from ATI. Table 6.3-9 shows the specifications for ATI force transducers with overload capacities close to those desired for this machine. The values listed for load capacity are the forces and torques about the x and y directions and the z direction. The force transducers are cylindrical in shape. The z direction is along the axis of the cylinder while the x and y directions are in the plane of the cylinder ends.

As the table shows, the Delta model force transducer is too weak to withstand the overload forces required. Even with the maximum torque loading aligned along the z-axis the force transducer does not achieve a safety factor of two. Both the Theta and the Omega 190 models are strong enough but they are both very heavy. The only remaining model is the Omega 160. At 2.7 kg, the Omega 160 heavier than desired, and the safety factor of 9.1 is higher than needed [2]. This larger-than-necessary load capacity is beneficial because force transducers are expensive and it would be best if the transducer were never in danger of being damaged while the machine is in operation. Moreover, the Omega 160 has high load capacity in all directions so an unexpected overload is less likely to damage it. One possible source of extra overload, for example, is if the patient slumps in the supports while leaning forward; this position would lengthen the moment arm of the vertical load even more and would surely damage a smaller force transducer. Still, a lighter force transducer would be preferred.

The next step is to choose the calibration range of the Omega 160 force transducer. Table 6.3-10 shows the sensing ranges and their resolutions for the Omega 160 transducer. Comparing the ranges available in Table 6.3-10 to those required in Table 6.3-7 shows that the SI-1000-120 and the US-200-1000 calibrated force transducers can meet the requirements. The force transducer with the greatest possible resolution is desired, so the Omega 160 US-200-1000 will be used for this machine.

Table 6.3-9: Force transducer overload capacity and size specifications [2]

Model	**Delta**	**Theta**	**Omega 160**	**Omega 190**	***Units***
F_{xy}	3.4	25	18	36	*kN*
F_z	12	61	48	110	*kN*
T_{xy}	220	2500	1700	5500	*N-m*
T_z	420	2700	1900	8100	*N-m*
Diameter	94.5	155	156	190	*mm*
Length	33.3	51.1	55.9	55.9	*mm*
Weight	0.91	5.0	2.7	6.4	*kg*
Safety Factor	1.2/1.9	13.4	9.1	29.4	

Table 6.3-10: Omega 160 force transducer sensing ranges and resolutions for DAQ systems [2]

Model	**US-200-1000**	**SI-1000-120**	**SI-1500-240**	**SI-2500-400**	***Units***
F_{xy} Range	892	1000	1500	2500	*N*
F_{xy} Resolution	0.035	0.063	0.125	0.125	*N*
F_z Range	2230	2500	3750	6250	*N*
F_z Resolution	0.070	0.063	0.125	0.188	*N*
T_{xy} Range	113	120	240	400	*N-m*
T_{xy} Resolution	0.0035	0.0063	0.0125	0.0125	*N-m*
T_z Range	113	120	240	400	*N-m*
T_z Resolution	0.0035	0.0031	0.0063	0.0125	*N-m*

6.4 Bearing selection

This section summarizes the bearing selections for the pelvis actuation module. This robot uses angular contact bearings for the load bearing joints, self-aligning bearings for the locating link joints, deep groove bearings for the vertical connection, and CARB toroidal bearings for the spline shaft supports.

6.4.1 Selecting bearing type

This robot requires bearings to act in four different functions. The first is to support the weight bearing robot arm against applied loads at the endpoint. The second is to connect the locating links to each other and to the load bearing links. The third is to connect the spline nuts to each other, constraining them to move vertically in unison but allowing them to rotate independently. The fourth bearing function is to support the end of the spline shafts opposite the motors.

The load bearing robot arm joints must carry combined moment, axial, and radial loads. Of these, the largest are the moment loads. Angular contact bearings are used for these two joints because, when paired, they can withstand all three kinds of loads while fitting in a compact package. For the locating links, only radial forces need be transmitted. Furthermore, moment loads should not be transmitted and the bearings should be able to compensate for angular misalignment in operation. Self-aligning bearings are ideal for this function because they resist radial loads but adapt to changes in angle much like ball ends. Also, self-aligning bearings have some capability to transmit axial loads.

In the case of the vertical connection bearings, the aim is to use the smallest bearing possible that will fit around the spline nut housings. These bearings will be large enough that the axial loads and moment loads that must be transmitted are relatively small. The lowest-profile ball bearings available are the deep-groove ball bearings, so these are selected for the spline nut connecting joints. As described in sections 4.2.4 and 6.9, the attachment to the spline nut housing will allow all three rotations to occur. Self-aligning bearings can fulfill this function without the use of flexures or other components, but the large size of the bearings make them impractical for this location.

The spline shaft support bearings are mounted 636 mm from the motors, and in separate housings. The weight of the motors will deform the chassis; to allow this assembly to function properly and without overconstraint, these bearings should allow angular and axial misalignment. Such bearings would also allow the shaft to undergo thermal expansion. A suitable bearing type is the SKF CARB toroidal bearing shown in Figure 6.4-1; these bearings have crowned rollers and races that, as desired for this application, allow both axial and angular displacement of the inner and outer races. These bearings also support very large loads. Once the bearing types for the joints are chosen, each joint must have bearings sized for it.

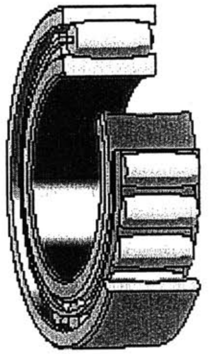

Figure 6.4-1: SKF CARB toroidal bearing [55]

6.4.2 Weight bearing joint bearings[3]

To size the bearings for the load bearing joints, first a method must be found to determine the loads on the bearings, and then these loads must be calculated for suitable bearing sizes. The load on angular contact bearings depends on spacing and orientation. Figure 6.4-2 shows a shaft with an applied moment supported by two angular contact bearings. Because the bearing balls can only support compressive loads, each bearing can potentially apply two forces as shown. For this calculation, the shaft, inner bearing race, and bearing balls are treated as a rigid body while the bearing load is modeled as occurring at the outer race. Also, the effect of preload is not considered.

The known quantities in this problem are the applied moment M_I, the bearing spacing a, the distance to the applied moment L, and the contact angle θ. The bearing reaction forces are unknown, though they must be positive as drawn. To find them, use force balance in x and y and moment balance at the end of the beam:

---

[3] This section is based largely on Slocum's Precision Machine Design p. 487.

$$\sum F_x = -F_1\cos\theta - F_2\cos\theta + F_3\cos\theta + F_4\cos\theta = 0 \tag{6.4-1}$$

$$\sum F_y = -F_1\sin\theta + F_2\sin\theta - F_3\sin\theta + F_4\sin\theta = 0 \tag{6.4-2}$$

$$\sum M = M_1 - F_1(a\sin\theta + R\cos\theta) + F_2(a\sin\theta + R\cos\theta) + F_3R\cos\theta - F_4R\cos\theta = 0 \tag{6.4-3}$$

There are four unknowns and only three equations. First adding and then subtracting the first two equations, however, shows that $F_2 = F_3$ and that $F_1 = F_4$. As no reaction force can be negative and preload is neglected, one pair of forces must be zero. Assume that $F_2 = F_3 = 0$; if the equations return negative forces then the assumption was incorrect. The moment equation now gives

$$F_1 = F_4 = \frac{M_1}{a\sin\theta + 2R\cos\theta} \tag{6.4-4}$$

which is positive for positive M_1. From this equation it is possible to determine the loads on the robot arm bearings. The next step is to find the moment loads on the joints as shown in Table 6.4-1. Then, these moments can be converted into bearing loads, and the bearing loads used to choose suitable bearings.

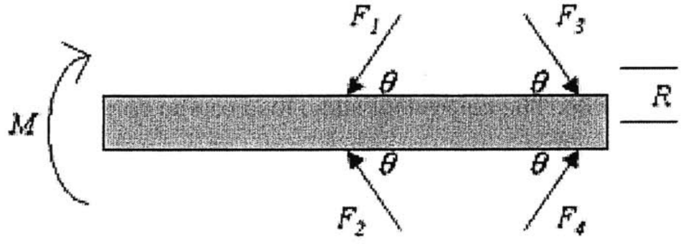

Figure 6.4-2: Shaft supported by angular contact bearings (adapted from [56]).

Table 6.4-1: Joint moment loads

Joint	Lever Arm	Force	Moment
	m	*N*	*N-m*
L1-L4	0.7874	624	492
L4-L7	0.2032	624	127

Standard practice is to choose bearings based on the expected life. However, for the gait robot this approach is not feasible. From the SKF website [55],

" Bearing size should be selected on the basis of static load ratings C_0 instead of on bearing life when one of the following conditions exist:

- the bearing is stationary and is subjected to continuous or intermittent (shock) loads;
- the bearing makes slow oscillating or alignment movements under load;
- the bearing rotates under load at very slow speed (n<10 r/min) and is only required to have a short life (the life equation in this case, for a given equivalent load P would give such a low requisite basic dynamic load rating C, that the bearing selected on a life basis would be seriously overloaded in service);
- the bearing rotates and, in addition to the normal operating loads, has to sustain heavy shock loads"

In this case, the load on the robot joint will only be at its maximum for a fraction of its use. Also, even though the robot may move at up to 2.15 Hz the bearings at the joints will not need to turn far, and thus their rotation speed will be limited. Therefore, the joint bearings are sized according to the static load rating. The SKF website contains a formula for calculating the equivalent static load P [55],

6.4-5

$$P = F_r + Y_0 F_a$$

where F_r is the radial load, F_a is the axial load, and Y_0 is a bearing factor. For angular contact bearings in the size range of interest, $Y_0 = 0.26$. The equivalent static load can be computed from the applied moment by using the reaction force F calculated in the previous section. This substitution yields an equivalent static load of

6.4-6

$$P = \frac{M_1}{a\sin\theta + 2R\cos\theta}\left(\sin\theta + Y_0\cos\theta\right)$$

To simplify the analysis used for selecting the bearings, two angular contact bearings will be assumed to be adjacent to each other in a back-to-back configuration. This arrangement makes the bearing spacing a function of the bearing size and type since the spacing and race diameter of angular contact bearings depends on the particular bearing, as shown in Figure 6.4-3. In section 6.7, a stiffness analysis of the joint is conducted that shows that separating the bearings increases stiffness significantly.

Table 6.4-2 shows the effective spacing, load capacity, moment load, resultant load, and safety factor for a number of SKF bearings. For all angular contact bearings in this range the contact angle is 40 degrees. The '2' in the second digit of the part number refers to a bearing that is of the smallest dimension for a given bore. This bearing type is preferred for this application because a larger shaft is stiffer. The effective bearing spacing used is the width of one bearing (labeled B in Figure 6.4-3); thus, the contact is assumed to occur at the centerline of each bearing. Furthermore, the race diameter is dimension *D1* from Figure 6.4-3, which measures the diameter of the large shoulder.

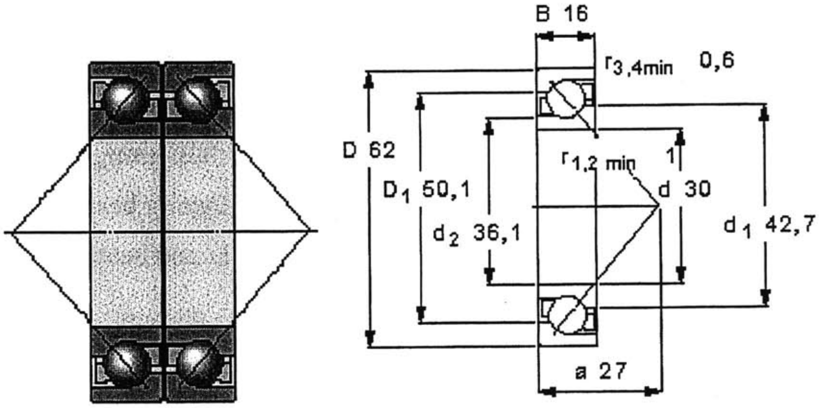

Figure 6.4-3: Angular contact bearings in a back-to-back configuration and the dimensions of angular contact bearings [55]

Table 6.4-2: Weight bearing joint bearing loads [55]

Model #	Effective Spacing	Race Diameter	Static Load Capacity	Moment Load	Equivalent Static Load	Safety Factor
	mm	*mm*	*kN*	*N-m*	*kN*	
7203	12	31.2	5.85	127	3.37	1.7
7204	14	37	8.3	127	2.86	2.9
7205	15	41.5	10	127	2.57	3.9
7206	16	50.1	15.6	492	8.37	1.9
7207	17	58.3	20.8	492	7.43	2.8
7208	18	65.6	26	492	6.68	3.9

The suggested safety factor for an SKF ball bearing that is rotating, has normal requirements for smooth running, and is subjected to pronounced shock loads over 1.5. For quieter running a safety factor of over two is suggested. Therefore, for this application the safety factor should be over two and thus the 7204 and 7207 bearings will be used in the load-bearing joints of the robot. This safety factor is less than the specified robot safety factor of four (see specifications, section 3.2.5) because overloading the bearings will plastically deform the bearing balls but will not cause the bearing to fail catastrophically.

6.4.3 Self-aligning bearings for locating links

The locating links must only transmit planar forces. From Table 6.1-2 on page 108, the axial force on the fore/aft link L_5 is 604 N and the axial force on the lateral link L_6 is 1715 N. These joints must transmit only radial loads and no moment loads, so self-aligning bearings like the one shown in Figure 6.4-4 are used. As for the load-bearing arm, the static load-carrying capacity is used to size the self-aligning bearings. Table 6.4-3 shows the specifications for numerous self-aligning bearings. Because shock loads may be present (in the plane as well as out of it), the self-aligning bearings should have a safety factor of two. Therefore, bearing #1200 is used for the joints of L_5 and bearing #1204 is used for the joints of L_6.

While the self-aligning bearings will be subjected mostly to radial loads, they should not fail if accidentally loaded axially. According to SKF, the approximate maximum allowable axial load in N, C_a, for these bearings is [55]

6.4-7
$$C_a = 3 \cdot B \cdot ID$$

where B and ID are the bearing width and inner diameter measured in mm. As show in Table 6.4-3, the maximum allowable axial load is 270 N and on bearing #1200 and 840 N on bearing #1204. Both of these values are acceptable.

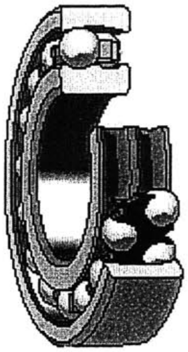

Figure 6.4-4: SKF self-aligning ball bearing [55]

Table 6.4-3: SKF self-aligning bearings [55]

Part #	ID	OD	B	C_0	C_a	w
	mm	mm	mm	N	N	kg
129	9	26	8	820	216	0.022
1200	10	30	9	1180	270	0.034
1201	12	32	10	1430	360	0.040
1202	15	35	11	1760	495	0.049
1204	20	47	14	3400	840	0.12
2204	20	47	18	4150	1080	0.14
2304	20	52	21	4750	1260	0.23

Key: ID - inner diameter, OD - outer diameter, B - bearing width, C_0 - static load capacity, w - bearing weight.

6.4.4 Deep-groove bearings for vertical connections

As described in section 4.2.4, a mechanism is required to make the spline-nuts move vertically in unison. This mechanism is connected to the arms through deep-groove ball bearings so that the arms may rotate relative to the vertical connection. The size of these bearings is dictated by the outer diameter of the spline-nut housings. For the 50 mm spline, 95 mm ID bearings must be used while 75 mm bearings may be used for the 40 mm splines. Each spline should have a preloaded bearing pair to eliminate play and to carry moment loads. For both splines, the smallest bearing that will fit is desirable. Table 6.4-4 shows the dimensions of the bearings selected.

The loads on the 40 mm spline bearings will be almost purely axial because of the mechanism to allow for misalignment. The magnitude of these forces is dependent on the linear actuator used: from Table 6.3-4, continuous force is 217 N and from Table 6.3-5, peak force is 1120 N. SKF defines the axial load-carrying capacity, C_a, of these bearings as half the radial static load capacity; as can be seen from Table 6.4-4, this capacity is 7 kN for the 61815 and is enough to carry peak motor loads.

Unlike the 40 mm spline bearings, the 50 mm spline bearings will be subjected to moment loads. These loads arise from the need to transmit vertical loads to the other spline bearings and to the linear motor. The maximum expected moment load is dependent on the linear actuator. For the 50 mm spline bearings it is also dependent on the moment arm separating the splines, the largest of which is 508 mm. The bearing spacing is about 76 mm. Therefore the radial load expected on the 50 mm spline bearings is 6.7 times the axial load: continuous radial load is 1450 N and peak radial load is 7490 N. Both of these loads are within the safe range for SKF 61819 deep-groove ball bearings.

Table 6.4-4: Deep-groove bearings [55]

Part #	*ID*	*OD*	*B*	C_0	C_a	*w*
	mm	*mm*	*mm*	*kN*	*kN*	*kg*
61815	75	95	10	14.3	7.15	0.15
61819	95	120	13	22.8	11.4	0.30

Key: ID - inner diameter, OD - outer diameter, B - bearing width,
C_0 - static load capacity, w - bearing weight.

6.4.5 CARB toroidal bearings for spline shaft support

The spline shafts must be supported on both ends. Toroidal bearings like the one shown in Figure 6.4-1 are ideal for this application: they allow for angular misalignment in operation and also allow axial displacement of the inner ring relative to the outer ring. This ability to adapt to operating conditions allows the gait trainer to be assembled without critical tolerances for parallelism between the motor and support bearing housings and also allows for thermal expansion of the shaft and structure. Table 6.4-5 lists the force requirement as well as the characteristics of the bearings chosen to support the shaft. Their static load capacity easily exceeds the expected loads for this application.

Table 6.4-5: Spline shaft support bearings [55]

	Force	Part #	ID	OD	B	C_0	w
Units	*N*		*mm*	*mm*	*mm*	*kN*	*kg*
50 mm Shaft	1680	C 2208	40	80	23	86.5	0.50
40 mm Shaft	320	C 2206	30	62	20	62	0.27

Key: ID - inner diameter, OD - outer diameter, B - bearing width, C_0 - static load capacity, w - bearing weight.

6.4.6 Bearing selection summary

Bearings for this machine are selected with the static load capacity of the bearings because shock loads are expected and because motion may be slow and oscillating. Three types of bearings are needed: angular contact bearings for the joints between load-bearing arms, self-aligning bearings for the joints between unloaded arms, and deep-groove bearings for the connection between the spline nuts. These bearings were sized with a safety factor of at least two to protect against permanent damage in case of shock loads. Table 6.4-6 lists the bearings selected.

Table 6.4-6: Bearing summary

At Joint Between	Type	Part No	Quantity
L1 and L4	Angular Contact	7207 BEGBP DB	2
L4 and L7	Angular Contact	7204 BEGBP DB	2
L2 and L5, L5 and L7	Self-Aligning	1200 ETN9	2
L3 and L6, L6 and L4	Self-Aligning	1204 ETN9	2
40 mm Splines to Vertical	Deep Groove	61815-2RS1 DB	4
50 mm Spline to Vertical	Deep Groove	61819-2RS1 DB	2
40 mm Spine Support	CARB	C 2206 TN9	2
50 mm Spline Support	CARB	C 2208 TN9	1

6.5 Robot arm cross-section selection

The robot arms must be strong enough to withstand body-weight support loads. This section sizes the robot arms according to their strength, starting with the load-bearing arm and including the upper and lower locating links.

One factor that impacts the design of all the arms is the material used. This design calls for moderate strength, high stiffness, and low weight. Materials that could be considered include aluminum, steel, and carbon fiber or fiberglass composites. Regarding stiffness-to-weight ratio, carbon fiber composites would outperform the metal ones. However, carbon fiber is not readily available, is expensive, difficult to machine, and somewhat hard to attach to. Steel is undesirable because it is heavy; an arm section that is light enough to be used on the arms would have unreasonably thin wall sections and may be prone to bucking. In the end, aluminum is the best solution: it is easily available and cheap, and it is easy to shape and attach to. In particular, 6061-T6 aluminum with tensile yield stress $\sigma_y = 275$ MPa and yield shear stress $\tau_y = 205$ MPa [3] is used on these arms. Future versions of this device could take advantage of the superior performance of carbon composites in this area.

6.5.1 Load-bearing arm

The most important arms in the robot linkage are the two load-bearing arms, L_1 and L_4. Worst-case loading conditions for these links are shown in Figure 6.5-1 and Figure 6.5-2. The two cases shown are for maximum bending loads and for maximum torsion loads: for maximum bending loads, the links are arranged in a straight line while for maximum torsion loads the links are at right angles. Table 6.5-1 shows the magnitude of these loads calculated from the linkage arrangement in Figure 6.5-1 and Figure 6.5-2 using an expected vertical load of 628 N from the specifications. Notice that the maximum torsion load on link L_1 equals the maximum bending load on link L_4. For reference, the link lengths are 16 inches for link L_1 and 23 inches for link L_4, as determined in Section 6.1. The specifications state that the minimum safety factor for the robot must be four; therefore the arm design load should be four times the quantities in Table 6.5-1.

To convert the required arm strength to suitable arm cross-sections, the minimum required section modulus and polar modulus is calculated. The section modulus z relates the applied moment M to the tensile stress of the material σ such that

6.5-1

$$\sigma = \frac{M}{z}$$

To resist torsion, the arm must have a polar section modulus z_P above a certain value so that an applied torque T creates a shear stress τ that is of acceptable magnitude:

6.5-2

$$\tau = \frac{T}{z_P}$$

Using these equations, the minimum z and z_P of the cross sections for arms L_1 and L_4 can be found, as shown in Table 6.5-2. The material used for the arms is 6061-T6 aluminum with tensile yield stress σ_y = 275 MPa and shear yield stress τ_y = 205 MPa.

Table 6.5-1: Loads on L_1 and L_4 links

Load	L_1	L_4	***Units***
Bending	745	492	*N-m*
Torsion	492	127	*N-m*

Table 6.5-2: Minimum section properties for arms L_1 and L_4 using 6061-T6 aluminum.

		L_1	L_4	***Units***
Section modulus	z	10.8	7.16	$m^3 \times 10^6$
Polar modulus	z_P	9.60	2.48	$m^3 \times 10^6$

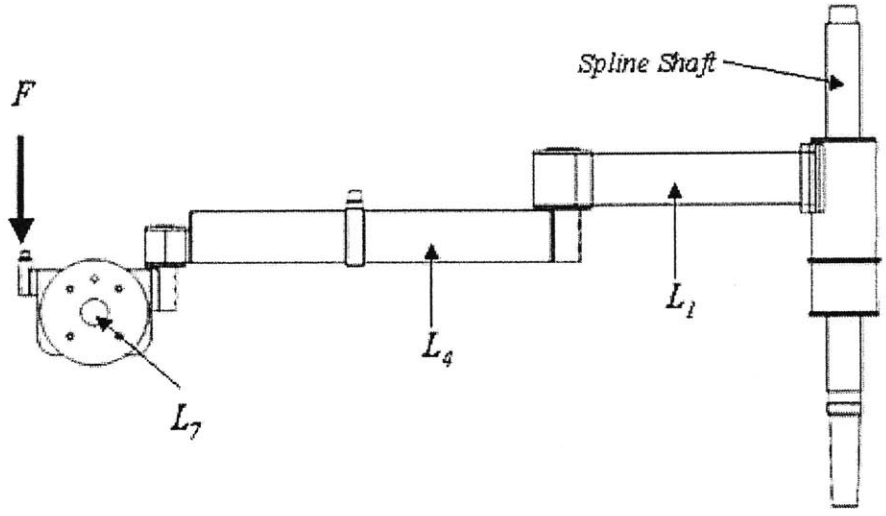

Figure 6.5-1: Load arm position for maximum L_1 bending

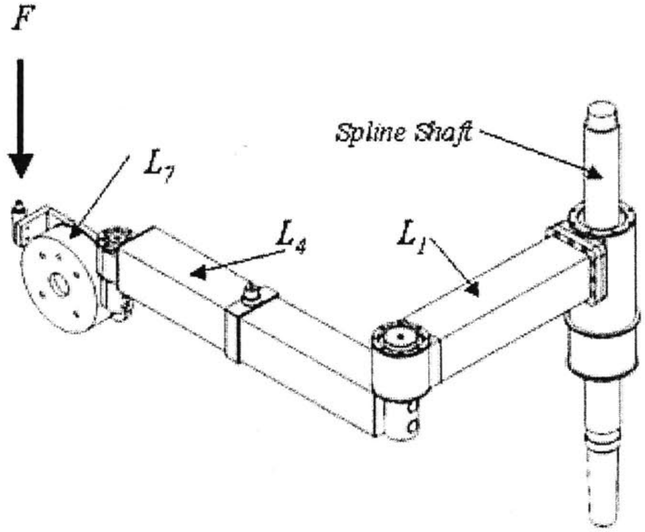

Figure 6.5-2: Load arm position for maximum L_1 torsion

From preliminary designs it was determined that the maximum outer dimension of each arm should be 3 inches. This dimension allowed for a suitably strong and stiff arm while leaving clearance in the vertical direction, so that the arms L_1, L_4, and L_2 did not interfere with each other. To select a suitable cross section for each arm, the available cross-sections must be evaluated. Hollow sections of uniform wall thickness with round, square, and rectangular shapes are considered. For a hollow rectangular cross-section, the section modulus z_{rect} is found from the formula [43]

6.5-3 $$z_{rect} = \frac{\left(b_o h_o^3 - b_i h_i^3\right)}{6h_o}$$

where b is the width and h is the height of the section, and the subscript o refers to the outer dimension and the subscript i refers to the inner dimension. The polar section modulus $z_{P,rect}$ of a rectangular section is found according to the formula [43]

6.5-4 $$z_{P,rect} = 2t(h_o - t)(b_o - t)$$

$$t = \tfrac{1}{2}(h_o - h_i) = \tfrac{1}{2}(b_o - b_i)$$

In this case, it is more convenient to express the polar modulus in terms of the thickness t of the rectangular section. For a hollow circular section, the section modulus z_{circ} is [43]

6.5-5 $$z_{circ} = \frac{\pi\left(d_o^4 - d_i^4\right)}{32d_o}$$

where d_0 is the outer diameter and d_i is the inner diameter of the section. The polar modulus $z_{P,circ}$ is

6.5-6 $$z_{P,circ} = \frac{\pi\left(d_o^4 - d_i^4\right)}{16d_o}$$

The final piece of information required to evaluate different cross-sections is the weight per length of section. Because the arms will be made of aluminum regardless of cross-section shape, the cross-sectional area is the only quantity needed for weight comparison. The cross-sectional area of a hollow rectangular section A_{rect} is

6.5-7 $$A_{rect} = \left(b_o h_o - b_i h_i\right)$$

and the cross-sectional area of a hollow circular section A_{circ} is

6.5-8
$$A_{circ} = \tfrac{1}{4}\pi\left(d_o^2 - d_i^2\right)$$

Using equations 6.5-3 through 6.5-8 it is possible to compare the available sections of aluminum. Figure 6.5-3 shows the section moduli for a variety of round and rectangular hollow sections. Note that, for the sections shown, rectangular sections in general perform better in bending than circular sections for similar cross-sectional area. Figure 6.5-4 shows the polar moduli of the selected sections. Some rectangular sections are comparable to circular sections, while some are significantly weaker in torsion than comparable circular sections.

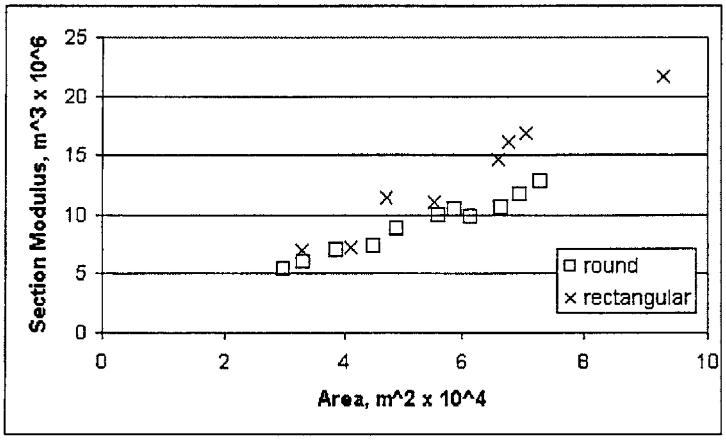

Figure 6.5-3: Section moduli of selected cross sections

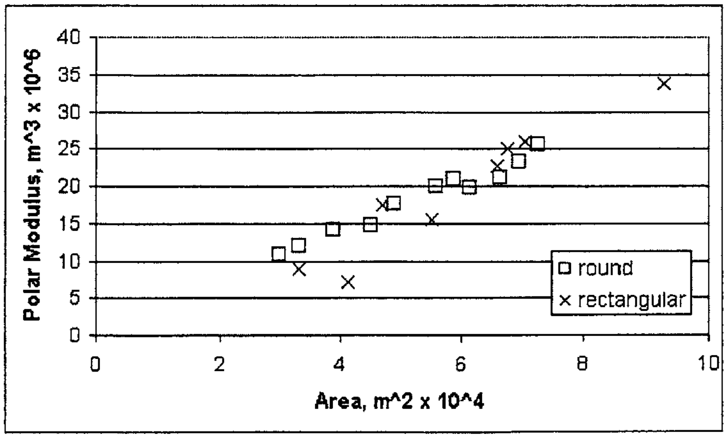

Figure 6.5-4: Polar moduli of selected cross sections

As a consequence of the data shown in Figure 6.5-3 and Figure 6.5-4, square hollow sections were chosen for the arms L_1 and L_4 of this design. Table 6.5-3 shows a comparison between the best circular and rectangular sections and the minimum requirements for the weight bearing arms. For the L_1 arm section, the square section achieves better section modulus and polar modulus while reducing weight. For the L_4 arm section, the square section is significantly heavier but still increases both torsional and bending strength.

Table 6.5-3: Comparison of selected circular and rectangular sections for L_1 and L_4 arms

Section	Section Modulus	Polar Modulus	Area
	$m^3 \times 10^6$	$m^3 \times 10^6$	$m^2 \times 10^4$
Minimum for L_1	10.8	9.60	
3 in. OD x 0.125 in. t Circular	12.8	25.5	7.28
3 x 3 in. x 0.094 in. t Rectangular	16.8	26.0	7.05
Minimum for L_4	7.16	2.48	
3 in. OD x 0.065 in. t Circular	7.05	14.1	3.87
3 x 3 in. x 0.062 in. t Rectangular	11.5	17.5	4.70

6.5.2 Upper locating link

The L_2 and L_3 arms do not have to transmit a significant torsional moment; the only loads on these arms are the bending loads induced by motor torque. The absence of other loads is due to the self-aligning ball bearings used for the joints between these arms and the L_5 and L_6 arms. To determine the moment load on the arm, only the peak motor torque is needed. As shown in section 6.3.1, the peak motor torque is 160 N-m. Table 6.5-4 shows the length, maximum moment, and minimum required section modulus computed from equation 6.5-1. As in the weight-bearing arms, the section modulus must account for a safety factor of four. Aluminum (6061-T6) will be used for these arms. The link lengths in Table 6.5-4 are from section 6.1: the length of arm L_2 is 16 inches and the length of arm L_3 is 5.5 inches. Square cross-sections were selected both for their superior performance in bending and to make them match the shape of the weight-bearing arms. Table 6.5-5 shows the selected cross-section for the L_2 and L_3 arms. The arms are over-designed so that a person who unwittingly leans on one of the locating links will not damage the device.

Table 6.5-4: Required properties for arms L_2 and L_3

Arm	Length	Max. Moment	Min. Section Modulus
	in.	*N-m*	*$m^3 \times 10^6$*
L_2	16	160	2.33
L_3	5.5	160	2.33

Table 6.5-5: Selected cross-section for arms L_2 and L_3

Section	Section Modulus	Area
	$m^3 \times 10^6$	$m^2 \times 10^4$
Minimum for L_2 and L_3	2.33	
1.5 x 1.5 in. x 0.125 in. t Rectangular	4.77	4.4

6.5.3 Lower locating link

The only loads the L_5 and L_6 arms transmit are axial; the self-aligning bearings on the joints connecting the L_5 and L_6 arms to the other links transmit no moments. Still, a minimum level of strength is required in case a person unwittingly leans on these links. Maximum axial loads on the L_5 and L_6 arms are given in section 6.1 and are reproduced here in Table 6.5-6 for reference along with the minimum cross-section area needed to transmit said load with a safety factor of four. Minimum cross-section area A is found from

6.5-9
$$\sigma = \frac{F}{A}$$

where F is the axial load and σ is the stress in the arm. Note that the minimum required area is an order of magnitude less than the areas of the other arms shown in Table 6.5-5 and Table 6.5-3.

Using a cross-section with the area shown in Table 6.5-6 would result in an arm prone to yielding in bending and to buckling in compression. Therefore, the arm must be sized to resist a minimum bending load of 20 kg or about 45 lbs; this is an estimated value for a load that a person might inflict on the machine without being aware that he or she may damage it. Both the L_5 and L_6 arms are modeled as simply supported beams. The maximum stress in such a beam occurs in the center and is given by [44]

$$\sigma = \frac{WL}{4z} \tag{6.5-10}$$

where W is the load, L is the length of the beam, and z is the section modulus. Using the length of the L_5 arm, the minimum section modulus for these links is 0.417 x 10^{-6} m^3. Table 6.5-7 shows the selected cross-section for the L_5 and L_6 arms.

Table 6.5-6: Required properties for arms L_5 and L_6

Arm	Length	Max. Force	Min. Section Area
	in.	*N*	*m^2 x 10^4*
L_5	23	604	0.0879
L_6	21.5	1715	0.249

Table 6.5-7: Selected cross-section for arms L_5 and L_6

Section	Section Modulus	Area
	m^3 x 10^6	m^2 x 10^4
Minimum for L_5 and L_6	0.417	0.249
0.75 x 0.75 in. x 0.065 in. t Rectangular	0.614	1.15

6.6 L_1-L_4 *shaft bolted joint analysis*

This section analyzes the loading on the shaft that connects the L_4 arm to the L_1 bearings. These bearings are 30 mm ID angular contact bearings that will be mounted on the L_1 arm. It is necessary to design a shaft that can withstand the required loads both from the bearings and from the mounting to the L_4 arm. A basic overview of the problem is first put forth to select materials and a basic geometry for the joint. Then the stiffness of a bolted joint is calculated, and the results are used in two models that approximate the loading on the system.

6.6.1 L_1-L_4 joint starting point and basic calculations

The starting geometry of the L_1-L_4 joint shaft is shown in Figure 6.6-1. As the figure shows, the shaft is held onto the arm end plate with two socket-head cap screws. This design was chosen as a starting point because a bolted joint allows for disassembly of the components. The alternatives are to make the pieces integral or to weld the shaft onto the endplate. Both options would require that similar materials be used in the shaft and arm endplate, but aluminum is preferred for the endplate so it can be brazed onto the arm and (as will be discussed shortly) steel is required for the shaft.

The first step in the back-of-the-envelope analysis phase is to choose a material for the shaft. Between the bearings and the L4 arm, the shaft must support a moment equal to the vertical load at the robot endpoint times the longest possible moment arm. This load creates a stress in the arm that is at a maximum at the outer fiber. The equations for this stress are

$$\sigma_{S,\max} = \frac{Mc_{\max}}{I_S} = \frac{F_{end} L_{arm} \cdot 0.5 d_S}{\frac{\pi d_S^4}{64}} = \frac{624N \cdot 0.7874m \cdot 0.015m}{4 \cdot 10^{-8} m^4} = 184MPa \qquad \textbf{6.6-1}$$

for endpoint force F_{end} = 624 N or 140 lbs. The yield stress of 6061-T6 aluminum is 275 MPa, which would make the safety factor of the shaft 1.5, much less than that the safety factor of four for the robot arms. Another option for shaft material is 7075 aluminum, which has a yield stress of 500 MPa. While a large improvement over weaker aluminum, 7075 still leaves a safety factor of only 2.7. To achieve a safety factor of four, high-strength steel with a yield stress of over 740 MPa is needed. Type 17-4 PH 1150 stainless steel, with an 869 MPa yield stress will be used for the shaft [3].

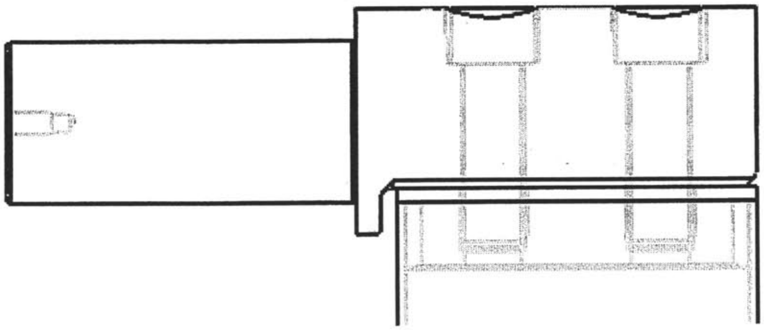

Figure 6.6-1: Starting design for L_1-L_4 joint shaft mounting.

Another part that requires careful selection of material is the fastener used. As will be seen in section 6.6.2 the preload on a bolted joint is very important to the load capacity of the joint. The larger the preload, the greater the normal force between the parts being mated and the greater the resistance to being pulled apart. In this L_1-L_4 shaft mount, normal force is important because it provides friction to resist torsion in the arm about its lengthwise axis. Due to the importance of a large preload, the strongest fasteners available are desired. American-unit fasteners are used throughout this machine, but unfortunately American-unit socket-head cap screws are not rated for strength. Therefore, metric screws are used for this joint. These screws will be blue-coated to distinguish them from the American-unit fasteners. They possess a 12.9 rating: the minimum proof strength of 970 MPa, minimum yield stress of 1100 MPa, and minimum ultimate tensile strength of 1220 MPa [43].

The final component of the joint is the endplate for the L_4 arm. Analyzing the section between the bolt and the arm as a cantilevered beam, the maximum moment M_{EP} is

6.6-2
$$M_{EP,b} = F_{EP}L_{EP,b} = \frac{F_{end}L_{arm}}{L_{EP}}L_{EP,b} = \frac{624N \cdot 0.7874m}{0.0762m} \cdot 0.0203 = 131N-m$$

where the subscript EP,b refers to the section of the endplate between the bolt and the arm and EP refers to the endplate as a whole. The maximum moment is 131 N-m for F_{end} = 624 N, L_{arm} = 787 mm, L_{EP} = 76.2 mm, and $L_{EP,n}$ = 20.3 mm. The highest bending stresses in the narrow section are

6.6-3
$$\sigma_{EP,b,\max} = \frac{M_{EP,b}0.5h}{\frac{1}{12}bh^3} = 53.7MPa$$

for endplate height h = *15.2 mm* and width b = *63.0 mm.* Because the section is short and stubby, the maximum shear stress $\tau_{EP,b,max}$ should be checked; it is [56]

6.6-4
$$\tau_{EP,n,\max} = \frac{3F_{EP}}{2bh} = 10.1MPa$$

Equations 6.6-3 and 6.6-4 show that a 6061-T6 aluminum endplate could support the required loads with a safety factor of 5.1.

6.6.2 Stiffness of a bolted joint

The method of determining the stiffness of a bolted joint for this analysis consists of finding the stiffness of the bolt used, then finding the stiffness of the material around the bolt, and finally putting them together to find the bolted joint stiffness. The geometry of a bolted joint is shown in Figure 6.6-2. The bolt has a shank diameter d_B and head diameter d_H, and its length is L_B. The material clamped by the bolt is L units long. Figure 6.6-2 also shows the cone of material affected by the bolt; the cone has an angle ϕ and reaches a maximum diameter d_C. Shigley gives the depth to which the threads apply clamping pressure on the endplate as half the bolt diameter [53].

To find the stiffness of the bolt, one must know the length L, bolt modulus E_B, and bolt tensile area $A_{B,T}$. Due to the threads in the shank the tensile area of a bolt is not equal to its nominal diameter. Norton [43] gives this tensile area as

6.6-5
$$A_{B,T} = \frac{\pi}{4}\left(\frac{d_p + d_r}{2}\right)^2$$

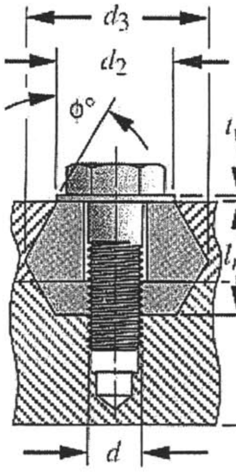

Figure 6.6-2: Bolted joint dimensions [43]

where d_p is the pitch diameter of the bolt and d_r is the minor diameter of the bolt. For metric fasteners of nominal diameter d_B and pitch p these values are

6.6-6 $$d_p = d_B - 0.649519p$$

6.6-7 $$d_r = d_B - 1.226869p$$

Using the length, area, and modulus of the bolt allows for the calculation of the bolt stiffness as follows:

6.6-8 $$k_B = \frac{A_{B,T} E_B}{L}$$

The next step is to find the stiffness of the material surrounding the bolt. This value can be approximated by assuming that only the material in a 30-degree cone is affected by the bolt, as shown in Figure 6.6-2. According to Shigley [53], the compressive stiffness of a cone of material with length t is

6.6-9 $$k = \frac{\pi E_m d_B \tan\phi}{\ln\frac{(2t\tan\phi + d_H - d_B)(d_H + d_B)}{(2t\tan\phi + d_H + d_B)(d_H - d_B)}}$$

In the geometry for this joint, the arm endplate and the shaft will be of different materials so their stiffness must be calculated separately. Furthermore, the cone of pressure will have its maximum diameter somewhere within the shaft provided that there is enough material under the bolt. The material stiffness then has three parts: the cone in the endplate, the diverting cone of material in the shaft measuring *L/2* in length, and the converging cone of material in the shaft measuring *(L/2 - 1/2 * d_B)* in length. They must be combined in series:

6.6-10 $$\frac{1}{k_m} = \frac{1}{k_e} + \frac{1}{k_{m,L}} + \frac{1}{k_{m,S}}$$

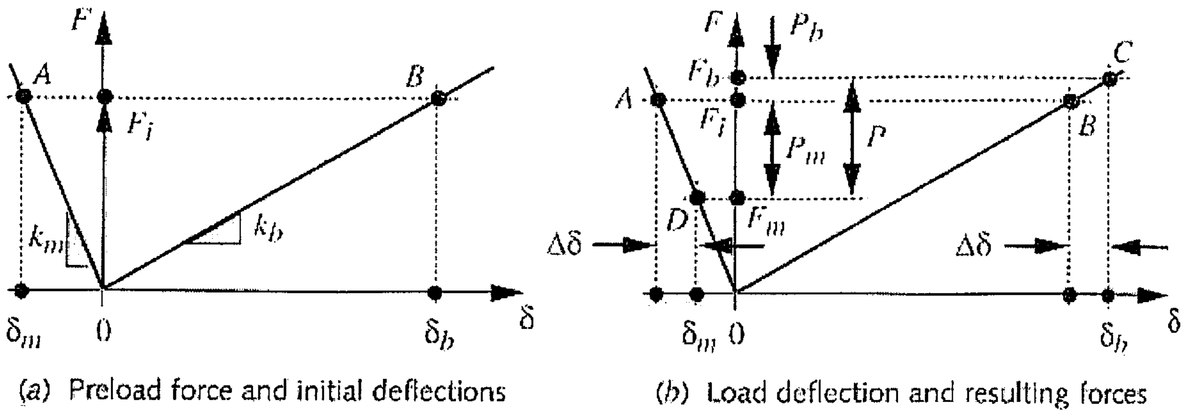

(*a*) Preload force and initial deflections (*b*) Load deflection and resulting forces

Figure 6.6-3: Effect of a tensile load on a preloaded bolted joint [43]

To find the stiffness of the combined bolt-material system, it is important to consider the preload on the bolt and how the preload affects the interaction between the material and the bolt. Figure 6.6-3 shows this interaction. When a preloaded joint is subjected to a tensile load, both the material and the bolt deform by the same amount. Because the material around the bolt is almost always stiffer than the bolt itself, the material assumes more of the load than does the bolt.

In mathematical terms, the fact that the bolt deflection equals the deflection of the material in the joint is expressed as [43]

6.6-11

$$\Delta = \frac{P_B}{k_B} = \frac{P_m}{k_m}$$

when the stiffness is treated as linear and P_B is the added load on the bolt and P_m is the added load on the material. Another relation that comes from Figure 6.6-3 is that the force P applied to the joint is split between the material and the bolt, or

6.6-12

$$P = P_B + P_m$$

Equations 6.6-11 and 6.6-12 can be combined to solve for each of P_B and P_m by substitution. The total force on the bolt and the material is the preload force F_i plus P_B for the bolt and the preload force F_i minus P_m for the material, as can be seen from Figure 6.6-3. In equation form, these relations are

6.6-13 $$F_B = F_i + \frac{k_B}{k_m + k_B} P$$

6.6-14 $$F_m = F_i - \frac{k_m}{k_m + k_B} P$$

Equations 6.6-13 and 6.6-14 hold only as long as the force on the material remains compressive; in other words, as long as $F_m > 0$. In equation form:

6.6-15 $$F_i > \frac{k_m}{k_m + k_B} P$$

This limitation exists because the material cannot support a tensile load. As long as the preload is not overcome, the additional load on the bolt is a small portion of the total joint load since the material stiffness is normally much greater than the bolt stiffness.

To illustrate the application of these equations, Table 6.6-1 shows the parameters and the results for an aluminum joint held with an M6 x 1.0 bolt rated to 12.9 strength. The table shows that the resultant joint stiffness is 630 N/µm, and that the load required to separate the joint when the bolt is preloaded to 90% of its proof strength is 21.6 kN. The analysis presented here follows that of Norton [43]. Slocum [56] has a fundamentally different way of analyzing joint stiffness, but the method requires parameters found from the literature that were not given for the materials used here. Therefore, Norton's analysis is used although a more thorough investigation using either Slocum's methods or finite-element software could be useful for future iterations of this design.

Table 6.6-1: Calculating the stiffness of a bolted joint

Parameters	*Label*	*Units*	*Values*
Bolt diameter	d	*m*	0.006
Bolt pitch	N	*m*	0.001
Bolt modulus	E_b	*N/m²*	2.08E+11
Shaft modulus	E_1	*N/m²*	2.08E+11
Endplate modulus	E_2	*N/m²*	6.90E+10
Shaft thickness at bolt	t_1	*m*	0.02425
Endplate thickness	t_2	*m*	0.0127
Shaft moment of inertia	I	*m⁴*	3.97608E-08
Pressure cone angle	ϕ	*rad*	0.523598776
Bolt preload	F_i	*N*	17500
Effective thread length	L_t	*m*	0.003
Bolt joint length	L	*m*	0.02725
Material stiffness	k_m	*N/m*	6.74E+08
Bolt tensile area	A_{bt}	*m²*	2.01234E-05
Bolt stiffness	k_b	*N/m*	1.54E+08
Bolt preload stress	σ_p	*Mpa*	869.6353292
Preloaded joint stiffness	k_j	*N/m*	8.28E+08
Joint separation load	F_{max}	*N*	21485.98

6.6.3 Determination of moment of inertia of L_1-L_4 shaft

The moment of inertia of the shaft must be known. The shaft cross-section is shown in Figure 6.6-4; it is a cylindrical shaft with radius r and a cutout h units from the center. The origin of the coordinate system is concentric with the shaft. The steps to finding the moment of inertia are to find the centroid of the area, find the moment of inertia about the origin, and then move the calculated moment of inertia to the centroid by using the parallel-axis theorem.

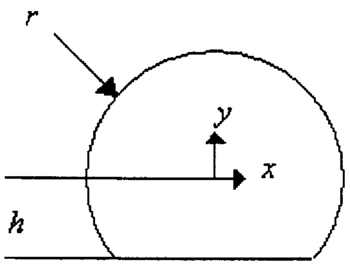

Figure 6.6-4: ***L_1-L_4*** **shaft cross-section**

The centroid of this area will has an *x* coordinate of zero due to symmetry. The *y*-coordinate is found from [43]

6.6-16
$$\bar{y} = \frac{\int y \cdot dA}{\int dA} = \frac{\frac{2}{3}\left(r^2 - h^2\right)^{3/2}}{h\sqrt{r^2 - h^2} + r^2\left(\frac{\pi}{2} - \sin^{-1}\frac{h}{r}\right)}$$

A table of integrals is used to compute the results [66]. Note that $dA = 2\sqrt{r^2 - y^2}dy$ for the calculation. The next step is to find the moment of inertia about the origin of the section. The results are

6.6-17
$$I_{Z'Z'} = \int_A y^2 dA = \frac{r^4}{4}\left(\frac{\pi}{2} + \sin^{-1}\frac{h}{r}\right) - \frac{h}{4}\sqrt{r^2 - h^2}\left(r^2 - 2h^2\right)$$

The final calculation is to move I_{ZZ} to coincide with the centroid using the parallel-axis theorem [66], which states that

6.6-18
$$I_{ZZ} = I_{Z'Z'} - \bar{y}^2 A$$

where A is the area of the cross section and is equal to the denominator of equation 6.6-16 and subscript *ZZ* refers to moment of inertia about the centroid. Table 6.6-2 shows the results of a spreadsheet calculation for the moment of inertia of a section with shaft diameter 49.3 mm with 10.2 mm deep flat cut into it.

Table 6.6-2: Moment of inertia of the L_1-L_4 joint shaft section

Parameters	*Label*	*Units*	*Values*
Shaft radius	r	*m*	0.024638
Cut location	h	*m*	0.014478
Section area	A	m^2	0.001623438
Centroid coordinate	y-bar	*m*	0.003253459
Moment about origin	I_{zz}	m^4	1.89E-07
Moment about neutral axis	$I_{z'z'}$	m^4	1.72E-07

6.6.4 Model of the joint as two springs and simple support

The first model for the L_1-L_4 joint shaft mounting is shown in Figure 6.6-5. The bolted joints are approximated as springs to model their force-displacement relationship. This model assumes that both bolted joints will be in tension while the plate provides a rigid simple support at the rear of the joint shaft. Also, since the model is two dimensional, the bolts are assumed to give knife-edge support across the width of the shaft, or into the page as it is shown in Figure 6.6-5. This assumption is warranted by the fact that the shaft width is only 2-5 times the width of the bolt, and by the fact that the bolted joint also provides some resistance to bending that is not modeled. The model parameters are the bolt locations along the shaft a and b, the stiffness of the two bolted joints k_1 and k_2, and the shaft modulus E_s and its moment of inertia I. The load at the end of the arm is converted into an applied moment M at the bearing shaft as shown.

Using singularity functions and the quantities defined in Figure 6.6-5, the loading $q(x)$ on the shaft is

6.6-19 $$q(x) = F_R < x >_{-1} + F_1 < x - a >_{-1} + F_2 < x - b >_{-1} + M < x - b >_{-2}$$

The negative integral of equation
6.6-19 gives the shear force $V(x)$ on the beam

6.6-20 $$V(x) = -F_R < x >^0 - F_1 < x - a >^0 - F_2 < x - b >^0 - M < x - b >_{-1} + C_1$$

where C_1 is a constant of integration that is equal to zero because the reaction loads are included in the loading equation. Performing the negative integral of equation 6.6-20 in turn gives the moment *M(x)* on the shaft:

6.6-21 $$M(x) = F_R < x >^1 + F_1 < x - a >^1 + F_2 < x - b >^1 + M < x - b >^0 + C_2$$

Again, C_2 is a constant of integration that equals zero because, due to the simple support, the moment at $x = 0$ must be zero. Two more integrations of equation 6.6-21 gives the displacement of the beam δ times the Young's modulus *E* and the moment of area *I*:

6.6-22 $$E_s I\delta(x) = \tfrac{1}{6}F_R < x >^3 + \tfrac{1}{6}F_1 < x - a >^3 + \tfrac{1}{6}F_2 < x - b >^3 + \tfrac{1}{2}M < x - b >^2 + C_3 x + C_4$$

In this case, the constant of integration C_4 is equal to zero because at $x = 0$ displacement is zero due to the simple support.

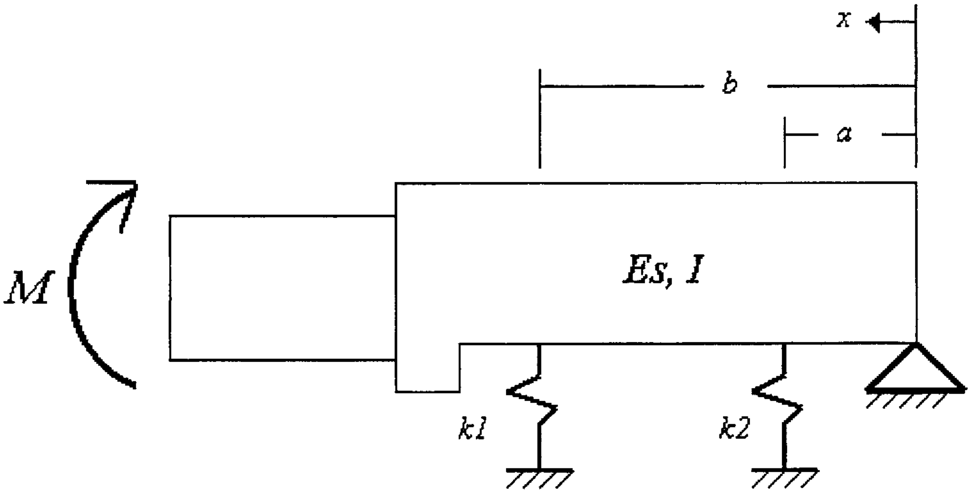

Figure 6.6-5: Model of the L_1-L_4 joint shaft mounting as two springs and a simple support

Thus far, the problem has four unknown quantities: the reaction force F_R, the forces at the bolted joints F_1 and F_2, and the constant of integration C_3. Three boundary conditions have already been used to solve for the other constants of integration. The remaining equations are the force balance, moment balance, and spring constitutive relations for the springs at the bolted joints. The sum of the forces on the beam is

6.6-23
$$\sum F = F_R + F_1 + F_2 = 0$$

while the sum of the moments about the simple support is

6.6-24
$$\sum M = M - F_1 \cdot a - F_2 \cdot b = 0$$

The final equations are the constitutive equations of the springs. As defined, a positive (downwards) displacement of the beam produces a negative (upwards) reaction force in the spring:

6.6-25
$$\delta(a) = \frac{-F_1}{k_1}$$

6.6-26
$$\delta(b) = \frac{-F_2}{k_2}$$

Finally, equations 6.6-23 through 6.6-26 can be combined with equation 6.6-22 to solve for the remaining unknowns with respect to the applied moment M, first by using 6.6-25 and 6.6-22 evaluated at a to solve for C_3 in terms of M and F_1 and then substituting that value into 6.6-22 evaluated at b to solve for F_1 in terms of M. After some algebra these steps yield

6.6-27 $$F_1 = M\frac{b^2 - a^2 - \dfrac{6E_sI}{k_2b}}{(b-a)^3 - b^2(b-a) + a^2(b-a) - \dfrac{6E_sIb}{k_1a} - \dfrac{6E_sIa}{k_2b}}$$

so F_1 and M can be used in equation 6.6-24 to find F_2 and then F_1 and F_2 can be used in equation 6.6-23 to find F_R. All the equations needed for this model have now been presented. They must now be evaluated using the model parameters that apply to this machine. Table 6.6-3 shows the values of the parameters used, the joint stiffness calculated, and the resulting loads.

Table 6.6-3 shows a very interesting feature of the two-spring model: F_1 and F_2 are opposite in sign for the values used, so one joint is loaded in tension and the other in compression. This relation is not true for lower values of joint stiffness. The fact that one joint is loaded in compression means that the deflection is positive at the joint, so the shaft is deflecting into the space occupied by the arm endplate. This movement is not included in the joint stiffness analysis of section 6.6.2 because the stiffness of the joint in compression is much greater. Therefore, another model is needed to account for this behavior.

6.6.5 One spring, cantilevered support model

A two-spring model results in one of the bolted joints being loaded in compression for the parameter values used. Because the compressive stiffness of a bolted joint is much greater than its tensile stiffness, a new model of the L_1-L_4 joint shaft mounting is developed here. As shown in Figure 6.6-6 on page 162, this new model consists of a beam to represent the shaft, a single bolted joint modeled as a spring and a cantilevered support that represents the second bolt and the support from the L_4 arm endplate. As in the previous model, the bolted joint is approximated as providing knife-edge support across the width of the shaft while providing no resistance to bending. The model parameters are the distance between the support and the bolt a, the stiffness of the bolted joint k_1, and the shaft modulus E_s and moment of inertia I.

As for the previous model, the first step is to express the loading q on the shaft with singularity functions

6.6-28 $$q(x) = M_R < x >_{-2} + F_R < x >_{-1} + F_1 < x - a >_{-1} + M < x - a >_{-2}$$

Table 6.6-3: Two-spring model results

Input Parameters	**Label**	**Value**	***Units***
Length to bolt 1	a	0.008636	*m*
Length to bolt 2	b	0.051816	*m*
Joint 1 stiffness	k_1	1.79E+09	*N/m*
Joint 2 stiffness	k_2	1.79E+09	*N/m*
Load at endpoint	F_{end}	2574.260858	*N*
Load safety factor	SF	4.13	
Applied moment	M	2026.973	*N-m*
Beam modulus	E_1	2.08E+11	N/m^2
Beam moment of inertia	I	8.33E-08	m^4
Poisson ratio	η	0.34	
Approx. beam height	h	0.015	*m*
Bolt diameter	d	0.01	*m*
Bolt length	L_m	0.035	*m*
Endplate modulus	E_2	6.90E+10	N/m^2
Beam thickness at bolt	t_1	0.01925	*m*
Endplate thickness	t_2	0.0127	*m*
pressure cone angle	ϕ	0.523598776	*rad*
Bolt modulus	E_b	2.08E+11	N/m^2
Bolt pitch	N	0.0015	*m*
Bolt preload	F_i	46107.90341	*N*
Bolt stiffness	k_b	4.97E+08	*N/m*
Preloaded joint stiffness	k_j	1.79E+09	*N/m*
Bolt preload stress	σ_p	795.1064653	*Mpa*
Force in joint 1	F_1	-7.76E+03	*N*
Integration constant	C_3	9.09E+00	
Force in joint 2	F_2	4.04E+04	*N*
Reaction force at support	F_R	-3.26E+04	*N*

where M_R is the reaction moment, F_R is the reaction force, F_1 is the force at the bolted joint and M is the applied moment. Next, equation 6.6-28 is integrated to find the shear V on the shaft

6.6-29
$$V(x) = -M_R < x >_{-1} - F_R < x >^0 - F_1 < x - a >^0 - M < x - a >_{-1} - C_1$$

As in the previous section, the fact that the reactions are included in the loading equation means that the constant of integration $C_1 = 0$. The moment M follows,

6.6-30
$$M(x) = M_R < x >^0 + F_R < x >^1 + F_1 < x - a >^1 + M < x - a >^0 + C_2$$

With $C_2 = 0$ because the reaction moment is included in the load q. Because of the cantilevered support, the beam must have no angle at $x = 0$, so the expression

6.6-31
$$E_s I\alpha(x) = M_R < x >^1 + \tfrac{1}{2} F_R < x >^2 + \tfrac{1}{2} F_1 < x - a >^2 + M < x - a >^1 + C_3$$

must be zero when evaluated at $x = 0$. Solving shows that $C_3 = 0$. Finally, the displacement of the beam is found through one more integration of equation 6.6-31,

6.6-32
$$E_s I\delta(x) = \tfrac{1}{2} M_R < x >^2 + \tfrac{1}{6} F_R < x >^3 + \tfrac{1}{6} F_1 < x - a >^3 + \tfrac{1}{2} M < x - a >^2 + C_4$$

where C_4 must equal zero because the cantilevered support at $x = 0$ prevents displacement.

Equations 6.6-28 through 6.6-32 leave three unknowns: the reaction moment M_R, the reaction force F_R, and the force at the bolted joint F_1. The three equations to use to find these unknowns are the force balance, moment balance, and Hooke's law for the bolted joint spring. The force balance is

6.6-33
$$\sum F = F_R + F_1 = 0$$

the moment balance is

6.6-34 $$\sum M = M + M_R - F_1 \cdot a = 0$$

and the spring constitutive equation is

6.6-35 $$\delta(a) = \frac{-F_1}{k_1}$$

Equations 6.6-33 through 6.6-35 are almost identical to those used for the previous model. Because there is one less equation and unknown, solving for F_1 in terms of M is simpler for this model than for the two-spring model. The result is

6.6-36 $$F_1 = M \frac{a^2}{\frac{2}{3}a^3 + \frac{2E_s I}{k_1}}$$

Once F_1 is known, F_R can be found from 6.6-33 and M_R from 6.6-34.

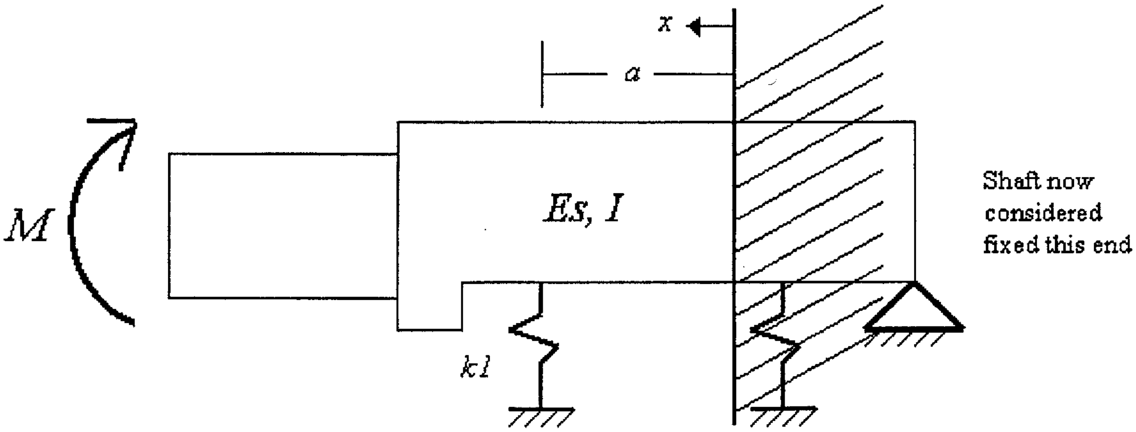

Figure 6.6-6: One spring, cantilevered support model of the L_1-L_4 joint shaft mounting

Because the shaft is short and stubby in the area being considered, transverse shear loading of the shaft should be considered in this problem. The shear deflections were estimated by approximating the shaft as a rectangular beam of similar dimensions. It was found that, while the shear deflections altered the load on the bolt by 3%, the effect was such to reduce the load on the joints. Therefore, to simplify the analysis presented here and to keep the analysis conservative, the shear deflections were dropped from the model.

The equations for the one spring, cantilevered support model have now been derived. The next step is to enter the equations into a spreadsheet and find bolt sizes, preloads, and spacing that will give the desired load-carrying capacity. Table 6.6-4 shows the results of the model using the same parameters as in the two spring model in Table 6.6-3: two M10 bolts spaced 38 mm (1.5 inches) apart, using a 46 kN preload force as before. Table 6.6-4 shows that these parameters keep the bolt stress below the yield stress of 1100 MPa even with a safety factor of four on the end-effector loads.

Table 6.6-4: Cantilevered, single spring model results

Parameter	**Label**	**Value**	***Units***
Distance between bolts	a_1	0.03818	*m*
Force in joint	F_1	5.24E+04	*N*
Reaction force	F_R	-5.24E+04	*N*
Reaction moment	M_R	-2.74E+01	*N-m*
Load on bolt	F_b	6.06E+04	*N*
Load on material	F_m	8251.991913	*N*
Stress on bolt	σ_b	1.05E+03	*Mpa*

6.7 L_1-L_4 *joint stiffness analysis*

The bolted joint between the L_1-L_4 shaft and the L_4 arm endplate was analyzed in section 6.6. This section will study the stiffness and strength of those two components in more detail. The previous section only examined the load on the bolted section; this section will calculate the loads and deflections in the other areas of the joint. First, the overall joint model is described. Then deflection due to bending and shear is examined. More detailed discussion follows about the bolted piece and the bearing shaft. Finally, all the pieces are put together in a complete model of the L_1-L_4 joint strength and stiffness. Results are also shown for when the model is applied to the L_4-L_7 joint

6.7.1 Overall joint model

Figure 6.7-1 shows a diagram of the L_1-L_4 joint in more detail than presented earlier. The joint is divided into nine pieces. Each piece has length, cross-section, material properties, and loading that are particular to that part. Five of the pieces are in the L_1-L_4 joint shaft, three are in the L_4 arm endplate, and one is shared between the two components. The properties of each piece are used to find the angle and deflection of each part. Then the angle and deflections are combined to yield the overall joint stiffness.

The overall joint stiffness is calculated as the linear stiffness felt at the endpoint. In other words, the joint stiffness is the force at the endpoint divided by the deflection at the endpoint, considering only the components in the L_1-L_4 joint. In equation form, this stiffness $k_{L1\text{-}L4}$ is

6.7-1
$$k_{L1-L4} = \frac{F_E L_P}{(\Delta_B - \Delta_T) L_A}$$

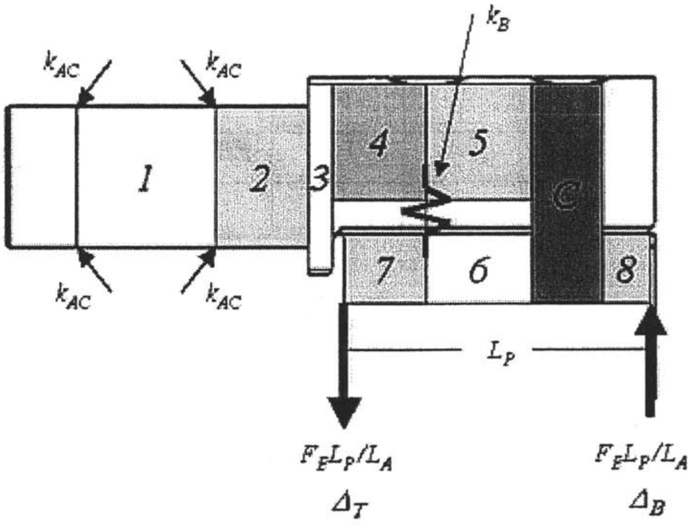

Figure 6.7-1: L_1-L_4 joint model

where F_E is the load at the endpoint, L_P is the length of the plate, L_A is the length of the arm from the L_1-L_4 joint to the endpoint, Δ_B is the total deflection at the bottom of the L_4 arm endplate and Δ_T is the total deflection at the top of the L_4 arm endplate.

To find the deflections at the top and bottom of the endplate, the deflections and angles of each component must be combined properly. For the top, this combination is

6.7-2
$$\Delta_T = \delta_C + \delta_6 + \delta_7 - \alpha_C(L_6 + L_7) + \alpha_6 L_7$$

where δ_i is the deflection of the i^{th} piece, α_i is the angle of the i^{th} piece, and L_i is the length of the i^{th} piece. The corresponding deflection at the bottom of the endplate is

6.7-3
$$\Delta_B = \delta_C + \delta_8 + \alpha_C(L_C + L_8)$$

The piece labeled 'C' is treated as perfectly rigid, and its total angle and deflection are a combination of the angles and deflections of all the pieces of the L_1-L_4 joint shaft. For the angle, the combination is simply

6.7-4
$$\alpha_C = \alpha_1 + \alpha_2 + \alpha_3 + \alpha_4 + \alpha_5$$

while the deflection of the 'C' piece is

6.7-5
$$\delta_C = \delta_1 + \delta_2 + \delta_3 + \delta_4 + \delta_5 + \alpha_1(L_2 + L_3 + L_4 + L_5) + \alpha_2(L_3 + L_4 + L_5) + \alpha_3(L_4 + L_5) + \alpha_4 L_5$$

Note that in equation 6.7-1, δ_C would cancel out from the definitions of Δ_B and Δ_T given in equations 6.7-2 and 6.7-3. The principle behind the combination of deflections and angles of the pieces is that each piece has the angle and deflection calculated relative to its neighbor. In other words, δ_i is the deflection of one end of the i^{th} piece relative to the other and not the total, absolute deflection relative to ground. The exception to this rule is the angle and deflection of the piece 'C', which is calculated in absolute terms.

Based on the geometry shown in Figure 6.7-1, the load and moment on each piece of the joint is shown on Table 6.7-1. The values are expressed in terms of the endpoint force F_E, bolt joint force F_B, arm length L_A, L_4 joint endplate length L_P, and the lengths of some pieces in the joint. The next step is to find the deflections of each piece of the joint shown in Figure 6.7-1. For most pieces this is a simple procedure because they are cantilevered beams with applied loads and/or moments at their ends. Three of the pieces warrant further examination: the two pieces that are bolted together and the piece that is supported by the joint bearings. These details are examined in the sections that follow.

Table 6.7-1: Loads and moments applied to each joint piece

Piece	Load	Moment
1	0	$F_E L_A$
2	0	$F_E L_A$
3	0	$F_E L_A$
4	0	$F_E L_A$
5	$-F_B$	$F_E L_A$
6	$F_B - F_E L_A/L_P$	$-F_E L_A/L_P{*}L_7$
7	$-F_E L_A/L_P$	0
8	$F_E L_A/L_P$	0

6.7.2 Basic model beam element

Most pieces of the L_1-L_4 joint can be treated as cantilevered beams because only the relative deflection and angle are important. The individual pieces then look like the beam in Figure 6.7-2. The piece has applied load F_i, applied moment M_i, reaction force F_{Ri}, and reaction moment M_{Ri}. The beam also has an elastic modulus E_i and cross-section moment of inertia I_i. The resultant endpoint deflection is δ_i and the endpoint angle is α_i.

The first step in this analysis is to find the reaction force and moment. These are found from a sum of forces,

6.7-6 $$\sum F = F_i - F_{Ri} = 0, \quad F_{Ri} = F_i$$

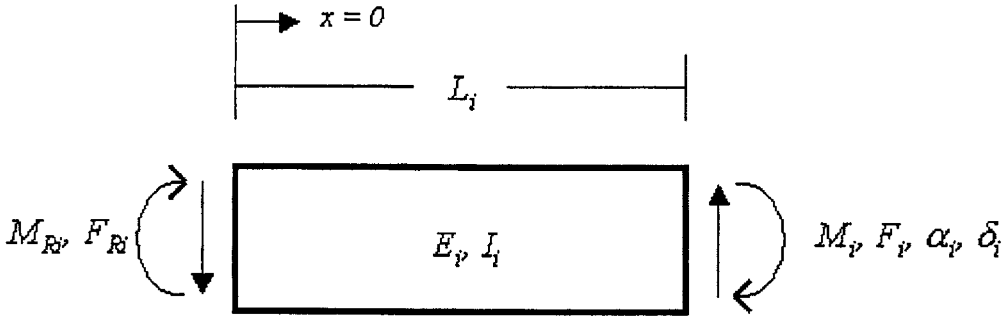

Figure 6.7-2: General L_1-L_4 joint piece

and a sum of moments

6.7-7 $$\sum M = M_i - M_{Ri} + F_i L_i = 0, \qquad M_{Ri} = M_i + F_i L_i$$

Then the load $q_i(x)$ along the beam is

6.7-8 $$q_i(x) = -F_i < x >_{-1} + (M_i + F_i L_i) < x >_{-2} + F_i < x - L_i >_{-1} - M_i < x - L_i >_{-2}$$

using variables as defined above. Two integrations give the shear $V_i(x)$ and moment $M_i(x)$ along the beam's length,

6.7-9 $$V_i(x) = F_i < x >^0 - (M_i + F_i L_i) < x >_{-1} - F_i < x - L_i >^0 + M_i < x - L_i >_{-1}$$

6.7-10 $$M_i(x) = -F_i < x >^1 + (M_i + F_i L_i) < x >^0 + F_i < x - L_i >^1 - M_i < x - L_i >^0$$

Because the reactions are included in the loading equation, the first two constants of integration are zero. Two more integrations give the angle $\alpha_i(x)$ and deflection $\delta_i(x)$ along the beam's length, 6.7-11 $$E_iI_i\alpha_i(x) = -\tfrac{1}{2}F_i < x >^2 + (M_i + F_iL_i) < x >^1 + \tfrac{1}{2}F_i < x - L_i >^2 - M_i < x - L_i >^1$$

6.7-12 $$E_iI_i\delta_i(x) = -\tfrac{1}{6}F_i < x >^3 + \tfrac{1}{2}(M_i + F_iL_i) < x >^2 + \tfrac{1}{6}F_i < x - L_i >^3 - \tfrac{1}{2}M_i < x - L_i >^2$$

The constants of integration are also zero for equations 6.7-11 and 6.7-12 because the beams are treated as cantilevered with zero angle and zero deflection at $x = 0$. The quantities of interest in this analysis are the angle and deflection at the endpoint. Substituting $x = L$ into equations 6.7-11 and 6.7-12 yields

6.7-13 $$\alpha_i(L_i) = \frac{2M_iL_i + F_iL_i^2}{2E_iI_i}$$

6.7-14 $$\delta_i(L_i) = \frac{3M_iL_i^2 + 2F_iL_i^3}{6E_iI_i}$$

These equations can be used for all the pieces once the load and moment applied to the piece as well as the piece geometry, cross-section, and material are known.

6.7.3 Shear deflection in beams

As shown in Figure 6.7-1, most pieces of the L_1-L_4 joint have short, stubby geometries so shear deflections could play an important role. According to Castigliano's theorem [43], the deflection due to shear δ_{shear} at a point is the partial derivative of the strain energy due to shear U_s with respect to the load F applied at the point:

6.7-15 $$\delta_{shear} = \frac{\partial U_s}{\partial F}$$

The strain energy due to shear is defined as

6.7-16 $$U_s = \int_V \frac{\tau^2}{2G} dV$$

where τ is the shear stress at any point in the beam and G is the shear modulus of the material. The shear stress is calculated as [43]

6.7-17 $$\tau_{xy}(y_1) = \frac{V}{Ib} \int_{y_1}^{c} y dA$$

where I is the moment of inertia of the cross section, V is the shear at the cross section and b is the width of the cross section and may depend on the height coordinate y. The integral in equation 6.7-17 is evaluated from y_1 to c where $2c$ is the height of the section. Equation 6.7-17 assumes that the shear stress is constant across the width b of the cross-section. In reality this is not the case, especially if the cross-section has varying width, but for this analysis it is assumed that the shear stress is averaged over the width as expressed in the equations.

A more convenient way to express equation 6.7-16 is

6.7-18 $$U_s = \frac{1}{2G} \int_0^L V^2 \int_{-b/2}^{b/2} \int_{-c}^{c} \left(\frac{\tau}{V} \right)^2 dydzdx$$

Equation 6.7-18 is a convenient expression because the shear stress is proportional to the shear on the beam but also depends on the cross section. Defining a new variable X such that

6.7-19 $$X = \int_{-b/2}^{b/2} \int_{-c}^{c} \left(\frac{\tau}{V} \right)^2 dydz$$

gives an integral that only depends on the cross-section of the beam. Finally, substituting for X and taking the derivative gives the shear deflection as

6.7-20 $$\delta_{shear,i} = \frac{X_i}{G_i} \int_0^L V_i \frac{\partial V_i}{\partial F_i} dx$$

Three cross-section shapes are used in the L_1-L_4 joint. In order of increasing complexity in calculating the shear deflection these cross-section shapes are rectangular, circular, and circular with a flat. Each cross-section has its own value of X that is used to calculate the shear deflection.

For a rectangular cross-section, equation 6.7-17 is simple because the width b of the beam is constant. Shear stress in a rectangular beam is [43]

6.7-21 $$\tau_{rect}(y) = \frac{V}{2I}\left[\left(\frac{h}{2}\right)^2 - y^2\right]$$

so that X_{rect} is

6.7-22 $$X_{rect} = \frac{bh^5}{120I^2}$$

where h is the height of the beam. For a circular cross-section, the shear stress becomes

6.7-23 $$\tau_{circ}(y) = \frac{2V\left(\frac{2}{3}\left(r^2 - y^2\right)^{3/2}\right)}{\pi r^4 \sqrt{r^2 - y^2}}$$

The integral X_{circ} is not easily computed by hand; instead, it was calculated using numerical methods. The integral is

6.7-24 $$X_{circ} = \int_{-r}^{r} \frac{32}{9\pi^2 r^8}\left(r^2 - y^2\right)^{5/2} dy$$

The final cross-section for which this process must be carried out is the cut-off circle. After a lengthy derivation, the result is

6.7-25
$$X_{cut-off} = \int_{-h}^{r} \frac{\left[\frac{2}{3}\left(r^2 - y^2\right)^{3/2} - \bar{y}\left(\frac{\pi r^2}{2} - y\sqrt{r^2 - y^2} - r^2 \sin^{-1}\frac{y}{r}\right)\right]^2}{2I^2\sqrt{r^2 - y^2}} dy$$

where *y-bar* is the location of the centroid and *I* is the section moment of inertia. Both quantities are defined in equations 6.6-16 through 6.6-18 on page 155.

The final step in evaluating the deflection of a beam due to shear is to evaluate equation 6.7-20 in terms of the shear on the beam as given by equation 6.7-9. At the end of the beam, the shear is equal to F_i (ignoring the discontinuity introduced by the concentrated moment applied at the end). Therefore the shear deflection at the end is

6.7-26
$$\delta_{shear,i} = \frac{X_i L_i}{G_i} F_i$$

This quantity should be added to the total deflection when analyzing the different pieces of the joint.

6.7.4 Bolted piece

The model used here to analyze the two bolted pieces in the L_1-L_4 joint is similar to the one in section 6.6.5. As shown in Figure 6.7-3, the model consists of two beams cantilevered to a common support with a spring between them. Each beam has its own load and moment applied to the endpoint. Once the force applied by the bolted joint is known, the force and moment at the endpoint of each piece can be used with equations 6.7-13, 6.7-14, and 6.7-26 to find the load and deflection at the endpoint of each beam.

Because the bolted joint between the beams is modeled as a spring, the force in the bolted joint F_B is proportional to the displacement, or

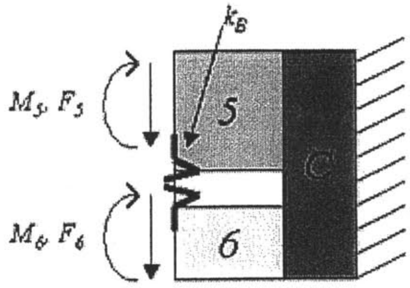

Figure 6.7-3: Model of the bolted pieces in the L_1-L_4 joint

6.7-27
$$F_B = k_B\left(\delta_5 - \delta_6\right)$$

The bolted joint stiffness k_B can be found from the equations given in section 6.6.2, and the deflections are calculated from equations 6.7-14, and 6.7-26 using the parameters for the two pieces that make up the bolted joint. For convenience, these two equations are combined here:

6.7-28
$$E_i I_i \delta_i\left(L_i\right) = \left(\frac{L_i^3}{3} + 2(1+\eta) I_i X_i L_i\right) F_i + \tfrac{1}{2} M_i L_i^2$$

Note that the applied moment M_i has no effect on the shear deflections of the beam.

The next step in finding F_B is to substitute equation 6.7-28 into 6.7-27. The applied forces and moments from Table 6.7-1 are substituted here as well. The result is

6.7-29
$$\begin{aligned}\frac{F_B}{k_B} &= \frac{1}{E_5 I_5}\left(-\frac{L_5^3}{3} F_B - 2(1+\eta_5) I_5 L_5 X_5 F_B + \frac{L_A L_5^2}{2} F_E\right) \\ &- \frac{1}{E_6 I_6}\left(\frac{L_6^3}{3}\left(F_B - \frac{L_A}{L_P} F_E\right) + 2(1+\eta_6) I_6 L_6 X_6\left(F_B - \frac{L_A}{L_P} F_E\right) - \frac{L_A L_6^2}{2L_P} F_E\left(L_7 + L_8\right)\right)\end{aligned}$$

After some algebra, the force in the bolt F_B can be found in terms of the endpoint force F_E as follows:

6.7-30 $$F_B = F_E L_A \frac{\frac{L_5^2}{2E_5 I_5} + \frac{L_6^2 \left(L_7 + L_8\right)}{2E_6 I_6 L_P} + \frac{L_6^3}{3E_6 I_6 L_P} + \frac{2\left(1+\eta_6\right) L_6 X_6}{E_6 L_P}}{\frac{1}{k_B} + \frac{L_5}{E_5 I_5}\left(\frac{1}{3} L_5^2 + 2\left(1+\eta_5\right) I_5 X_5\right) + \frac{L_6}{E_6 I_6}\left(\frac{1}{3} L_6^2 + 2\left(1+\eta_6\right) I_6 X_6\right)}$$

The above value for the force in the bolted joint can now be entered into the cantilevered-beam equations from section 6.7.2 to find the resultant deflection and stiffness of the piece.

6.7.5 Bearing shaft

The bearing shaft is the only piece that is connected to ground. It is supported by four springs at an angle θ that represent the stiffness of the angular contact ball bearings, as shown in Figure 6.7-4. Each spring has a stiffness k_{AC} and produces a force F_1, F_2, F_3, or F_4; the forces act at angles θ and at distance R_B from the shaft centerline. The shaft is also subject to an axial force F_E.

The sum of the forces acting on the shaft in the x and y directions is

6.7-31 $$\sum F_x = \left(-F_1 + F_2 - F_3 + F_4\right)\cos\theta - F_E = 0$$

6.7-32 $$\sum F_y = \left(-F_1 + F_2 + F_3 - F_4\right)\sin\theta = 0$$

while the sum of the moments is

6.7-33 $$\sum M = -M_1 + \left(F_2 - F_4\right)L_1 \sin\theta + \left(F_1 + F_2 - F_3 - F_4\right)R_B \cos\theta = 0$$

The shaft is supported by springs; therefore, the boundary conditions are the constitutive force-displacement equations for those springs:

6.7-34

$$\delta_0 = -\frac{(F_3 - F_1)\sin\theta}{k_y}$$

6.7-35

$$\delta_L = -\frac{(F_2 - F_4)\sin\theta}{k_y}$$

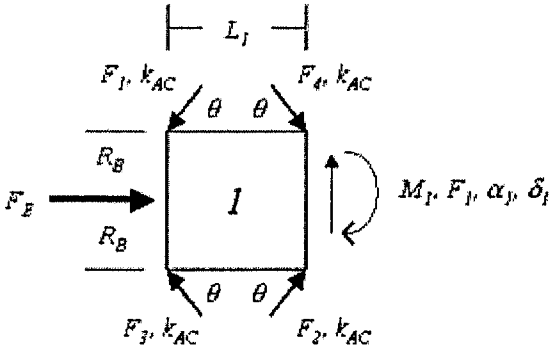

Figure 6.7-4: Bearing shaft supported by four springs

Because there are not enough equations to solve for four unknowns, one extra equation must be added. As in section 6.4.2, then, there is an assumption that $F_3 = 0$. The angular contact bearings cannot produce a negative force, so if at the end of the analysis one of the non-zero forces is negative this assumption must be revised.

To solve for the forces, subtract equation 6.7-32 from equation 6.7-31, and use the assumption that $F_3 = 0$ to find:

6.7-36

$$F_4 = \frac{F_E}{2\cos\theta}$$

Next, solve 6.7-31 for F_1,

6.7-37 $$F_1 = F_2 - \frac{F_E}{2\cos\theta}$$

then solve 6.7-33 for F_2,

6.7-38 $$F_2 = \frac{F_E}{2\cos\theta} + \frac{M_1}{L\sin\theta + 2R_B\cos\theta}$$

and finally substitute 6.7-38 into 6.7-31 to find F_1 in terms of known quantities.

6.7-39 $$F_1 = \frac{M_1}{L\sin\theta + 2R_B\cos\theta}$$

Now the loading condition of the shaft is known and the loading equation of the general joint element from Figure 6.7-2 and equation 6.7-8 can be used. Substituting in for forces and moments,

6.7-40 $$\begin{aligned} q_1(x) &= (F_3 - F_1)\sin\theta < x >_{-1} + (M_1 + (F_3 - F_1)R_B\cos\theta) < x >_{-2} \\ &+ (F_2 - F_4)\sin\theta < x - L_1 >_{-1} - (F_2 - F_4)R_B\cos\theta < x - L_1 >_{-2} \end{aligned}$$

To simplify this expression and the ones that follow, substitute F_0 for the force at $x = 0$ and so forth:

6.7-41 $$q_1(x) = F_0 < x >_{-1} + M_0 < x >_{-2} + F_L < x - L_1 >_{-1} - M_L < x - L_1 >_{-2}$$

Integrating the loading equation four times gives the displacement equation,

6.7-42 $$E_1 I_1 \delta_1(x) = -\tfrac{1}{6}F_0 < x >^3 + \tfrac{1}{2}M_0 < x >^2 + \tfrac{1}{6}F_L < x - L_1 >^3 - \tfrac{1}{2}M_L < x - L_1 >^2 + C_3 x + C_4$$

The first two constants of integration are zero because the reaction forces are included in the loading equation, but the third and fourth constants must be found by invoking equations 6.7-34 and 6.7-35. The former is the easier result to obtain.

6.7-43

$$E_1I_1\delta_1(0) = C_4 = -E_1I_1\frac{F_0}{k_y}$$

6.7-44

$$C_4 = \frac{E_1I_1M_1\sin\theta}{k_y\left(L_1\sin\theta + 2R_B\cos\theta\right)}$$

Solving for C_3 is more involved. Shear deflections must be taken into account.

6.7-45

$$E_1I_1\delta_1(L) = -\tfrac{1}{6}F_0L_1^{\,3} + \tfrac{1}{2}M_0L_1^{\,2} + C_3L_1 + C_4 + \delta_{SHEAR}(L) = -E_1I_1\frac{F_L}{k_y}$$

6.7-46

$$C_3 = \frac{M_1\sin\theta}{2L_1\left(L_1\sin\theta + 2R_B\cos\theta\right)}\left[\frac{-4E_1I_1}{k_y} + \frac{L_1^{\,3}}{3} - L_1^{\,2}\left(L_1 + 2R_B\cot\theta\right) - R_BL_1^{\,2}\cot\theta - \frac{4X_1L_1\left(1+\eta_1\right)}{E_1}\right]$$

The next step is to find the appropriate spring stiffness to input into the above equations. SKF gives preload specifications for its angular contact bearings that include a displacement and a force applied in the axial direction [55]. Calling the former Δ_P and the latter F_P, these can be related to find the stiffness in the axial direction of each spring in this model:

6.7-47

$$k_x = \frac{\Delta_P}{F_P}$$

The contact angle of the bearing can then be used to relate the axial stiffness to the radial stiffness, 6.7-48 $$k = \frac{k_x}{\cos^2\theta} = \frac{k_y}{\sin^2\theta}$$

Table 6.7-2 shows the specifications for bearing preload given by SKF. All that remains is to enter these equations and values into a spreadsheet to find a result for the L_1-L_4 joint stiffness.

Table 6.7-2: Approximate stiffness of SKF angular contact bearings [55]

Preload		Clearance *µm*	Force *N*	Stiffness
GA	*max*	0	0	
	min	-4	160	40
GB	*max*	-2	60	
	min	-10	630	71.25
GC	*max*	-8	450	
	min	-16	1280	103.75

6.7.6 Results of L_1-L_4 joint model

Table 6.7-3 on page 178 and Table 6.7-4 on page 179 show the results of applying the above model to the L_1-L_4 and L_4-L_7 joints. The table shows the stiffness in two ways: as an angular stiffness and as a linear stiffness extrapolated to the robot endpoint at the center of the L_7 link. The endpoint is at the center of this link because that is where the force transducer is located. The L_1-L_4 joint has an angular stiffness of 96400 N-m/rad while the L_4-L_7 joint has an angular stiffness of 21400 N-m/rad. While the former joint is angularly stiffer, the longer lever arm means that it is an order of magnitude less stiff at the endpoint: the L_1-L_4 joint has 0.2 N/µm stiffness at the endpoint versus 2.1 N/µm for the L_4-L_7 joint.

Table 6.7-3: L_1-L_4 Joint model results

L1-L4 Joint Inputs	**Labels**	**Values**	***Units***
Endpoint force	F_e	2496	*N*
Length of arm	L_a	0.6858	*m*
Length of plate	L_p	0.073152	*m*
Bolt spacing	D_{bolt}	0.03556	*m*
Bolt diameter	d	0.01	*m*
Bolt pitch	p	0.0015	*m*
Pressure cone angle	ϕ	0.52359878	*rad*
Bolt joint stiffness	k_{bj}	1.60E+09	*N/m*
Bolt preload	F_i	4.20E+04	*N*
Force in bolt joint	F_{bj}	39538.8146	*N*
Safety factor against separation	SF_b	1.39583502	
Stress in bolt	σ_b	887.216009	*MPa*
Effective width of plate	b_p	0.04445	*m*
Thickness of plate	h	0.01524	*m*
Diameter of bearing seat	d_b	0.035	*m*
Diameter of wide shaft	d_w	0.049276	*m*
Cut distance from shaft center	h_s	0.014478	*m*
Shaft modulus	E_s	2.08E+11	N/m^2
Poisson of shaft	η_s	0.28	
Plate modulus	E_p	6.90E+10	N/m^2
Poisson of plate	η_p	0.34	
Bolt modulus	E_b	2.08E+11	N/m^2
Bearing stiffness	k_{AC}	1.77E+08	*N/m*
Bearing contact angle	θ	0.6981317	*rad*
Bearing radius	R_b	0.0185	*m*
Deflection at top of plate	Δ_T	1.01E-04	*m*
Deflection at bottom of plate	Δ_B	1.40E-03	*m*
Angular stiffness of joint	K_α	9.64E+04	*N-m/rad*
EQ. stiffness of Joint at endpoint	K_J	2.05E+05	*N/m*

Table 6.7-4: L_4-L_7 Joint model results

L4-L7 Joint Inputs	**Labels**	**Values**	***Units***
Endpoint force	F_e	2496	*N*
Length of arm	L_a	0.1016	*m*
Length of plate	L_p	0.0508	*m*
Bolt spacing	D_{bolt}	0.0254	*m*
Bolt diameter	d	0.006	*m*
Bolt pitch	p	0.001	*m*
Pressure cone angle	ϕ	0.52359878	*rad*
Bolt joint stiffness	k_{bj}	9.09E+08	*N/m*
Bolt preload	F_I	1.50E+04	*N*
Force in bolt joint	F_{bj}	7846.37068	*N*
Safety factor against separation	SF_b	2.44371905	
Stress in bolt	σ_b	830.287338	*MPa*
Effective width of plate	b_p	0.03048	*m*
Thickness of plate	h	0.0127	*m*
Diameter of bearing seat	d_b	0.02	*m*
Diameter of wide shaft	d_w	0.03048	*m*
Cut distance from shaft center	h_s	0.010414	*m*
Shaft modulus	E_s	2.08E+11	*N/m^2*
Poisson of shaft	η_s	0.28	
Plate modulus	E_p	6.90E+10	*N/m^2*
Poisson of plate	η_p	0.34	
Bolt modulus	E_b	2.08E+11	*N/m^2*
Bearing stiffness	k_{AC}	9.37E+07	*N/m*
Bearing contact angle	θ	0.6981317	*rad*
Bearing radius	R_b	0.01695	*m*
Deflection at top of plate	Δ_T	1.59E-04	*m*
Deflection at bottom of plate	Δ_B	7.60E-04	*m*
Angular stiffness of joint	K_α	2.14E+04	*N-m/rad*
EQ. stiffness of joint at endpoint	K_J	2.08E+06	*N/m*

6.8 Vertical connection sub-module design

Three spline shafts allow the robot linkage to move in the vertical direction. As noted in section 4.2.4 the three shafts will not be perfectly parallel and they will not keep the spline nuts spaced apart a constant distance. This is a similar problem to that faced by the planar linkage itself: there are more constraints than degrees of freedom. In the planar linkage the problem was solved by replacing four of the six one-DOF-pin-joints with three-DOF-spherical-joints. The same solution is required here. By adding mobility to the structure that connects the spline nuts, the forced congruence is removed while the ability to move vertically in unison is retained. The system is also connected to a linear motor module with a linear bearing for a total of four interconnected vertical guides.

6.8.1 Vertical connection sub-module requirements

The simplest vertical connection module would consist of a structure that rigidly connects the bearings on the spline nut housings, the linear motor, and the body-weight support spring. The bearings associated with the spline nuts each allow only two motions: vertical translation and rotation about the vertical axis. This configuration creates a problem with overconstraint. The vertical connection structure has six degrees of freedom but seventeen constraints, four each from the spline nut bearings and five from the linear motor bearing.

The vertical connection sub-module is shown in Figure 6.8-1. This module is meant to restrict the vertical translation without interfering with the other five degrees of freedom of each spline-nut and bearing assembly so that shimming and exact alignment are not necessary. This module must be able to account for typical misalignments in manufacturing and assembly. The magnitudes of the expected misalignments are shown in Table 6.8-1. The module should allow 3 mm of motion for the location spline nuts and 1 mm of motion for the linear motor. There must also be 1° of angular misalignment allowed between the components. By adding these eleven degrees of freedom, the number of constraints on the vertical connection structure is reduced from seventeen to six. The main spline is responsible for four of the constraints, the locating spline 2 provides an additional constraint, and the linear motor introduces the vertical constraint. The mechanism that connects the linear motor to the main spline must be designed to sustain at least the peak force generated by the linear motor, or 1120 N as stated in section 6.3.2 and as repeated in Table 6.8-1 below. The other two splines also need to be able to carry some load, though as was the case for the locating link cross-sections in section 6.5.2 the required load is only 200 N.

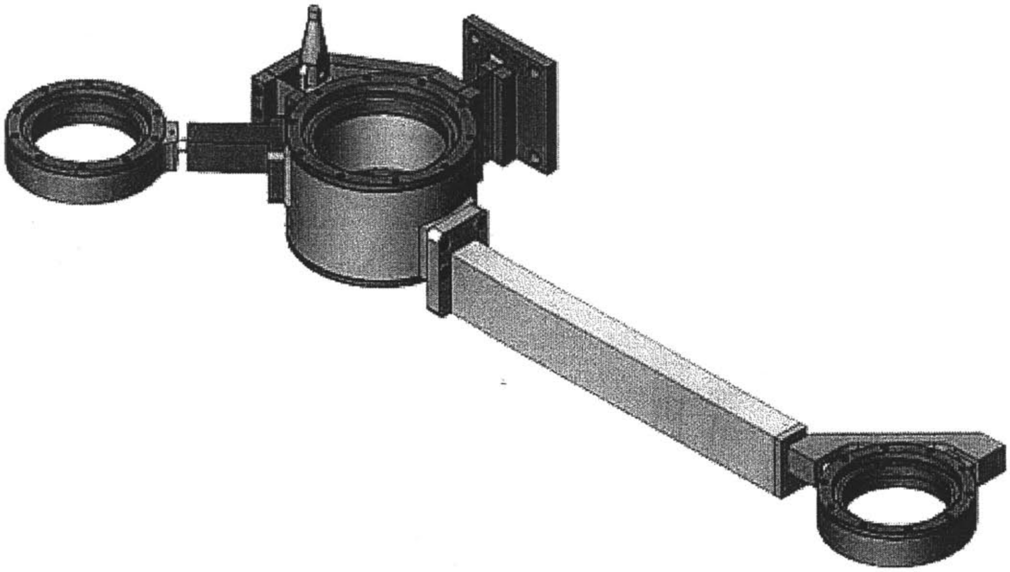

Figure 6.8-1: Vertical connection sub-module

Table 6.8-1: Vertical connection requirements for each spline

	Linear Motor	Spline 2	Spline 3	*Units*
Degrees of freedom	4	3	4	
Vertical load	1120	200	200	*N*
Translation	1	3	3	*mm*
Rotation	1	1	1	*degrees*

6.8.2 Load-bearing connection design

The connection between the linear motor and the main spline nut must transmit vertical loads up to 1120 N. Because the main spline nut is connected to the load-bearing arm that supports the force sensor, this connection is in the force-feedback path. Ideally the feedback path would have as high a bandwidth as possible, so the load-bearing connector must be stiff and should be free of clearance or play. These requirements make flexural bearings the ideal medium for transmitting these vertical loads. Figure 6.8-2 shows a flexure capable of the task: it consists of two orthogonal flexure blades, each capable of a translation and a twist. The flexure blades were arranged as shown in Figure 6.8-2 so that the rotational misalignments of the spline nut would have no moment arms.

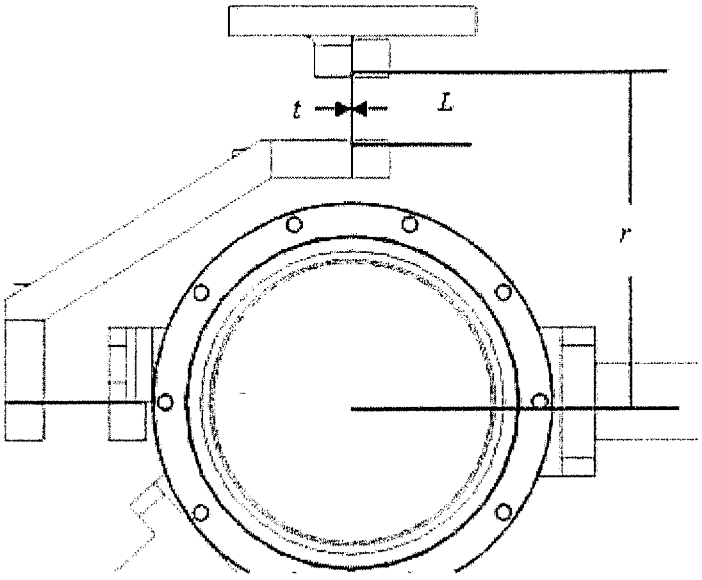

Figure 6.8-2: Four-degree-of-freedom clamped flexure

The material, cross-section, and length of these flexure blades must be selected so as to ensure the safety of the device in response to static loads and fatigue. Also, the clamping mechanism must be designed so as to avoid fretting corrosion at the interface between the bolted parts. A clamped flexure is used for this application because it allows the use of very thin yet strong spring-tempered stainless steel flexure blades. Spring-tempered stainless steel has yield strength 965 MPa and endurance limit 552 MPa [3]. The strength of the material used impacts the load-carrying capacity of the flexure, the maximum deflection the flexure can sustain, and the flexure's ability to survive cyclic loading.

Three deformations of the flexure are examined: 'bending' deformations occur vertically along the flexure's stiffest direction, 'flexing' deformations occur horizontally perpendicular to the length of the flexure, and 'twisting' deformations occur about a horizontal axis that runs through the length of the flexure. Vertical loads F transmitted across the flexure blades produce bending stresses σ_{bend}

6.8-1

$$\sigma_{bend} = \frac{6Fr}{th^2}$$

where t is the thickness of the flexure, h is the height of the blade and r is the lever arm of the vertical force. In the flexure shown in Figure 6.8-2 r is the distance from the center of the spline shaft to the far clamping edge of the flexure [44].

Flexing deflections δ are found using a 'fixed-free' beam-bending model [44],

6.8-2 $$\delta = \frac{4pL^3}{Eht^3}$$

where p is the force in the flexing direction, E is the young's modulus, and L is the length of the flexure blade. The resulting tensile stress σ_{flex} is

6.8-3 $$\sigma_{flex} = \frac{6pL}{ht^2}$$

In twist, the flexure is a rectangular beam. The twisting angle theta in response to a torque T is

6.8-4 $$\theta = \frac{TL}{KG}$$

where G is the shear modulus of the material and K is a twisting stiffness factor defined for a rectangular beam as [43]

6.8-5 $$K = ht^3\left[\frac{1}{3} - 0.21\frac{t}{h}\left(1 - \frac{t^4}{12h^4}\right)\right]$$

The shear stress τ_{twist} resulting from the deformation is

6.8-6 $$\tau_{twist} = \frac{T}{Q}$$

The constant Q is the polar section modulus of the rectangular section, defined as [43]

6.8-7

$$Q = \frac{h^2 t^2}{3h + 1.8t}$$

Equations 6.8-1 through 6.8-7 were used to design the flexure shown in Figure 6.8-2. Table 6.8-2 shows the result of the design: the flexure blades are 21.6 mm long, 74.7 mm tall, and 0.79 mm thick (or 0.031 inches, a readily-available sheet thickness [37]).

The flexure assembly is meant to allow one translation and one rotation at each flexure blade, but additional deformations could occur. A finite-element analysis of the flexure assembly was conducted[4] to measure its vertical displacement arising from vertical loads. Figure 6.8-3 shows the displacement resulting from a static 250 N vertical force. As shown on Table 6.8-3, maximum vertical displacement is 0.1034 mm so the stiffness is 2.42 N/μm. A frequency analysis of the flexure was also conducted to ensure that no unconstrained vibrations occurred at low frequency. Table 6.8-4 lists the modes of vibration and their frequencies; the lowest-frequency mode shape is shown graphically in Figure 6.8-4. In this mode, each flexure flexes and the connecting structure deforms, allowing the connecting structure to rotate about a vertical axis located approximately at the spline shaft. The frequency of this vibration is 1250 Hz, so it should not interfere with the operation of the robot.

---

[4] The author would like to thank Antonio Makiyama at Interactive Motion Technologies for providing the finite element analysis shown in this section.

Table 6.8-2: Flexure design

Parameter	Label	Value	*Units*
Length	L	21.6	*mm*
Thickness	t	0.787	*mm*
Height	h	74.7	*mm*
Lever Arm of Vertical Force	r	111	*mm*
Elastic Modulus	E	193	*GPa*
Shear Modulus	G	77.2	*GPa*
Yield Stress	σ_y	965	*MPa*
Endurance Limit	σ_E	552	*MPa*
Max. Bending Stress	$\sigma_{bend,max}$	170	*MPa*
Flexing Force	p	174	*N*
Max. Flexing Stress	$\sigma_{flex,max}$	488	*MPa*
Twisting Torque	T	0.752	*N-m*
Max. Twisting Stress	$\tau_{twist,max}$	49.1	*MPa*

Table 6.8-3: Results of static FEA analysis

	Value	*Units*
Vertical Load	250	*N*
Max. Stress	29.6	*MPa*
Max. Strain	0.000253	
Max. Displacement	0.1034	*mm*
Stiffness	2.42	*N/micron*

Table 6.8-4: Results of frequency FEA analysis

Mode	Frequency
	Hz
1	1248.5
2	1727.1
3	2113.8
4	4034.8
5	4965.6

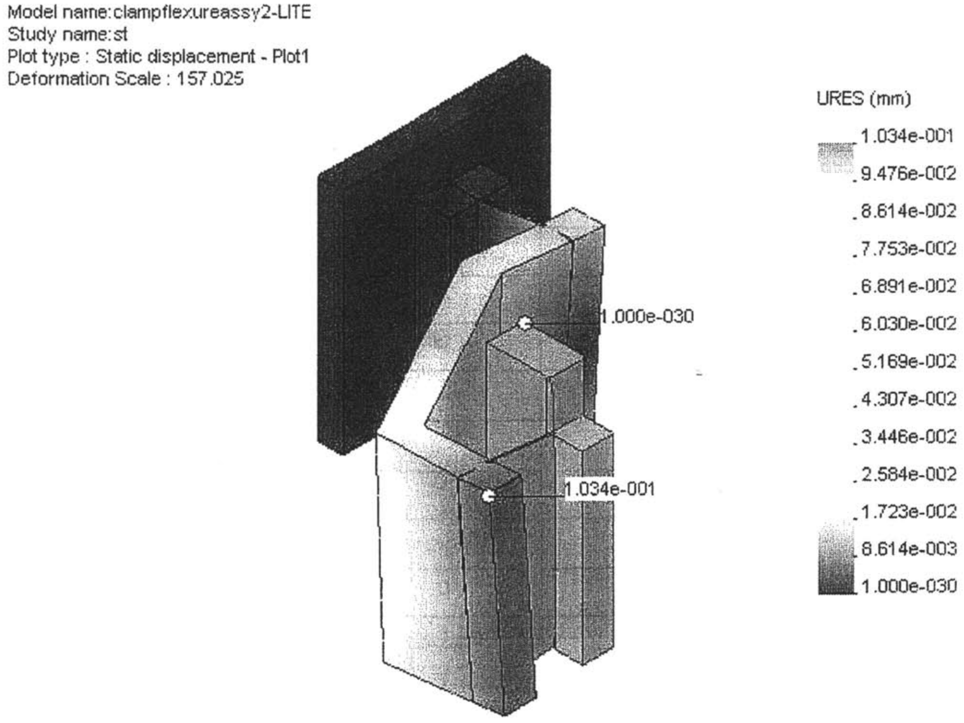

Figure 6.8-3: Finite element analysis of flexure; displacement from 250 N vertical load

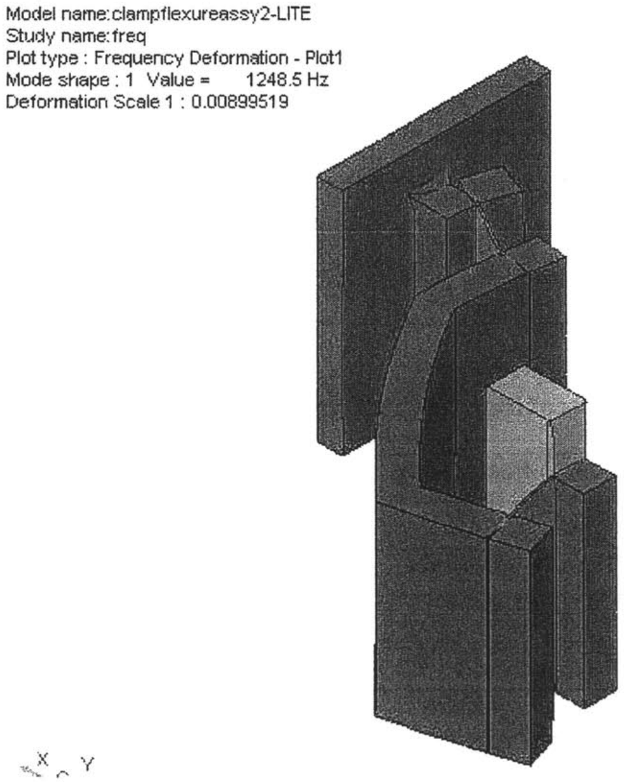

Figure 6.8-4: Finite element analysis of flexure, lowest frequency mode, *f = 1250 Hz*

6.9 Body-weight support sub-module design

In section 4.2.5, numerous energy storage elements as well as an active element were proposed as ways to generate body-weight support forces. The passive elements were coil springs, constant force springs, gas charge springs, and surgical tubing springs while the active element was a Copley linear motor. A linear motor has already been specified for this robot; see section 6.3.2. The purpose of this linear motor is to modulate the output force in the vertical direction. The bulk of the vertical force must still come from a passive energy storage element. Each type of energy storage element is first investigated with calculations to ascertain their relative merit and a workable solution is found.

6.9.1 Calculations for each option

Before analyzing the energy storage elements considered for this sub-module, it is worth examining the governing equations of a block and tackle transmission such as the one shown in Figure 6.9-1. The ball spline already serves to guide the motion so a rope pulling upwards on the spline nut is a feasible way of applying forces to this system. A block and tackle converts tension in a low force/high displacement input line into high force/low displacement tension at the output line, much the same way as a gear train converts a high speed/low torque input into a low speed/high torque output. For an input tension T_i and a block and tackle ratio N, the output tension T_o is

6.9-1

$$T_o = N \cdot T_i$$

while the displacement of the output line x_o given an input line displacement of x_i is

6.9-2

$$x_o = \frac{1}{N} \cdot x_i$$

In this case, the relationship between the stiffness at the input line K_i and one at the output line K_o is also needed:

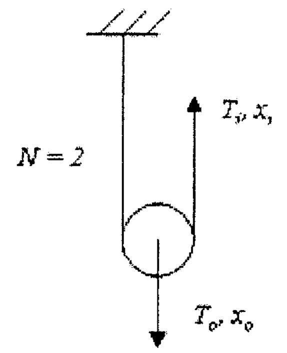

Figure 6.9-1: Block-and-tackle with N = 2

6.9-3
$$K_o = \frac{T_o}{x_o} = \frac{N \cdot T_i}{\frac{1}{N} \cdot x_i} = N^2 \cdot K_i$$

Equation 6.9-3 is only applicable for linear stiffness at both the input and the output. These block and tackle equations show that the mechanism is capable of being used to adjust both the force and the stiffness on the output side. Any passive element can be connected to the robot endpoint through a block and tackle.

The first passive element, the coil spring, is straightforward to analyze. Only coil springs configured as extension springs are studied due to the likelihood of using cables in tension to transmit forces between the energy storage element and the vertically mobile linkage. Begin by defining a quantity C, called the spring index and calculated from the nominal spring diameter *D* and the wire diameter *d* by

6.9-4
$$C = \frac{D}{d}$$

Useful values of *C* are between 4 and 12 [43]. The lower *C* is the stiffer the spring will be. The stress in the coil τ_{coil} is given by

6.9-5
$$\tau_{coil} = K_w \frac{8FD}{\pi d^3}$$

where *F* is the force on the spring and K_w is Wahl's factor

Table 6.9-1: Torsional yield stress S_{ys} for Type 302 stainless steel in static and fatigue loading [43]

Load Cycles	Torsional Yield Strength, S_{ys}
	MPa
Static	455
10^5	468
10^6	429
10^7	390

6.9-6
$$K_w = \frac{4C-1}{4C-4} + \frac{0.615}{C}$$

The shear stress allowed in type-302 stainless steel springs is shown in Table 6.9-1 for both the static condition and for cyclic loads.

Equations 6.9-4 through 6.9-6 allow one to find the stress on the coil for a given force, but they do not give guidance with respect to selecting proper values of D, d, and C. These parameters can be determined from the spring stiffness constant K by

6.9-7
$$K = \frac{F - F_i}{y} = \frac{d^4 G}{8D^3 N_a}$$

where y is the spring displacement, F_i is the force required to overcome the initial tension of the spring, G is the modulus of rigidity of the material, and N_a is the number of active coils in the spring. It is assumed that one coil out of the spring is not active [43], so the spring body length L_b is

6.9-8
$$L_b = d(N_a + 1)$$

Finally, the natural frequency f_n of "surging" can be calculated

6.9-9
$$f_n = \frac{d}{\pi D^2 N_a}\sqrt{\frac{G}{32\rho}}$$

using all the parameters as defined above plus ρ, the mass density of the spring material. In the section 6.9.2, coil springs are analyzed in terms of the requirements of the body-weight support sub-module.

The next available energy storage element is the constant force spring. This type of spring is susceptible to fatigue wear. This is the case because, as the spring unrolls, the only material that becomes stressed is that in the quarter-circumference just prior to straightening. The straight section of material is already stressed while the material that remains in the coil simply rotates without any strain. This pattern of change in stress means that any displacement that rotates the coil by as little as a quarter turn produces one full stress cycle in the spring material. In other words, unlike in a coil spring where the stress in the material is proportional to the load, material in a constant force spring undergoes a full stress cycle with every movement.

Assuming a step rate of one step per second, the spring would undergo 60 cycles in a minute and 3600 in an hour. If the device is used eight hours a day it will experience one million cycles in just under seven weeks. While constant force springs can be designed to possess longer fatigue life, an 8.61 lb. constant force spring that can withstand one million cycles measures 9.30 inches in diameter and 4 inches in width [62]. Table 6.9-2 shows springs with similar force ratings and different life ratings: by comparison, a 10.6 lb. spring rated for 2500 cycles measures just 1.16 inches in diameter and 1 inch in width [62]. As these springs show, the price for longer life is less stress in the wound spring, which translates into significantly lower force output for a given size spring. At these rates it would take five to six constant force springs to support the static weight of the linkage, and every one of the springs would have to be changed in two-month intervals. Unless no other solution is acceptable, constant force springs should not be used to generate any part of the body-weight support force.

In charged gas springs, the only two factors than can be controlled are the travel and the force of the spring. The manufacturer does not publish data regarding life, maximum duty cycle, friction, or even spring constant. Therefore, it is safer to use charged gas springs to provide either a static force or a short-duration high-force stroke. It is best to avoid continuous use since heat built up in the spring could cause the gas inside to expand and to thereby raise the pressure inside the cylinder.

The final energy storage element available is the surgical tubing spring. The maximum load these springs are rated to is 77 pounds; available springs are shown in Table 6.9-3. These springs can stretch to almost three times their original length. The longest springs have a free length of 123 inches, and extend to thirty feet in length.

Table 6.9-2: Sample constant force springs [62]

Life	Force	Inner Diameter	Width
cycles	*lbs.*	*in.*	*in.*
2,500	10.6	1.156	1
5,000	9.04	1.85	1
13,000	9.48	2.219	1.5
20,000	8.74	3.297	1.5
35,000	9.50	4.97	2.5
100,000	8.69	6.66	4
1,000,000	8.61	9.30	4

Table 6.9-3: Properties of off-the-shelf surgical tubing springs with 77 lb. load rating [37]

Overall Length	Deflection at Load	Rate
in.	*in.*	*lbs./in.*
19	24	3.21
31	48	1.60
43	72	1.07
55	96	0.80
79	144	0.53
123	240	0.32

6.9.2 Choosing a design

Table 6.9-4 shows the specifications that apply to the body-weight support module. The output force and output stiffness values are repeated from Table 3.2-9 on page 52, while the total force includes the force required to support the weight of the linkage.

Coil spring designs with and without block-and-tackle transmissions are shown in Table 6.9-5. A spring index of 12 yields the shortest spring for each transmission ratio. These springs are still large and have a low natural frequency; in particular the one-to-one ratio spring has a natural frequency equal to the maximum step rate specification for the robot. Coil springs would meet the requirements but they are not the ideal solution.

The most appealing option is the surgical tubing spring. Three springs of the type shown in Table 6.9-3 provide the required force. Longer springs can be used to lower the stiffness, and they can be wrapped around pulleys as shown in Figure 6.9-2. These pulleys must have a large enough diameter to prevent stress concentrations from damaging the springs prematurely.

Table 6.9-4: Body-weight support module specifications

	Value	*Units*
Output Force	628	*N*
Output Stiffness	700	*N/m*
Total Force	890	*N*

Table 6.9-5: Coil spring designs

Parameters				*Units*
Block-and-tackle ratio	1	2	4	
Max endpoint force	890	890	890	*N*
Endpoint stiffness	700	700	700	*N/m*
Spring constant	700	2800	11200	*N/m*
Spring travel*	1.27	0.636	0.318	*m*
Spring material	302-SS	302-SS	302-SS	
Stress in coil	421	423	421	*MPa*
Body length	0.558	0.286	0.154	*m*
Surging frequency	2.18	4.37	8.70	*Hz*

* - Spring travel calculation ignores initial tension of spring

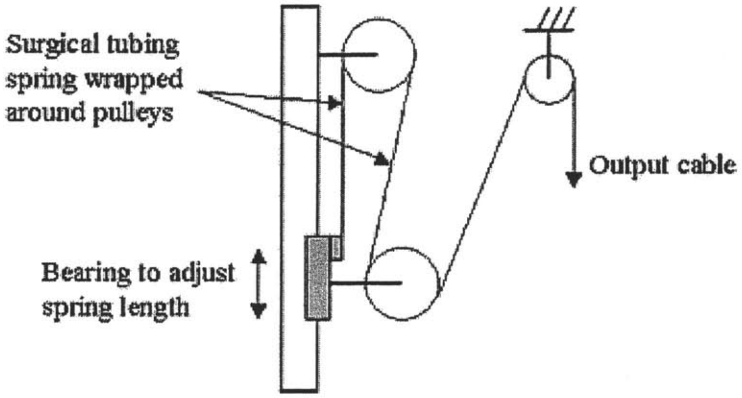

Figure 6.9-2: A configuration of surgical tubing BWS with pulleys to reduce package length

Chapter 7: Final Design Details

This chapter contains an overview of the pelvis actuation module designed in this thesis as well as drawings of the principal assemblies the module contains. The detailed part drawings are not included in this document.

7.1 Design overview

The solid model for the pelvis actuation module is shown in Figure 7.1-1. It is composed of the planar linkage assembly, the motor/spline shaft assemblies, and the chassis.

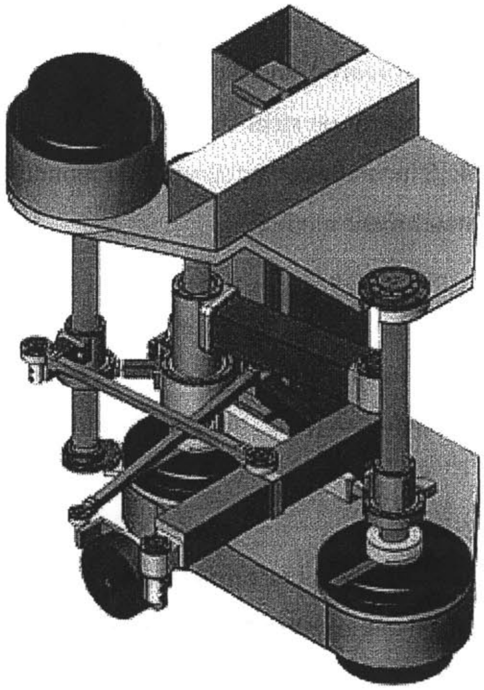

Figure 7.1-1: Pelvis actuation module

7.2 Planar linkage sub-assemblies

The planar linkage assembly, shown on page 197, has seven sub-assemblies: three spline-nut housing assemblies, three robot arms, and the vertical connection assembly. Two of the robot arms are locating links and one is the load-bearing arm.

The spline nut housing assembly for the 50mm spline nuts is shown on page 198 on the drawing labeled MHR-02-003. The spline nuts are held in the housing with two endcaps. They are constrained in rotation by two keys that are inserted through the housing wall and covered by aluminum plates. A flange with twelve threaded holes serves as a mounting point for the load-bearing robot arm; it has a raised lip to locate the corresponding flange on the arm. The outside surface of the housing is the mounting surface for the deep-groove ball bearings that connect the robot arms in the vertical direction. The two housings for the locating link spline-nuts are similar in design but hold only one spline nut and have four threaded insert holes to mate to the locating link robot arms.

Page 199 shows the load-bearing arm assembly, drawing number MHR-03-004. This arm is made of three links: the L_1 'upper arm', the L_4 'forearm', and the L_7 'end effector'. The joints between the arms have angular-contact ball bearings that mount on steel shafts. The forearm link also has a shaft in its middle that attaches the locating link. The end effector serves as a mount for the ATI force transducer, which will in turn hold the patient attachment module.

The locating link that aligns the end effector is shown in drawing MHR-04-005 on page 200. The joint bearings self-aligning ball bearings, and the links are of much narrower cross-sections than the load-bearing arm. A similar locating link attaches to the L_4 'forearm' mentioned above and locates the end effector laterally.

The final planar linkage sub-assembly is the vertical connection, shown on page 201 in drawing number MHR-05-005. This assembly links the spline-nuts so that they move in unison in the vertical direction but are not overconstrained in the other directions. It has a large bearing housing that mounts on the outside of the load-bearing spline-nut housing. This housing is in turn connected to the linear motor by a clamped-blade flexure and to the other spline nuts through plain-bearing gimbal assemblies.

REVISIONS				
ZONE	REV.	DESCRIPTION	DATE	APPROVED

ITEM NO.	QTY.	PART NO.	DESCRIPTION
1	1	MHR-02-003	S.N. Housing 50 Assy
2	1	MHR-03-004	Load-bearing Arm Assy
3	1	MHR-04-005	F/A Locating Link Assy
4	1	MHR-02-004	S.N. Housing 40 Assy #1
5	1	MHR-04-006	Lat. Locating Link Assy
6	1	MHR-02-005	S.N.Housing 40 Assy #2
7	1	MHR-05-005	Vertical Connect Assy

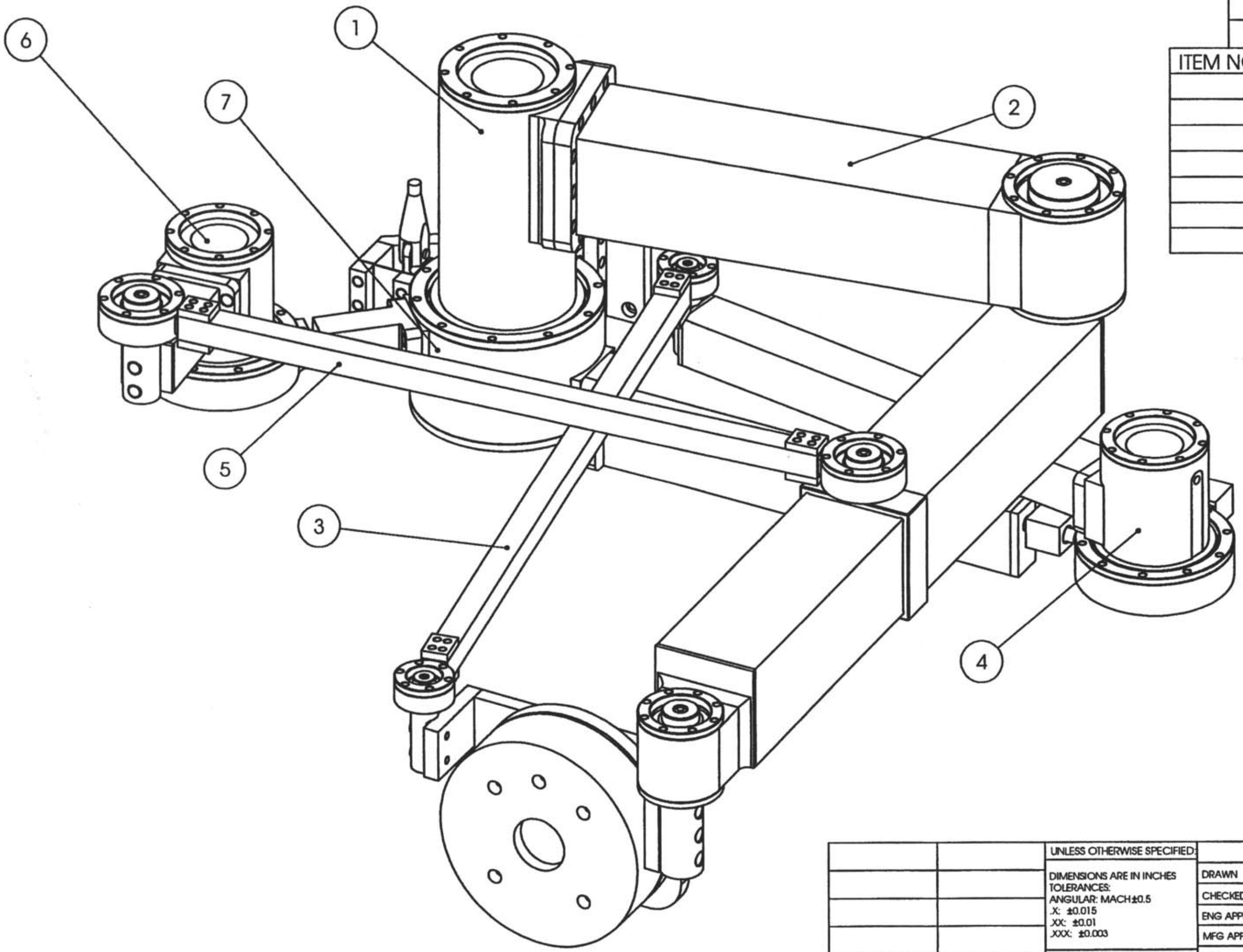

PROPRIETARY AND CONFIDENTIAL

THE INFORMATION CONTAINED IN THIS DRAWING IS THE SOLE PROPERTY OF MIT NEWMAN LAB. ANY REPRODUCTION IN PART OR AS A WHOLE WITHOUT THE WRITTEN PERMISSION OF MIT NEWMAN LAB IS PROHIBITED.

NEXT ASSY	USED ON
APPLICATION	

UNLESS OTHERWISE SPECIFIED:

DIMENSIONS ARE IN INCHES
TOLERANCES:
ANGULAR: MACH±0.5
.X: ±0.015
.XX: ±0.01
.XXX: ±0.003

INTERPRET GEOMETRIC TOLERANCING PER:

MATERIAL
–

FINISH
–

DO NOT SCALE DRAWING

	NAME	DATE
DRAWN	MHR	4/19/2004
CHECKED		
ENG APPR.		
MFG APPR.		
Q.A.		

QUANTITY REQUIRED
1

MIT Newman Lab

TITLE:

Complete Arm Assy

SIZE B
DWG. NO. MHR-00-001
REV --

SCALE: 1:3
WEIGHT:
SHEET 1 OF 2

REVISIONS				
ZONE	REV.	DESCRIPTION	DATE	APPROVED

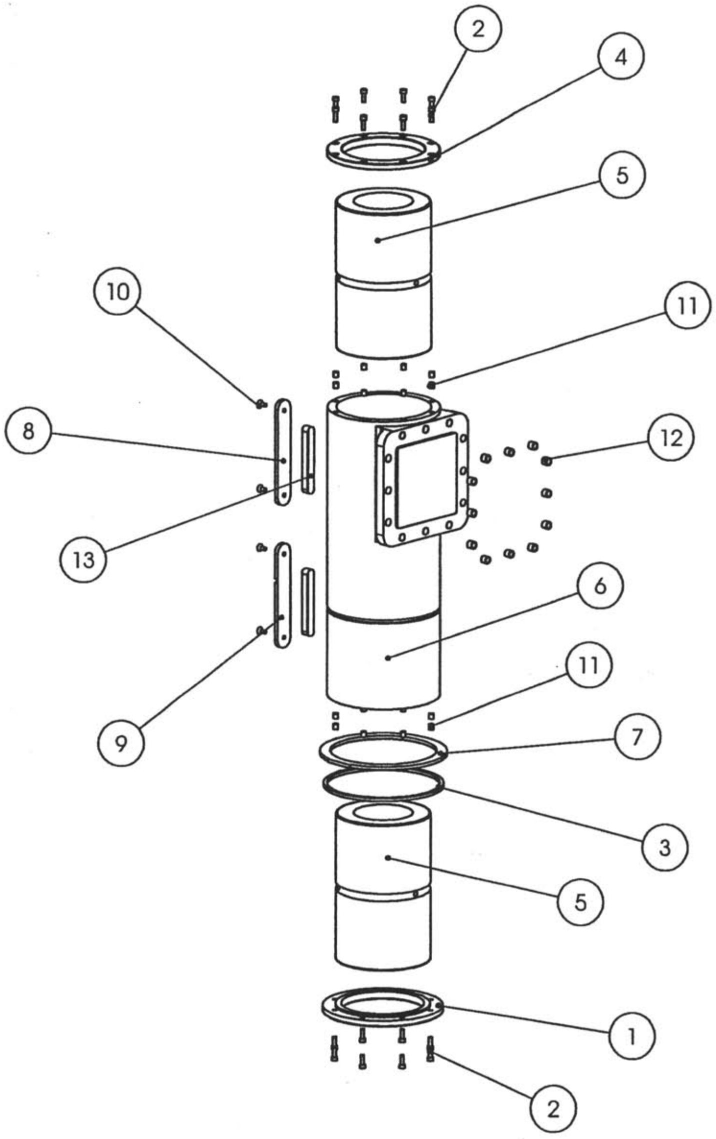

ITEM NO.	QTY.	PART NO.	DESCRIPTION
1	1	MHR-02-11	S.N.H. 50 Bottom Endcap
2	16	McMaster 91251A107	4-40 x 0.31 SHCS
3	1	MHR-02-14	S.N.H. 50 Bearing Spacer
4	1	MHR-02-10	S.N.H. 50 Top Endcap
5	2	LT50	50mm Ballspline Nut
6	1	MHR-02-06	Spline Nut Housing LT50
7	1	McMaster 97633A495	External Retaining Ring for 3.75in Shaft
8	1	MHR-02-16	S.N.H. 50 Upper Key Cover
9	1	MHR-02-17	S.N.H. 50 Lower Key Cover
10	4	McMaster 91253A106	4-40 x 0.25 FHSCS
11	16	McMaster 90296A102	4-40 x 0.168 Screw-Lock Helicoil Insert
12	12	McMaster 90296A301	M5-0.8 x 5mm Screw-Lock Helicoil Insert
13	2	LT50 Key	LT50 Key

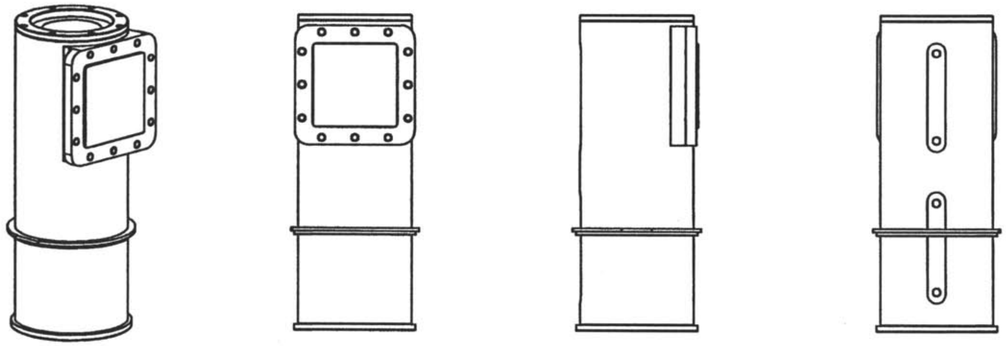

PROPRIETARY AND CONFIDENTIAL

THE INFORMATION CONTAINED IN THIS DRAWING IS THE SOLE PROPERTY OF MIT NEWMAN LAB. ANY REPRODUCTION IN PART OR AS A WHOLE WITHOUT THE WRITTEN PERMISSION OF MIT NEWMAN LAB IS PROHIBITED.

NEXT ASSY	USED ON
APPLICATION	

UNLESS OTHERWISE SPECIFIED:
DIMENSIONS ARE IN INCHES
TOLERANCES:
ANGULAR: MACH±0.5
.X: ±0.015
.XX: ±0.01
.XXX: ±0.003

INTERPRET GEOMETRIC TOLERANCING PER:

MATERIAL

FINISH

DO NOT SCALE DRAWING

	NAME	DATE
DRAWN	MHR	3/12/2004
CHECKED		
ENG APPR.		
MFG APPR.		
Q.A.		

QUANTITY REQUIRED
1

MIT Newman Lab

TITLE:

S.N. Housing 50 Assy

SIZE	DWG. NO.	REV
B	MHR-02-003	--

SCALE: 1:4 WEIGHT: SHEET 1 OF 1

REVISIONS				
ZONE	REV.	DESCRIPTION	DATE	APPROVED

ITEM NO.	QTY.	PART NO.	DESCRIPTION
1	1	MHR-03-18	L1-L4 Joint BB Endplate
2	2	McMaster 91255A263	10-32 x 0.375 BHSCS
3	1	MHR-04-12	L6 BB Endplate
4	1	MHR-03-001	Arm L1 Assy
5	1	MHR-03-003	Arm L7 Assy
6	1	MHR-03-002	Arm L4 Assy
7	2	McMaster 92146A550	#10 Spring-Lock Washer
8	12	McMaster 91303A084	M5-0.8 x 16mm 12.9 SHCS

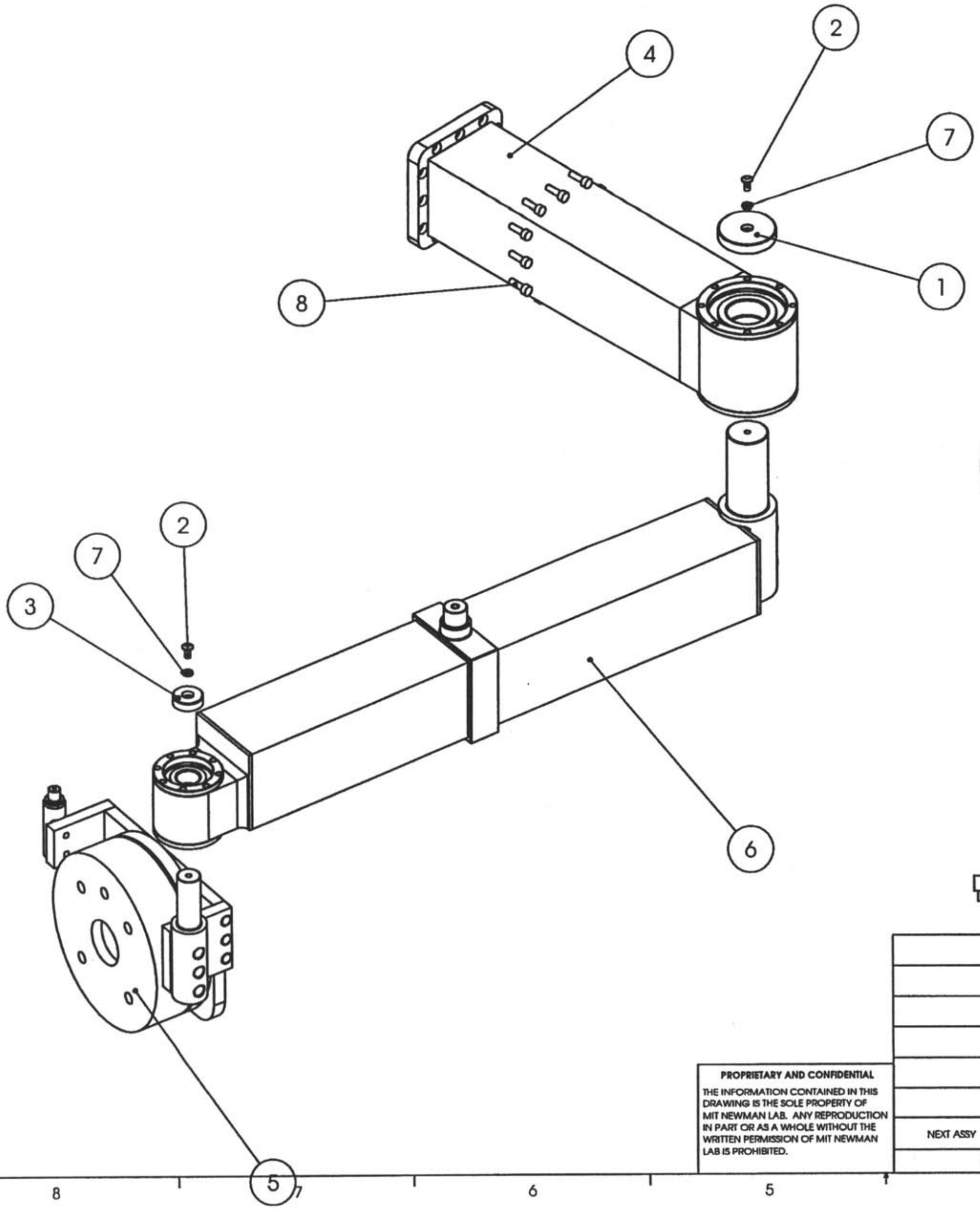

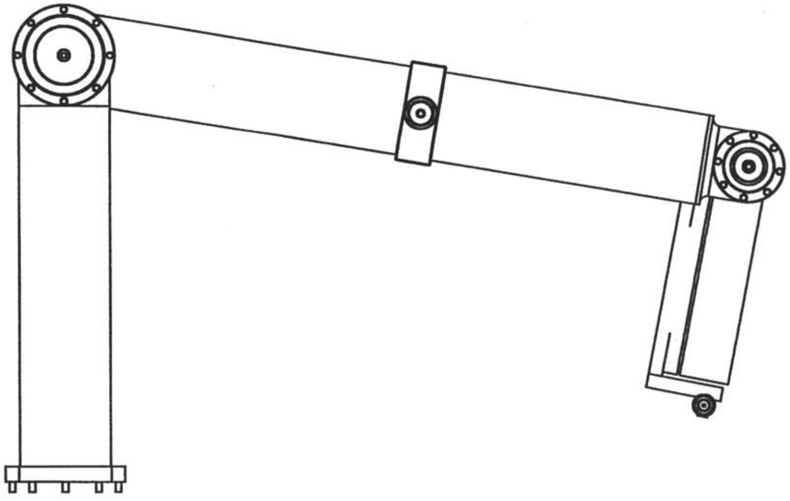

PROPRIETARY AND CONFIDENTIAL

THE INFORMATION CONTAINED IN THIS DRAWING IS THE SOLE PROPERTY OF MIT NEWMAN LAB. ANY REPRODUCTION IN PART OR AS A WHOLE WITHOUT THE WRITTEN PERMISSION OF MIT NEWMAN LAB IS PROHIBITED.

NEXT ASSY	USED ON
APPLICATION	

UNLESS OTHERWISE SPECIFIED:
DIMENSIONS ARE IN INCHES
TOLERANCES:
ANGULAR: MACH±0.5
.X: ±0.015
.XX: ±0.01
.XXX: ±0.003
INTERPRET GEOMETRIC TOLERANCING PER:
MATERIAL —
FINISH —
DO NOT SCALE DRAWING

	NAME	DATE
DRAWN	MHR	4/12/2004
CHECKED		
ENG APPR.		
MFG APPR.		
Q.A.		

QUANTITY REQUIRED
1

MIT Newman Lab

TITLE:
Load-bearing Arm Assy

SIZE B
DWG. NO. MHR-03-004
REV --
SCALE: 1:4
WEIGHT:
SHEET 1 OF 1

REVISIONS

ZONE	REV.	DESCRIPTION	DATE	APPROVED

ITEM NO.	QTY.	PART NO.	DESCRIPTION
1	1	MHR-04-003	Arm L5 Assy
2	1	MHR-04-001	Arm L2 Assy
3	2	McMaster 91255A106	4-40 x 0.25 BHSCS
4	2	MHR-04-11	L5 BB Endplate
5	2	McMaster 92146A530	# 4 Spring-Lock Washer
6	4	McMaster 91303A081	M5-0.8 x 12mm 12.9 SHCS

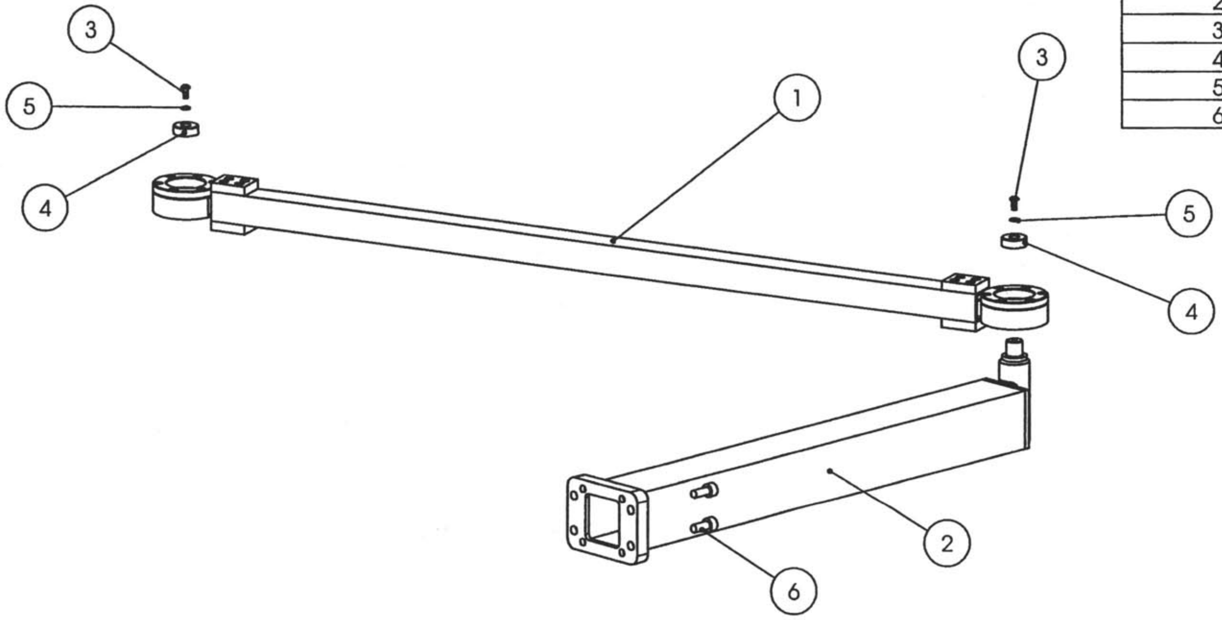

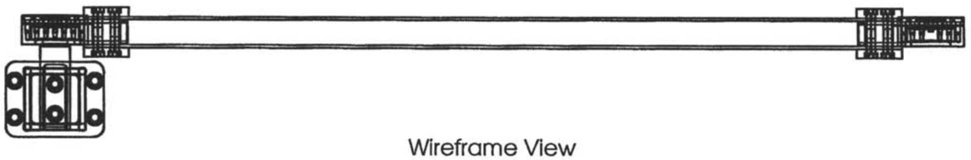

Wireframe View

PROPRIETARY AND CONFIDENTIAL

THE INFORMATION CONTAINED IN THIS DRAWING IS THE SOLE PROPERTY OF MIT NEWMAN LAB. ANY REPRODUCTION IN PART OR AS A WHOLE WITHOUT THE WRITTEN PERMISSION OF MIT NEWMAN LAB IS PROHIBITED.

NEXT ASSY	USED ON
APPLICATION	

UNLESS OTHERWISE SPECIFIED:
DIMENSIONS ARE IN INCHES
TOLERANCES:
ANGULAR: MACH±0.5
.X: ±0.015
.XX: ±0.01
.XXX: ±0.003
INTERPRET GEOMETRIC TOLERANCING PER:
MATERIAL
--
FINISH
--
DO NOT SCALE DRAWING

	NAME	DATE
DRAWN	MHR	4/9/2004
CHECKED		
ENG APPR.		
MFG APPR.		
Q.A.		

QUANTITY REQUIRED
1

MIT Newman Lab

TITLE:
F/A Locating Link Assy

SIZE	DWG. NO.	REV
B	MHR-04-005	--

SCALE: 1:3 WEIGHT: SHEET 1 OF 1

ITEM NO.	QTY.	PART NO.	DESCRIPTION
1	1	MHR-05-001	Spline 1 DGBB Housing Assy
2	1	MHR-05-002	Spline 2 DGBB Housing Assy
3	1	MHR-05-003	Spline 3 DGBB Housing Assy
4	1	MHR-05-004	Flexure Assy
5	1	MHR-05-04B	Spline 2 Cnct Brazement
6	8	McMaster 91303A081	M5-0.8 x 12mm 12.9 SHCS
7	1	MHR-05-07	Spline 3 Connector
8	2	McMaster 6621K18	PEEK 0.375 D x 0.5 L Plain Bearing
9	1	McMaster 3473T72	3/32 in Wire Rope End Fitting 7x19
10	1	MHR-05-08	BWS/Flexure Mount
11	3	McMaster 91303A126	M6-1.0 x 16mm 12.9 SHCS

REVISIONS				
ZONE	REV.	DESCRIPTION	DATE	APPROVED

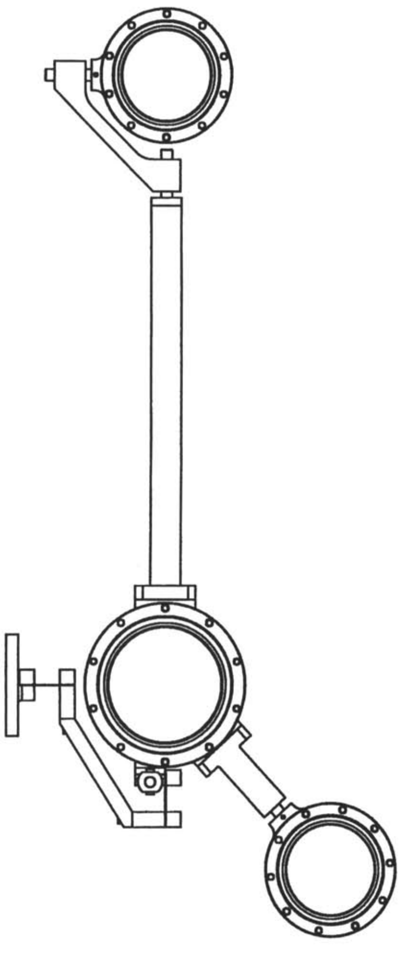

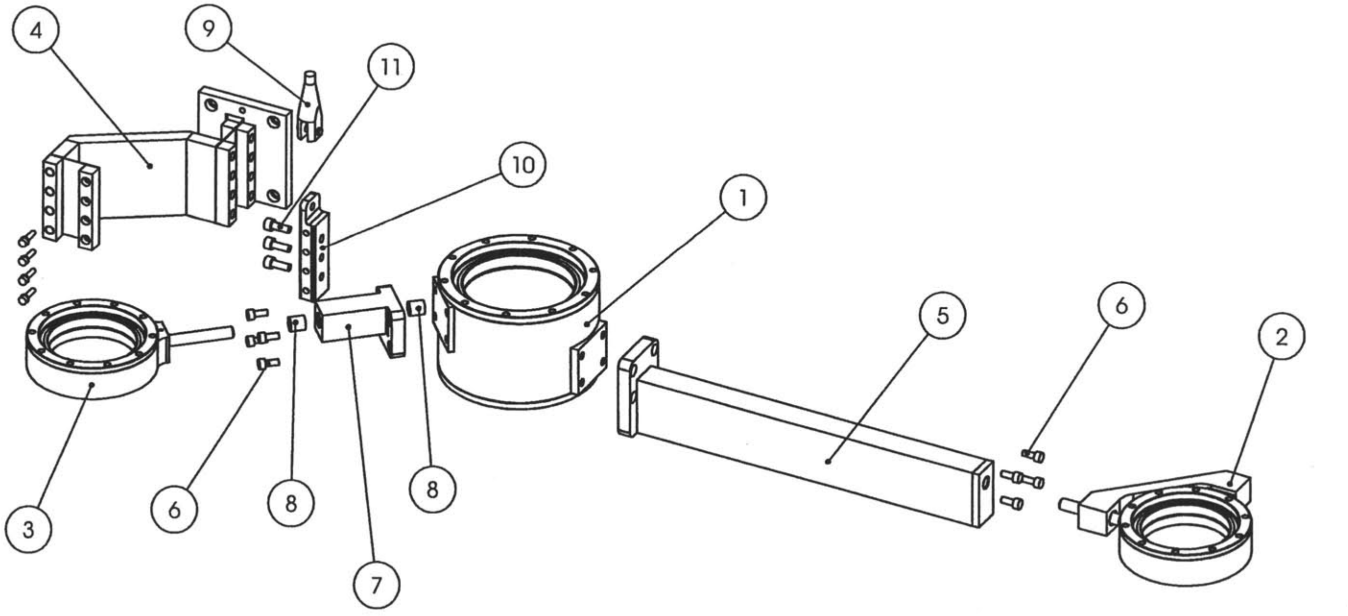

PROPRIETARY AND CONFIDENTIAL

THE INFORMATION CONTAINED IN THIS DRAWING IS THE SOLE PROPERTY OF MIT NEWMAN LAB. ANY REPRODUCTION IN PART OR AS A WHOLE WITHOUT THE WRITTEN PERMISSION OF MIT NEWMAN LAB IS PROHIBITED.

NEXT ASSY	USED ON
APPLICATION	

UNLESS OTHERWISE SPECIFIED:
DIMENSIONS ARE IN INCHES
TOLERANCES:
ANGULAR: MACH±0.5
.X: ±0.015
.XX: ±0.01
.XXX: ±0.003
INTERPRET GEOMETRIC TOLERANCING PER:
MATERIAL
--
FINISH
--
DO NOT SCALE DRAWING

	NAME	DATE
DRAWN	MHR	4/19/2004
CHECKED		
ENG APPR.		
MFG APPR.		
Q.A.		

QUANTITY REQUIRED
1

MIT Newman Lab

TITLE:

Vertical Connect Assy

SIZE B
DWG. NO. MHR-05-005
REV --
SCALE: 1:4
WEIGHT:
SHEET 1 OF 1

Chapter 8: Conclusions

This section examines the accomplishments of this project, including an evaluation of the design, an outline of future work required in this project, and finally a summary of contributions made in this thesis.

8.1 Evaluation of design

The first step in the review of the accomplishments in this thesis is the evaluation of the final product: the design. This evaluation is carried out with regard to three areas: the design process, the design itself, and proposed improvements for a future version.

8.1.1 Design process

This thesis outlines the design process behind the gait robot. It is arranged in a logical manner that begins with the background, proceeds to determining the functional requirements and a set of target specifications needed to meet them, considers the conceptual options and decides on the best course of action, shows a mockup to prove the concept, and then makes detailed calculations to back up the actual design. While these sections are presented in a logical order here there were some small deviations in the actual order of progress. Most of the deviations were not serious but in retrospect, adhering more strictly to the textbook process could have been beneficial.

In terms of the order of design steps, the only section that was out of place was the compilation of specifications for the machine. Instead of being laid out after defining the functional requirements but before selecting a concept, the specifications were not fully defined until after the mockup was built and before the start of the final design; before this point they existed as a collection of numbers without the authoritative or complete character of true specifications. While the final specifications were available in time to guide the final design, the concept selection was carried out using the preliminary numbers.

Having an official specifications document prior to the concept selection would have lent more authority to preliminary calculations made at that point.

Another change to the design process that could have been beneficial in this project is the interplay between concepts and specifications, or comparing desired values to achievable values. In particular this type of decision-making would have been useful in the concept design stage. The current concept was chosen because it was a good way to fulfill the specifications, but changes to the specifications, in particular the workspace required, could allow the use of other concepts. In the end, the most useful method for testing the specifications is to have a working machine, so the interplay between specifications and concepts is not complete; as will be seen in the next section the prototype pelvis robot can help in the next iteration of the design.

The construction of the mockup was a time-consuming procedure but it proved valuable. The mockup showed the viability of the four-degree-of-freedom concept selected for the pelvis actuation module and also allowed for some gait analysis that showed that gait was relatively unimpeded by the device. In retrospect, the mockup was too involved to be a simple "proof-of-concept", but its capacity to reveal information about body-weight support and the effect of friction and inertia on gait was not fully utilized.

Finally, one part of the design not covered in this thesis is the overground propulsion module. Because time did not permit the design of this apparatus, throughout the design of the pelvis actuation module the propulsion module was largely ignored. Calculations into the bandwidth and power requirements of this module prior to the design of the pelvis actuation module could have allowed specifications for maximum weight or other such limitations on the pelvis device. Still, the current procedure yielded a pelvis module that should work very well even if it is limited to use with a treadmill.

8.1.2 Final design

The final design produced by this thesis is shown in *Chapter 7: Final Design Details*. The best aspect of the pelvis actuation module is its parallel four-degree-of-freedom mechanism. This novel approach to parallel motion using ball-splines is the advancement that makes the high-mobility pelvis actuator possible; the large forces and low impedance required of the actuators rendered serial approaches unusable. The details that accompany this overall concept are sound as well from the design standpoint, including the use of a single load-bearing arm and the assembly that connects the spline nuts in the vertical direction. Also, the mechanical design seems to be relatively easy to manufacture and assemble.

Another aspect of the design is not as desirable: the placement of the lateral motor in the 'upper chassis' as opposed to in the 'lower chassis' with the other motors leads to complications in the design of the chassis and increases chassis weight. Space constraints in the linkage design necessitated that the lateral motor be placed in its current location, but in retrospect the space should have been created to place the motor lower.

In the end, the pelvis actuation module looks like a promising start to building a gait therapy robot. As designed it should meet most of the design specifications outlined in this thesis.

8.1.3 Suggested improvements

The pelvis robot designed here is a prototype for a gait-training device. This section outlines likely places for improvement between this prototype and the next iteration of the machine. These include the revision of the target specifications, resizing of the frontal workspace, relocation of the lateral motor, use of transmissions for the planar actuators, and re-design of the body-weight support module to be independent of the planar actuation module.

The first stage in the evolution of this design is to study the use of the prototype to refine the target specifications for the next version. All the target specifications should be reviewed: the workspace required of the machine, the forces it must output, and allowable endpoint impedances. This process mostly involves testing the device, studying the usage patterns, and recording any complaints or comments.

The review of the specifications should specifically weigh the benefits of reducing the frontal workspace. The size of the workspace in the fore/aft direction is the single biggest determinant of machine size and cost. First, the long travel necessitates long lever arms for the planar motors, so more massive motors must be used. Second, the long lever arm increase moment loads on the planar linkage, increasing the strength required of the robot arms and making them heavier. Both the heavier robot arms and the longer lever arms raise the stiffness required to maintain acceptable natural frequency in the vertical direction; this stiffness applies to the spline shafts, spline nuts, robot arms, and robot arm joints.

Moreover, the longer, heavier robot arms increase the inertia of the device in the vertical direction and increase the expected workload on the linear motor for that degree of freedom. Finally, the increased weight of the actuators and linkage increase the loads on the supporting structure, further increasing total machine weight. Reducing the size of the frontal workspace would reduce the size and weight of almost every component of the pelvis actuation module.

There are two reasons for a long frontal workspace: the first is to ensure that the patient never reaches the end of the workspace even during a stationary stepping task and the second is to reduce the accelerations required of the overground propulsion module. The former reason for a longer frontal workspace can be overruled by the substantial mechanical gains realized from the change. The latter reason is more difficult to overcome; the pelvis actuator module with reduced frontal travel would require larger accelerations of the overground module because the overground module would have less distance to react to changes in patient overground speed. It is likely that the reduction in weight is not enough to allow the overground module to attain the desired accelerations.

A purely mechanical change that should be made to the pelvis robot is the relocation of the lateral actuator, as mentioned in the previous section. The location of this actuator increases the demands on the supporting structure, so if any way can be found to relocate it so that it is on the bottom chassis plane it should be implemented.

Another mechanical change that may prove advantageous is the inclusion of transmissions for the planar motors. As mentioned in section 4.2.1 the capstan drive transmission seems suitable for this application. A prototype should be used to evaluate the impedance and feel that this element would create. Making this change would reduce the actuator size and weight and add freedom in locating the motors relative to the splines.

Finally, a redefining of the boundaries between the body-weight support module and the pelvis actuation module would improve the function in both areas of the machine. As stated in section 4.1.2, an overhead, independent body-weight support wire was not considered due to restrictions on machine overall height, but these restrictions might be relaxed. This configuration would allow the combination of the body-weight support and fall support systems. The linear motor that actuates the vertical degree of freedom would still act through the planar linkage but all other vertical forces would now travel through the overhead wire instead. Therefore, the planar linkage could be made lighter, lowering the inertia and raising the natural frequency of the system. Moreover, a 'mechanical fuse' could be inserted into the design to protect both the robot and the patient in case of falls.

8.1.4 Other applications

The pelvis actuation module is a novel, four-degree-of-freedom, parallel robot. In its current form it is intended for gait rehabilitation in general and gait rehabilitation for stroke patients in particular. However, this device it should be just as useful for patients suffering from spinal cord injuries, multiple sclerosis, and Parkinson's disease. Furthermore, it could be used in orthopedics to aid in recovery after hip replacement surgery, for example.

Outside of rehabilitation, the four-degree-of-freedom robot might be applied in manufacturing, particularly in assembly. Mechanical assembly is a known possible application of impedance-controlled robots. The size and mobility of this machine could allow it to perform tasks other machines could not. The primary limitation of this design is the relatively low stiffness in the vertical direction; this property of the machine would limit the amount of mass it carries in the endpoint. On the other hand, in an application where the robot must only guide an object and not carry it this design could be ideal. In a way, such an application would be very similar to the gait therapy application because the patient is still placing most of his or her weight on the ground.

8.2 Future work

This thesis is the start of the development of a complete gait therapy robot. Much future work is required, first on the pelvis actuation module itself, then on the other modules of the gait trainer, and finally in putting individual modules and the entire collection through clinical trials.

8.2.1 Further work on pelvis actuation module

Most of the components of the pelvis actuation module have been designed; the body-weight support system and the chassis are the only components remaining. To complete the physical system, these last parts must be designed and the entire machine must be manufactured and assembled.

The completed robot must then be modeled, characterized, and controlled. Detailed models of this machine could calculate the friction at the endpoint based on the load and the position of the linkage, the stiffness and natural frequency both in the vertical direction and in the horizontal plane, and the dynamic response of the robot arms to force inputs. Predictions made by these models could be tested against the physical performance of the machine in the characterization process, during which the friction, damping, and inertial parameters of the robot are determined experimentally. Finally, a control algorithm for the robot can be devised. The author can only guess at the complexity associated with the control of a four-degree-of-freedom robot. Once the basic structure of the controller is created, it must be refined and evolved according to what the desired trajectory and output impedance is during gait training.

The last component of the pelvis module is a user interface. This aspect of the design includes both the interface with the controller and the mechanical interface between the user and the machine. The former mostly involves a simple computer program that is intuitive and user-friendly. The latter includes a control panel with easily-identified switches as well as extra kill switches in case of emergencies and a simple user manual that details operations necessary for the adjustment of the machine.

8.2.2 Additional components

Only the pelvis actuation module has been designed at the moment. The design, construction, and characterization of the overground propulsion module could prove to be just as difficult as that of the pelvis actuation module. It also remains to devise a method to control both modules so that they work together. While this kind of problem has been attacked in the past, it is not a difficulty simply solved. The patient attachment module requires only design and construction and no control or actuation. A suggested course of action regarding this module is given in section 4.1.4, and a mockup is tested in this thesis as well. Still, the patient attachment is suited to the 'build and test' method of design, and a few iterations of a solution are required. A fall support method must also be incorporated into this machine as described in section 4.1; this module requires mechanical design only.

8.2.3 Clinical trials

After the gait trainer is complete it should be tested with humans. The first tests should be used to make sure the device could be used safely with a variety of healthy and impaired populations. Clinical trials with stroke patients can then determine the proper intervention procedure and best control algorithm is for training. Studies should also evaluate the gait trainer as used in the step-up task and as used for standing balance training.

Further clinical trials should be used to assess the effectiveness of the therapy over a longer period of time. These trials could compare robot therapy to conventional therapy to ensure that the use of the robot is at least comparable to training with a therapist. In addition, studies could focus on the difference between gait training while walking on the ground versus gait training while walking on a treadmill.

Besides being used in studies to test recovery, this robot could also be used to study the response of gait to external force inputs. Such a study could aim to explain human balance reactions and other phenomena that occur while walking. Furthermore, it would be interesting to attempt to use force inputs at the pelvis to attempt to make the gait pattern of a treadmill walker match the gait pattern of an overground walker. Finally, the gait trainer can be used on healthy subjects to study perception, reflex, and muscle function of the lower body.

8.3 Contributions to the field

The largest contribution of this thesis to the state of the art is in the design of a novel four-degree-of-freedom robot mechanism with parallel actuation. This configuration has the advantages that there are no singularities within the workspace and that the four degrees of freedom are as close to independent as possible. No other such devices exist to the best of the author's knowledge. It is hoped that this method for achieving high mobility mechanisms without resorting to serial configurations of actuators is used in other applications.

Another novel aspect of this thesis is the linkage design. The conceptual division of a multiple-degree-of-freedom linkage into several single-degree-of-freedom cranks could be applied to the design of other linkages. The technique would be most useful to other three-degree-of-freedom linkages having different workspace dimensions, though it could be applicable to simpler two-degree-of-freedom devices as well.

The specifications devised for the complete gait trainer are also valuable contributions. With that blueprint, an entirely new device can be designed from the concept selection stage forward, saving the time and effort required for a literature search.

Finally, the mockup of this device is a novel piece of hardware. It represents a mobile body-weight support system that supports body weight without the error motions associated with a pendulum system. Even though the novelty of this device will be entirely surpassed by the completed gait trainer, the mockup itself could be redesigned as a passive device for body-weight support.

Appendix A: Supplementary Calculations

A.1 Crank equations

This appendix summarizes the crank forward and inverse kinematics.

A.1.1 Forward kinematics

The crank forward kinematics are exactly the same as for a two-link mechanism when expressed in terms of the angles θ and α. Figure A.1-1 shows the parameters of the crank, including the link lengths L1 and L2 and the crank width d.

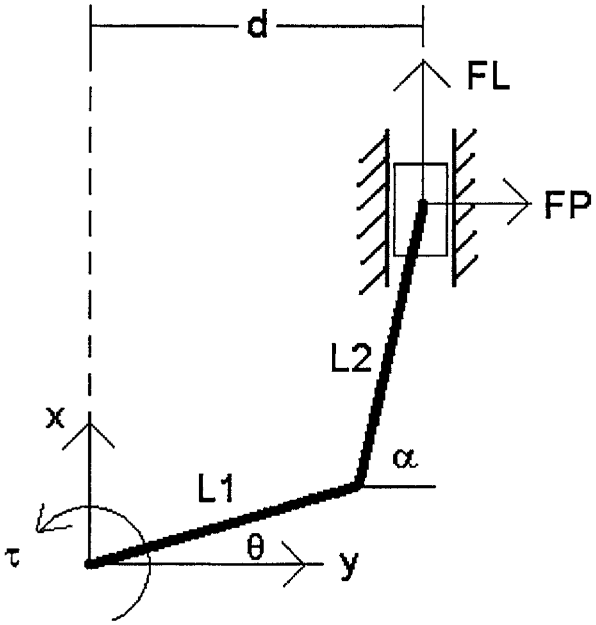

Figure A.1-1: One-degree-of-freedom crank mechanism

In terms of the above variables, the endpoint position along the slider is found from

A.1-1 $$x = L_1 \sin\theta + L_2 \sin\alpha$$

Differentiating once and rearranging the terms gives

A.1-2 $$\dot{x} = \dot{\theta} L_1 \frac{\sin(\alpha - \theta)}{\sin\alpha}$$

The geometry of the crank must be used to find α. In terms of the above variables, α is

A.1-3 $$\alpha = \cos^{-1}\left(\frac{d - L_1 \cos\theta}{L_2}\right)$$

The crank output forces can be found from free-body diagrams of the links. The force along the crank is

A.1-4 $$F_L = \frac{\tau \sin\alpha}{L_1 \sin(\alpha - \theta)}$$

while the 'parasitic', or perpendicular force into the slider bearing is

A.1-5 $$F_P = \frac{\tau \cos\alpha}{L_1 \sin(\alpha - \theta)}$$

A.1.2 Inverse kinematics

The inverse kinematics of the crank are found using the dimensions shown in Figure A.1-2. In addition to θ and α, the angle γ and ϕ are defined to simplify the calculations. The former is the angle that the crank endpoint position vector makes with the horizontal and the latter is the relative angle between the two links.

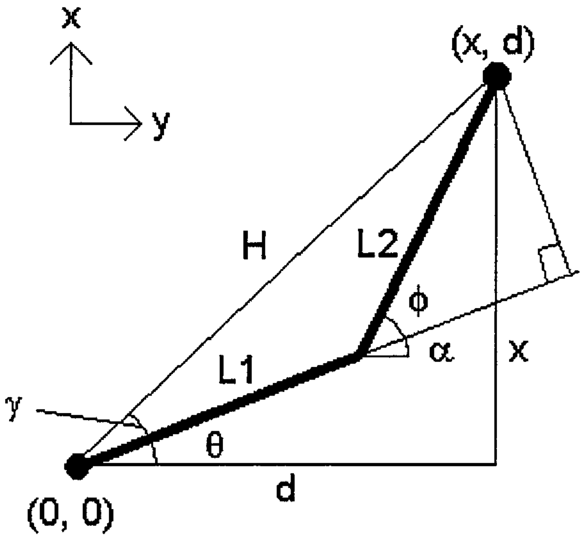

Figure A.1-2: Crank inverse kinematics

Because the crank has only one degree of freedom, the inverse kinematics only needs to find θ, the angle of the crank actuator link. The known values are the dimensions of the cranks and the position x of the end effector. This calculation requires several steps, the first of which is finding the angle ϕ,

A.1-6
$$\cos\phi = \cos(\alpha - \theta) = \frac{x^2 + d^2 - L_2{}^2 - L_1{}^2}{2L_1L_2}$$

From f, the angle (γ - θ) between the actuator link and the endpoint position vector can be found,

A.1-7
$$\tan(\gamma - \theta) = \frac{L_2 \sin\phi}{L_1 + L_2\cos\phi}$$

Then, the known endpoint position is used to isolate γ,

A.1-8
$$\gamma = \tan^{-1}\left(\frac{x}{d}\right)$$

and finally the equations are solved for θ as follows:

$$\theta = \tan^{-1}\left[\frac{x\left(d^2+x^2+L_1^2-L_2^2\right)-d\sqrt{4L_1^2L_2^2-\left(x^2+d^2-L_1^2-L_2^2\right)^2}}{d\left(d^2+x^2+L_1^2-L_2^2\right)+x\sqrt{4L_1^2L_2^2-\left(x^2+d^2-L_1^2-L_2^2\right)^2}}\right]$$

A.2 Singularity functions

Singularity functions are a convenient way to express loading conditions on beams. They are used in Chapter 6: Design Analysis because they allow one equation to represent discontinuous loading on a beam. Without singularity functions, separate solutions to beam bending equations would have to be found for each section of the beam between discontinuous loads. Therefore, the model in this thesis would require four equations instead of two.

The first singularity function is the unit doublet function, which is shown in Figure A.2-1(a). In a loading equation, the doublet function indicates an applied concentrated moment at x=a. The function in Figure A.2-1 (b) is the unit impulse function, which in a loading equation represents an applied concentrated load. Also shown are the unit step functions and unit ramp functions.

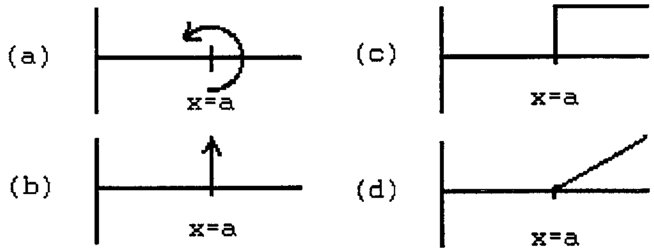

Figure A.2-1: Singularity functions: (a) unit doublet, (b) unit impulse, (c) unit step, (d) unit ramp

The singularity functions in Figure A.2-1 are related through integration. Notice that the area under the unit step function from *0* to *x* is the value of the unit ramp function. Although not as obvious, the area under the unit impulse function is also equal to the value of the unit step function. This relationship between the singularity functions is shown in equations A.2-1 through A.2-3.

A.2-1 $$n=-2; \qquad \int_{-\infty}^{x} < x-a >^{-2} dx = < x-a >^{-1}$$

A.2-2 $n = -1;$ $$\int_{-\infty}^{x} < x - a >^{-1} \, dx = < x - a >^{0}$$

A.2-3 $n \geq 0;$ $$\int_{-\infty}^{x} < x - a >^{n} \, dx = \frac{< x - a >^{n+1}}{n+1}$$

The value of a singularity function at a point x is zero if the quantity inside triangular brackets is negative. For the unit doublet and unit impulse, in fact, the value of the function is zero everywhere except at $x = a$. The unit step function has value of one for every x greater than a. Evaluating any other singularity function at a point $x > a$ simply results in the substitution of normal parenthesis for the triangular brackets. Thus, the unit ramp function has value x at any point $x > a$.

Bibliography

1. Aisen ML, Krebs HI, Hogan N, et al. The Effect of Robot-Assisted Therapy and Rehabilitative Training on Motor Recovery Following Stroke. *Archives of Neurology* 1997; **54**: 443-446.
2. ATI Industrial Automation. *Multi-Axis Force/Torque Sensors.* < http://www.ati-ia.com/sensors.htm > (7 May 2004).
3. Automation Creations, Inc. *MatWeb - The Online Materials Information Resource.* < http://www.matweb.com/index.asp?ckck=1 > (7 May 2004).
4. Buerger SP. *Characterization and Control of an Interactive Robot.* MSME Thesis, Massachusetts Institute of Technology, February 2001.
5. Celestino JR. *Characterization and Control of a Robot for Wrist Rehabilitation.* MSME Thesis, Massachusetts Institute of Technology, June 2003.
6. Charnnarong J. *The Design of an Intelligent Machine for Upper-Limb Physical Therapy.* MSME Thesis, Massachusetts Institute of Technology, September 1991.
7. Charness A. *Stroke/Head Injury: A Guide to Functional Outcomes in Physical Therapy Management.* Rockville: Aspen Systems Corp, 1986.
8. Chen G, Schwandt D, Van der Loos HFM, et al. Compliance-adjustable, force-sensing harness support for studying treadmill training in neurologically impaired subjects. *6th Annual Gait and Clinical Movement Analysis Meeting, Shriners Hospitals for Children, Northern California, Sacramento, CA, April 25-28* 2001.
9. Colombo G, Joerg M, Schreier R, Dietz V. Treadmill training of paraplegic patients using a robotic orthosis. *Journal of Rehabilitation Research and Development* 2000; **37**: 693-700.
10. Colombo G, Wirz M, Dietz V. Driven gait orthosis for improvement of locomotor training in paraplegic patients. *Spinal Cord* 2001; **39**: 252-255.
11. Copley Controls Corp. *Copley Controls Corp. Home page.* < http://www.copleycontrols.com > (7 May 2004).
12. Crandall SH, Dahl NC, Lardner TJ. *An Introduction to the Mechanics of Solids; Second Edition with SI Units.* New York: The McGraw-Hill Companies, Inc., 1999.
13. da Cunha Filho IT, Lim PAC, Qureshy H, et al. A comparison of regular rehabilitation and regular rehabilitation with supported treadmill ambulation treadmill training for acute stroke patients. *Journal of Rehabilitation Research and Development* 2001; **38**: 245-255.
14. Danaher Corporation. *MotionVillage Welcome Center.* < http://www.motionvillage.com > (7 May 2004).
15. Davies PM. *Steps to Follow: The Comprehensive Treatment of Patients with Hemiplegia.* New York: Springer, 2000.
16. Dietz V, Colombo G, Jensen L. Locomotor activity in spinal man. *The Lancet* 1994; **344**: 1260-1263.

17. Farley CT, McMahon TA. Energetics of walking and running: insights from simulated reduced-gravity experiments. *Journal of Applied Physiology* 1992; **73**: 2709-2712.
18. Gazzini F, Fadda A, Torre M, Macellari V. WARD: a pneumatic system for body weight relief in gait rehabilitation. *IEEE Transactions on Rehabilitation Engineering* 2000; **8**: 506-513.
19. Gurley Precision Instruments. *Gurley Precision Instruments.* < http://www.gurley.com > (7 May 2004).
20. Harris-Love ML, Forrester LW, Macko RF, et al. Hemiparetic gait parameters in overground versus treadmill walking. *Neurorehabilitation and Neural Repair* 2001; **15**: 105-112.
21. Hesse S, Helm B, Krajnik J, Gregoric M, Mauritz KH. Treadmill training with partial body weight support: influence of body weight release on the gait of hemiparetic patients. *Journal of Neurological Rehabilitation* 1997; **11**: 15-20.
22. Hesse S, Konrad M, Uhlenbrock D. Treadmill walking with partial body weight support versus floor walking in hemiparetic subjects. *Archives of Physical Medicine & Rehabilitation* 1999; **80**: 421-427.
23. Hesse S, Uhlenbrock D. A mechanized gait trainer for the restoration of gait. *Journal of Rehabilitation Research and Development* 2000; **37**: 701-708.
24. Hogan N. Impedance control: an approach to manipulation. Part I, Part II, Part III. *Journal of Dynamic Systems, Measurement, and Control* 1985; **107**: 1-24.
25. Hudson CC, Krebs DE. Frontal plane dynamic stability and coordination in subjects with cerebellar degeneration. *Experimental Brain Research* 2000; **132**: 103-113.
26. Inman VT, Ralston HJ, Todd F. *Human Walking*. Baltimore: Williams & Wilkins, 1981.
27. Johansson BB. Brain plasticity and stroke rehabilitation: the Willis lecture. *Stroke* 2000; **31**: 223-230.
28. Kapandji IA. *The Physiology of the Joints, Volume 2.* New York: Churchill Livingstone, 1987.
29. Kerrigan DC, Frates EP, Rogan S, Riley PO. Hip hiking and circumduction: quantitative definitions. *American Journal of Physical Medicine & Rehabilitation* 2000; **79**: 247-252.
30. Kirker SGB, Jenner JR, Simpson DS. Changing patterns of postural hip muscle activity during recovery from stroke. *Clinical Rehabilitation* 2000; **14**: 618-626.
31. Kirker SGB, Simpson DS, Jenner JR, et al. Stepping before standing: hip muscle function in stepping and standing balance after stroke. *Neurology Neurosurgery, & Psychiatry* 2000; **68**: 458-464.
32. Kosak MC, Reding MJ. Comparison of partial body weight-supported treadmill training versus aggressive bracing walking post stroke. *Neurorehabilitation and Neural Repair* 2000; **14**: 13-19.
33. Kraan GA, van Veen J, Snijders CJ, Storm J. Starting from standing: why step backwards? *Journal of Biomechanics* 2001; **34**: 211-215.
34. Krebs HI, Hogan N, Aisen ML, Volpe BT. Robot-aided neurorehabilitation. *IEEE Transactions on Rehabilitation Engineering* 1998; **6**: 75-87.
35. Macko RF, DeSouza CA, Tretter LD, et al. Treadmill aerobic exercise training reduces the energy expenditure and cardiovascular demands of hemiparetic gait in chronic stroke patients: a preliminary report. *Stroke* 1997; **28**: 326-330.

36. Matjacic Z, Johannesen IL, Sinkjaer T. A multi-purpose rehabilitation frame: a novel apparatus for balance training during standing of neurologically impaired individuals. *Journal of Rehabilitation Research and Development* 2000; **37**: 681-691.
37. McMaster-Carr Supply Company. *Online Catalog.* < http://www.mcmaster.com > (7 May 2004).
38. Miyai I, Yagura H, Oda I, et al. Premotor cortex is involved in restoration of gait in stroke. *Annals of Neurology* 2002; **52**: 188-194.
39. Mobility Research. *Litegait I.* Rev. Feb. 2000. < http://www.litegait.com/newpage/prod01.htm > (12 Aug. 2003).
40. Nadeau S, Arsenault AB, Gravel D, Bourbonnais D. Analysis of the clinical factors determining natural and maximal gait speeds in adults with a stroke. *American Journal of Physical Medicine & Rehabilitation* 1999; **78**: 123-130.
41. Nelles G, Spiekermann G, Jueptner M, et al. Evolution of functional reorganization in hemiplegic stroke: a serial positron emission tomographic activation study. *Annals of Neurology* 1999; **46**: 901-909.
42. Nilsson L, Carlsson J, Danielsson A, et al. Walking training of patients with hemiparesis at an early stage after stroke: a comparison of walking training on a treadmill with body weight support and walking training on the ground. *Clinical Rehabilitation* 2001; **15**: 515-527.
43. Norton RL. *Machine Design: An Integrated Approach. 2nd Ed.* Upper Saddle River: Prentice Hall, 2000.
44. Oberg E, Jones FD, Horton HL, Ryffel HH. *25th Edition Machinery's Handbook.* New York: Industrial Press, Inc., 1996.
45. Online Dynamics, Inc. *Autolev.* < http://www.autolev.com > (7 May 2004).
46. Pavol MJ, Owings TM, Grabiner MD. Body segment inertial parameter estimation for the general population of older adults. *Journal of Biomechanics* 2002; **35**: 707-712.
47. Pohl M, Mehrholz J, Ritschel C, et al. Speed-dependent treadmill training in ambulatory hemiparetic stroke patients: a randomized controlled trial. *Stroke* 2002; **33**: 553-558.
48. Prokop T, Schubert M, Berger W. Visual influence on human locomotion: modulation to changes in optic flow. *Experimental Brain Research* 1997; **114**: 63-70.
49. Ryan AS, Dobrovolny CL, Smith GV, Silver KH, Macko RF. Hemiparetic muscle atrophy and increased intramuscular fat in stroke patients. *Archives of Physical Medicine and Rehabilitation* 2002; **83**: 1703-1707.
50. Schmidt H, Sorowka D, Hesse S, Bernhardt R. Development aspects of a robotized gait trainer for neurological rehabilitation. *2001 Proceedings of the 23rd Annual EMBS International Conference,* 2001; 1340-1343.
51. Schmidt H, Sorowka D, Hesse S, Bernhardt R. Robotic walking simulator for neurological gait rehabilitation. *Proceedings of the Second Joint EMBS/BMES Conference* 2002; 2356-2357.
52. Sensable Technologies, Inc. *Sensable Technologies.* < http://www.sensable.com > (7 May 2004).
53. Shigley JE, Mischke CR. *Mechanical Engineering Design, Fifth Edition.* New York: McGraw-Hill, Inc., 1989.

54. Siddiqi N, Gazzini F, Des Jardins J, Chao EYS. The use of a robotic device for gait training and rehabilitation. *Medicine Meets Virtual Reality.* IOS Press, 1997.

55. SKF Group, The. *Welcome to SKF.com.* < http://www.skf.com > (7 May 2004).

56. Slocum AH. *Precision Machine Design.* Dearborn: Society of Manufacturing Engineers, 1992.

57. Smith WD, Smith LH. *McGraw-Hill On-Site Guide to Building Codes 2000: Commercial and Residential Interiors.* New York: McGraw-Hill, 2001.

58. Spyropoulos P, Pisciotta JC, Pavlou KN, et al. Biomechanical gait analysis in obese men. *Archives of Physical Medicine and Rehabilitation* 1991; **72**: 1065-1070.

59. Stabilus USA. *Welcome to Stabilus.* < http://www.stabilus.com/default_e.asp > (7 May 2004).

60. Staff of Anthropology Research Project, eds. Anthropometric Source Book Volume I: Anthropometry for Designers. *NASA Reference Publication 1024.* Yellow Springs: Webb Associates, 1978.

61. State of South Carolina. *S.C. Code of Regulations Chapter 61 Department of Health and Environmental Control.* Rev. Mar. 2001. < www.lpitr.state.sc.us/coderegs/chap61/61-16.htm > (22 Jul. 2003).

62. Stock Drive Products/Sterling Instrument. *Welcome to SDP/SI.* < http://sdp-si.com/index.asp > (7 May 2004).

63. Stolze H, Kuhtz-Buschbeck JP, Mondwurf C, et al. Gait analysis during treadmill and overground locomotion in children and adults. *Electroencephalography and Clinical Neurophysiology* 1997; **105**: 490-497.

64. Tan HZ, Srinivasan MA, Eberman B, Cheng B. Human factors for the design of force-reflecting haptic interfaces. *Dynamic Systems and Control* 1994; **55**: 353-358.

65. THK America, Inc. *THK Technology.* < http://www.thk.com/technology_en.html > (7 May 2004).

66. Thomas GB, Finney RL. *Calculus and Analytic Geometry.* 9th Ed. Reading, MA: Addison-Wesley Publishing Company, 1996.

67. Tilley AR. *The Measure of Man and Woman: Human Factors in Design.* New York: Wiley, 2002.

68. Ulrich KT, Eppinger SD. *Product Design and Development.* Boston: McGraw-Hill, 2000.

69. Umphred DA. *Neurological Rehabilitation.* Philadelphia: Mosby, 2001.

70. van Ingen Schenau GJ. Some fundamental aspects of the biomechanics of overground versus treadmill locomotion. *Medicine & Science in Sports & Exercise* 1980; **12**: 257-261.

71. Visintin M, Barbeau H. The effects of body weight support on the locomotor pattern of spastic paretic patients. *Le Journal Candien des Sciences Neurologiques* 1989; **16**: 315-325.

72. Visintin M, Barbeau H, Korner-Bitensky N, et al. A new approach to retrain gait in stroke patients through body weight support and treadmill stimulation. *Stroke* 1998; **29**: 1122-1128.

73. Wang, CYE, Bobrow JE, Reinkensmyer DJ. Swinging from the hip: use of dynamic motion optimization in the design of robotic gait rehabilitation. *Proceedings of the 2001 IEEE International Conference on Robotics & Automation* 2001; 1433-1438.

74. Werkmeister J. *Design and Fabrication of the Mesomill: A Five-Axis Milling Machine for Meso-Scaled Parts.* MSME Thesis, Massachusetts Institute of Technology, June 2004.

75. Werner C, von Frankenberg S, Treig T, Konrad M, Hesse S. Treadmill training with partial body weight support and electromechanical gait trainer for restoration of gait in subacute stroke patients: a randomized crossover study. *Stroke* 2002; **33**: 2895-2901.
76. Wheeler JW. *An Ankle Robot for a Modular Gait Rehabilitation System.* MSME Thesis, Massachusetts Institute of Technology, June 2004.
77. White SC, Yack HJ, Tucker CA, et al. Comparison of vertical ground reaction forces during overground and treadmill walking. *Medicine & Science in Sports & Exercise* 1998; **30**: 1537-1542.
78. Williams D. *A Robot for Wrist Rehabilitation.* MSME Thesis, Massachusetts Institute of Technology, June 2001.
79. Wilson MS, Qureshy H, Protas E, et al. Equipment specifications for supported treadmill ambulation training: a technical note. *Journal of Rehabilitation Research and Development* 2000; **37**: 415-422.